



# UNIVERSITÀ DEGLI STUDI DI PADOVA

Dipartimento di Fisica e Astronomia “Galileo Galilei”

Corso di Laurea Magistrale in Fisica

Tesi di Laurea

## Preliminary Modelling for the Proton Boron Capture Therapy (PBCT)

Relatore

Prof. Marco Mazzocco

Correlatore

Dr. G.A.Pablo Cirrone

Dr.ssa Giada Petringa

Laureando

Davide Chiappara

Anno Accademico 2018/2019



# Abstract

Radiotherapy is one of the most common treatments received nowadays for tumour control. Heavy particles use, compared to photons, is one of the most fast-growing techniques, as it grants great tumour control saving healthy tissues as well. The most used ions are protons and  $^{12}\text{C}$ . The former have an efficiency close to photons (they are usually considered only 10% more effective), whereas the latter are usually more effective and are recommended especially for radiation resistant tumours. Nevertheless, proton facilities and treatments cost far less than carbon ones, therefore many *radiotherapy enhancements* have been theorized and analyzed over the last decades in order to improve the quality of cheaper techniques to obtain results similar to expensive ones. In this thesis work, an innovative technique for protontherapy enhancement, called Proton Boron Capture Therapy (PBCT), will be briefly discussed and studied. The idea is to exploit a nuclear reaction involving  $^{11}\text{B}$  that produces three high LET alpha particles that could enhance protons lethality: if a boron-containing drug is located close to tumour cells, the occurrence of this reaction should permit effective treatment also of radiation resistant tumours. Moreover the shape of the cross section as a function of incoming proton energy, should grant an enhancement only in the tumour region while saving healthy tissues. The biological effectiveness of this technique has already been published [1].

In this work both an *experimental* approach (using techniques such as clonogenic assay) and a *modelling* approach (using mainly TALYS and Geant4 toolkits) are discussed. Moreover, a semi-analytical study permitted to understand whether the exploited reaction was responsible for the enhancement of biological effectiveness or not.

The results of this thesis suggest that alpha particles creation, due to  $p + ^{11}\text{B}$ , cannot explain the experimental increase of radiation lethality. Nevertheless, some of the tools obtained can still be used for future studies of this technique. In chapter 1 a brief introduction on radiotherapy will be given, together with some information about protontherapy and radiotherapy enhancement; in chapter 2 experimental facilities and methods will be presented; in chapter 3 some experimental results will be described and discussed; in chapter 4 the computational methods which have been used will be described and in chapter 5 the software that have been written will be described and discussed, as well as with the results obtained from simulations. In chapter 6 a conclusion to this thesis work will be given, and in Appendix A a description of some libraries (ParticleHP) used in this thesis can be found.

---

# Abstract

La radioterapia ad oggi é uno dei trattamenti piú usati per la cura dei tumori, e l'uso degli adroni é una delle tecniche che si stanno sviluppando piú velocemente, in contrasto alla radioterapia tradizionale che fa uso di fotoni. Rispetto a questi ultimi, le particelle dotate di massa permettono di distruggere il tumore senza danneggiare eccessivamente i tessuti sani adiacenti. Gli ioni piú usati per questo genere di terapia sono i protoni e il  $^{12}\text{C}$ . I protoni hanno un'efficienza molto simile a quella dei fotoni (solitamente si considerano essere soltanto il 10% piú efficaci), mentre gli ioni carbonio sono piú efficaci e raccomandati soprattutto per i tumori radioresistenti. Nonostante questo, gran parte delle strutture adroterapiche equipaggiano solamente protonterapia dato che gli strumenti costano molto meno di quelli di carbonterapia, quindi sono state teorizzate e studiate parecchie tecniche di *potenziamento della radioterapia* negli ultimi decenni per poter ottenere con metodi relativamente economici lo stesso effetto che si ottiene con i piú cari. In questo lavoro di tesi si discute e si studia brevemente una tecnica innovativa chiamata *terapia di cattura protonica del boro* (PBCT). L'idea é quella di sfruttare una reazione nucleare: se é presente del  $^{11}\text{B}$  in prossimità del tumore, un protone del fascio terapeutico potrebbe interagire con tale nucleo e andare a produrre tre particelle alpha dall'alto LET, che migliorerebbero l'efficacia del trattamento stesso. La forma della sezione d'urto al variare dell'energia del protone, inoltre, aiuterebbe a potenziare la letalità del fascio solamente in prossimità del tumore, senza rovinare i tessuti sani. L'efficacia biologica di questa tecnica é già stata pubblicata [1].

In questo lavoro di tesi si discute un approccio *sperimentale* (con tecniche quali lo studio clonogenico) e un approccio *modellistico* (usando principalmente TALYS e Geant4). Inoltre, uno studio semi-analitico ha permesso di capire se la reazione sfruttata fosse la reale responsabile dell'aumento dell'efficacia biologica misurata sperimentalmente.

I risultati di questa tesi suggeriscono che la creazione di particelle alpha dovute alla reazione  $p+^{11}\text{B}$  non é in grado di spiegare l'aumento sperimentale della letalità dei protoni, ma alcuni degli strumenti discussi in questa tesi potrebbero, un domani, venire usati per uno studio piú esaustivo di questa tecnica. Nel capitolo 1 si farà una piccola introduzione sulla radioterapia, discutendo anche l'adronterapia, la protonterapia e il potenziamento della radioterapia; nel capitolo 2 si presenteranno le sedi sperimentali e i metodi sperimentali usati; nel capitolo 3 si descriveranno e discuteranno alcuni risultati sperimentali; nel capitolo 4 si tratterà dei metodi computazionali usati e nel capitolo 5 si descriveranno i programmi scritti e i risultati ottenuti. Nel capitolo 6 si troverà una conclusione a questo lavoro e nell'Appendice A una descrizione di alcune librerie (ParticleHP) utilizzate in questa tesi.



# Contents

<b>1</b>	<b>Introduction</b>	<b>7</b>
1.1	Radiotherapy . . . . .	7
1.2	Cells killing through ionizing radiation . . . . .	8
1.3	Medical physics quantities . . . . .	9
1.4	Hadrontherapy advantages . . . . .	10
1.4.1	Dose-depth curve and ballistic advantages . . . . .	11
1.4.2	Higher LET and OER . . . . .	11
1.4.3	Cost of the treatment . . . . .	13
1.5	Protontherapy and carbontherapy . . . . .	14
1.5.1	Facility and ballistics . . . . .	14
1.5.2	LET, RBE and OER . . . . .	15
1.6	Radiotherapy enhancement . . . . .	16
1.6.1	Radiosensitizing drugs . . . . .	16
1.6.2	Use of Nanoparticles . . . . .	17
1.6.3	Induced nuclear reactions: the case of Boron Neutron Capture Therapy (BNCT) . . . . .	17
1.6.4	The Proton Boron Capture Therapy . . . . .	19
1.7	Physical quantities . . . . .	21
1.7.1	Cross section . . . . .	21
1.7.2	Production Cross section . . . . .	21
1.7.3	Multiple processes . . . . .	22
<b>2</b>	<b>Experimental Methods</b>	<b>23</b>
2.1	Experimental facilities . . . . .	23
2.1.1	Laboratori Nazionali del Sud - CATANA . . . . .	23
2.1.2	CNAO . . . . .	26
2.2	Clonogenic assay . . . . .	26
2.3	Chromosome aberrations with FISH approach . . . . .	27
2.4	CR39 detector . . . . .	30
<b>3</b>	<b>Experimental campaign</b>	<b>31</b>
3.1	First experimental proof . . . . .	31
3.2	Radiobiology at CNAO . . . . .	35
3.3	CR39 analysis . . . . .	35
3.4	Present and future perspectives: NEPTUNE . . . . .	37
<b>4</b>	<b>Computational Methods</b>	<b>39</b>
4.1	Monte Carlo methods . . . . .	39
4.2	Geant4 . . . . .	40
4.2.1	Geometry . . . . .	40
4.2.2	Physics models . . . . .	41
4.2.3	Primary generators . . . . .	42
4.2.4	Simulation outputs . . . . .	43
4.3	ROOT . . . . .	43

4.4	TALYS . . . . .	44
4.5	Hadrontherapy . . . . .	45
4.5.1	Geomtery . . . . .	45
4.5.2	Primary Generator . . . . .	46
4.5.3	Physics . . . . .	46
4.6	Hadr03 . . . . .	47
4.6.1	Geometry . . . . .	48
4.6.2	Primary generator . . . . .	48
4.6.3	Physics . . . . .	48
4.6.4	Output . . . . .	48
<b>5</b>	<b>Computational results</b>	<b>51</b>
5.1	EXFOR . . . . .	51
5.2	The $^8\text{Be}$ problem . . . . .	52
5.3	TALYS application . . . . .	52
5.4	Energy span . . . . .	54
5.4.1	Cross section uncertainty . . . . .	54
5.4.2	Process cross section . . . . .	54
5.4.3	Fixed energy . . . . .	55
5.4.4	Different cross sections . . . . .	56
5.5	Hadrontherapy with CR39 . . . . .	56
5.6	TALYS results . . . . .	57
5.6.1	Alpha production cross section . . . . .	57
5.6.2	Alpha spectrum . . . . .	60
5.6.3	Other particles . . . . .	61
5.6.4	Future perspectives . . . . .	62
5.7	Cross section . . . . .	62
5.8	Physicslists study . . . . .	63
5.8.1	Energy span validation . . . . .	63
5.8.2	Physicslists in Geant4 . . . . .	64
5.8.3	ParticleHP . . . . .	67
5.8.4	Future perspectives . . . . .	69
5.9	Semi-analytical analysis . . . . .	70
5.10	CR39 simulation . . . . .	77
<b>6</b>	<b>Conclusions</b>	<b>79</b>
<b>A</b>	<b>TENDL libraries</b>	<b>81</b>
A.1	CrossSections . . . . .	81
A.2	F files . . . . .	82
A.3	F files structure . . . . .	85
A.3.1	dataType3: cross section . . . . .	85
A.3.2	dataType6: energy and angular correlation . . . . .	86
A.4	Modification to the ParticleHP . . . . .	88





# Chapter 1

## Introduction

Tumours treatment is one of the most studied subject in modern medicine. When a patient develops cancer, different kinds of treatment are used to try and remove it in the best possible way. Main treatments include [2] *physical removal*, where the main part of the tumour is removed through surgery, *chemotherapy*, where drugs are used to weaken the tumour and block its spreading, *immunotherapy* where an immune response is enhanced or suppressed, *hormone therapy* where drugs are used to inhibit activity of hormones that influence tumour growth, *genetic treatment* where some genes are taken inside cancer cells through a vector and *radiotherapy*, where ionizing radiations are used to try and destroy the tumour tissue.

Approximately 50% of all cancer patients receive radiation therapy during their course of illness [3]. In this work enhancing of a particular kind of radiotherapy named *protontherapy*, that is the most common type of *hadrontherapy*, will be studied.

### 1.1. Radiotherapy

Radiotherapy is a treatment exploiting the ionizing radiations damage induced to human cells. After the discovery of radiation and its study, in the 20<sup>th</sup> century it was discovered that some kinds of radiation can interact with human body, being helpful or dangerous.

Ionizing radiation is radiation with enough energy so that during an interaction with an atom, it can remove tightly bound electrons from the orbit of an atom, causing the atom to become charged or ionized [4]. This radiation, ionizing biological tissues, can lead to damaging of the tissue itself, and depending on which structures are harmed the damage may be fixed by the organism or lead to cell death. Radiotherapy exploits ability of ionizing radiation to kill a tumour: in fact on one hand cells burning may lead to cancer onset (and this is important for radioprotection), on the other hand radiation could be used in a smart way to kill some cells, like cancerous ones.

Today there are two different kinds of radiotherapy: the *conventional radiotherapy* where photons or electrons are used to burn tumoural tissue and *hadrontherapy* where hadrons (like protons, neutrons and heavier ions), are considered.

Whether tumour can be vanquished by radiotherapy or not depends on several variants, of which some of the most studied are [5]:

- Tumour burden: the number of cancer cells is restrictive when treating tumours because the bigger the tumour is the harder it is to vanquish all tumoural cells and heal the disease.

- 
- Tumour microenvironment/hypoxia: a peculiar microenvironment is created when a tumour is nearby, in particular tissue hypoxia (absence of oxygen) as a consequence of structurally and functionally disturbed microcirculation and the deterioration of diffusion conditions has been found from many experimental data [6]. This changes effectiveness of radiotherapy, as will be discussed later.
  - Inherent or acquired treatment resistance: some tumours are more radio-resistant than others, and even the same kind of tumour can behave differently on different patients. This resistance can emerge due to a variety of reasons including host environmental factors as well as genetic or epigenetic alterations in the cancer cells [7].
  - Repopulations during the treatment: radiotherapy is often fractionated and therefore repopulation can play a role in treatment failure [8].

All these issues are indubitably correlated to *medicine* and *biology*, and a concurrent physical approach, like the one discussed in this work, can surely increase the effectiveness of radiotherapy.

## 1.2. Cells killing through ionizing radiation

Ionizing radiation can kill cells in different ways, depending on the *structure* being damaged by radiation and on the *way* damage is done to the structure itself.

When radiation passes through cells, it can deposit energy, mainly through *ionization*. Considering for example classical radiotherapy, involving photons, processes that lead to energy loss are:

- **Photoelectric effect:** this effect happens when the photon interacts with an electron of the matter, usually in one of the internal shells. After a photoelectric interaction the photon ceases its existence and an electron is created (together with its corresponding ion) and accelerated. Usually also secondary low energy photons due to electronic rearrangement of the ion are produced.
- **Compton scattering:** this is a scattering between the photon and a quasi-free electron of the matter. After the scattering the electron is accelerated and the photon changes its quadrimomentum.
- **Pair production:** in this type of interaction the photon, under the high electric fields created by nuclei, creates a pair of charged leptons, in particular an electron and a positron that have each half the energy of the photon and have back-to-back direction in the center of mass frame.

The cross section of these different effects strongly depends on the energy of the photon and the nature of the material. Looking at possible effects, when matter is targeted by photons energy is transferred mainly through interaction with electrons: the energy is given to electrons, bonds are broken and atoms are ionized.

Concerning heavy particles on the other hand, the energy deposit inside matter happens mainly through:

- **Electromagnetic interaction:** if the hadron is charged (like protons or ions), it can lose part of its energy through effects like *Coulomb scattering*, *Bremsstrahlung radiation* and other electromagnetic interactions. This plethora of effects can lead to production of photons and electrons of different energy and ionize atoms in the matter.
- **Hadronic interaction:** hadronic interaction happens when the hadron collides with another hadron inside the matter (mostly inside a nucleus). It can be *elastic* when there is only an energy tradeoff (that can lead also to production of some excited states that decay through particles

---

emission) or *inelastic* if there is an exchange of nucleons between the hadrons that lead to the production of new nuclei that can travel or decay emitting particles.

Ionizing radiation can harm a cell in two different ways: damage is *direct* when a cell structure is directly ionized (and therefore damaged) by radiation itself, while it is *indirect* when the cell structure is not damaged by radiation itself but by something that has been produced by radiation. The damage may be caused for example by produced electrons or produced free radicals.

Not all damage dealt to cells is lethal. Modern biology, in fact, guarantees that a cell can fix most of the damage that is dealt to it. Lethal damage is mainly the one dealt to the most vulnerable part of the cell: the DNA inside the nucleus (also some damages to mitochondria have been proven to be lethal, but death due to DNA damage is far more common). Damage due to ionizing radiation can lead to single strand breaks (*SSB*) when the DNA helix breaks in one point, i.e. only one strand of the chain breaks; and double strand breaks (*DSB*) when the DNA helix breaks in two points, i.e. both strands of the chain break. Cells have an innate ability to repair damage, and can fix most of damage to DNA as well. But if damage is dealt in a massive way, for example if there is one or more DSB, the cell goes through mitotic failure and can therefore be considered dead.

This is a key-concept when talking about radiotherapy: the best way to kill a cell is to release a *large* amount of energy in *close* spots of the *DNA*.

### 1.3. Medical physics quantities

In order to describe and compare the different types of radiotherapy, some quantities will be introduced here.

- **Dose:** it is the most common quantity when talking about energy exchange, not only through radiation. It is defined as the ratio between energy deposited in the target and its mass. Its standard unit of measure is the *gray* (Gy), equivalent to one joule per kilogram of matter. It is used as a quantity to describe deposited energy in the given target.
- **Equivalent Dose:** it is a quantity connected to radioprotection, defined as the dose multiplied by a factor accounting for radiation periculosity. Heavier ions have a multiplication factor of 20 whereas photons have a multiplication factor of 1, and so on. It is measured in *Sievert* (Sv), and has been introduced because biological effect strongly depends on particle nature.
- **Effective dose:** another quantity connected to radioprotection, in particular interaction between ionizing radiation and human bodies: it can be obtained multiplying the equivalent dose by a factor accounting for the vulnerability of the organ the radiation hits; a multiplicative factor of 0.12 must be taken into account for lungs whereas skin has a multiplicative factor of 0.01 and so on for every organ. It is measured, like equivalent dose, in *Sievert* (Sv).
- **Linear Energy Transfer:** also known as *LET*. It is the linear density for energy deposited by a charged particle along its trajectory when only contribution below a given energy threshold  $\Delta$  is considered, i.e. the ratio between local deposited energy  $dE$  in an infinitesimal segment  $dl$  and the segment itself. When  $\Delta$  is taken equal to infinity all energy trade contributions are considered and the LET becomes the *stopping power*. It is a quantity used in micro and nano dosimetry and is usually measured in  $\text{keV}\mu\text{m}^{-1}$  or in  $\text{MeVcm}^{-1}$ .
- **Relative Biological Effectiveness:** also known as *RBE*, it is a radiobiological quantity. When using cells, the same effect can be achieved using different doses for different type of radiation. The RBE is the ratio between the dose needed to achieve a given effect with the reference radiation (photons) and the dose needed to achieve exactly the same effect using another kind

of radiation. Usually RBE is calculated considering a given fraction of survival in clonogenic experiments: for example  $RBE_{10}$  for protons is the ratio between dose needed to reach 10% survival using photons and 10% survival using protons. RBE calculation is quite complicated and depends not only on the type of radiation and its energy (and therefore its LET), but may depend also on the kind of cells and the dose rate.

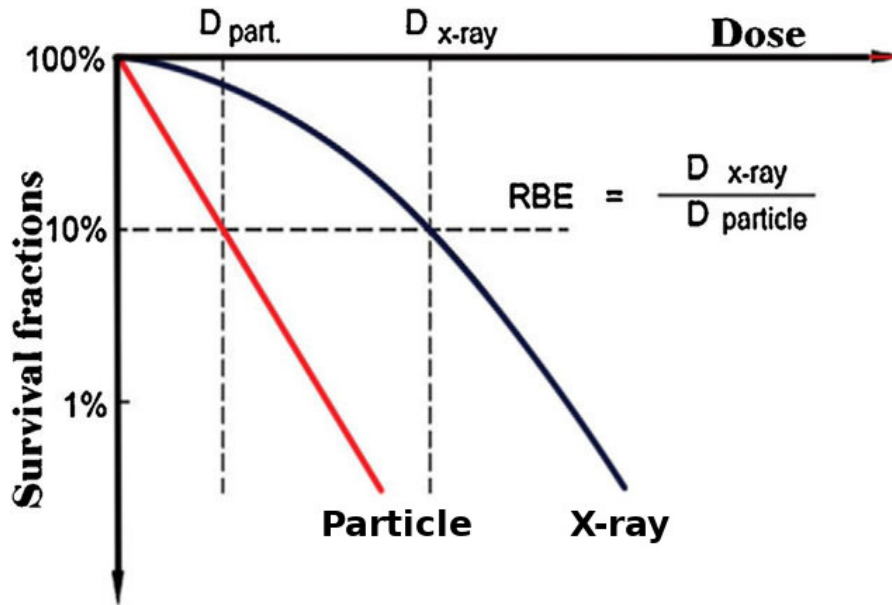


**Figure 1.1:** Example of RBE estimation for a given particle therapy. In this case, with particles the same effect (survival of 10%) is reached with less dose when compared to photons, particles have therefore a higher RBE and are more effective [9].

- **Dose Modifying Factor:** also known as *DMF* it is like the RBE but is used to compare same kind of radiation in different environments (for example when a radiosensitizer is used or not).
- **Oxygen Enhancement Ratio:** also known as *OER* it is the ratio between dose needed to achieve a given result in a hypoxic region and the dose needed to achieve the same result in an oxygenated region.
- **Therapeutic index:** it is defined as the ratio of treatment efficiency to side effect. It is important because killing the tumour is not the only purpose of clinical radiotherapy: although increasing radiation lethality improves the probability to vanquish cancer in the patient, the ballistic precision of radiation is crucial; damage should be dealt to cancer cells only, saving healthy tissues. This index is the one meant to be improved when a *better* type of radiotherapy is used.

## 1.4. Hadrontherapy advantages

Although most of cancer treatments through radiotherapy are done with conventional radiotherapy, hadrontherapy has started to be considered useful because of its numerous advantages, and the number of patients treated with particles is strongly rising in the last decades. Here the most important advantages will be shortly listed together with some drawbacks.

In this section charged particle hadrontherapy will be considered<sup>1</sup>, as the main topic of this work is the discussion of enhancement of proton therapy.

<sup>1</sup>A small parentheses regarding BNCT will be discussed later

The comparison here is meant to be done considering *similar doses*: as dose measures the ratio between energy and mass, a higher dose will translate in a higher energy deposited in the tissue and higher probability to damage cells.

### 1.4.1 Dose-depth curve and ballistic advantages

Interaction of charged hadrons with matter is far different from interaction of photons with matter, as already described in Section 1.2, hence producing different depth dose curves. While photons show a dose deposited exponential decrease after an initial maximum, hadrons present a narrow peak, known as *Bragg peak*, at the end of their path after which the dose rapidly decreases to zero. This is considered one of the most important advantages of hadrontherapy over conventional radiotherapy because of the *precision* of the treatment: if the spot where damage is delivered by the beam is less spread, then it is easier to damage the tumour while saving healthy tissues, and this way improve the therapeutic capacity. This is the main reason why hadron therapy is often suggested when treating with tumours in vulnerable zones like the head or the neck.

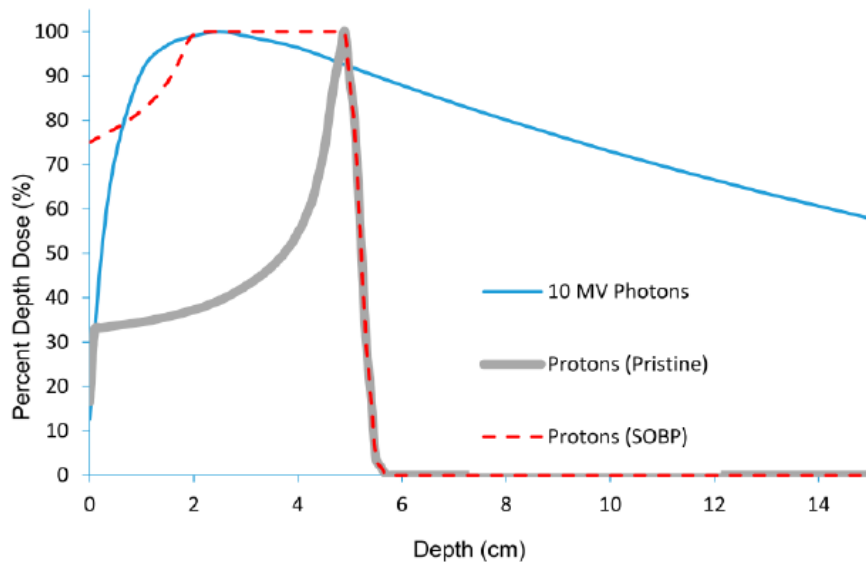


**Figure 1.2:** Comparison between dose-depth curves of photons and protons. Also a *Spread Out Bragg Peak* is exhibited (see text for more details) [10].

In Figure 1.2 the depth-dose curve for photons and hadrons is plotted, together with the *Spread Out Bragg Peak* (SOBP). The SOBP represents the dose distribution curve used for a clinical cancer treatment: it is obtained from many superimposed monoenergetic Bragg peaks of different energy and used to homogeneously cover the whole tumour region.

Moreover, charged hadrons are in general *easier* to control than photons: they can be deflected, accelerated and decelerated using electromagnetic fields and their range is shorter and therefore need thinner stoppers when compared to photons.

### 1.4.2 Higher LET and OER

In Section 1.4.2 it was highlighted how to kill cells damage should be as close as possible, in order to destroy in an unfixable way DNA strands. Heavy particles, when compared to photons, tend to release more energy in closer spots, provoking more DSBs that are also closer. In Figure 1.3 a representation shows how heavier particles lead to greater number of DSBs.

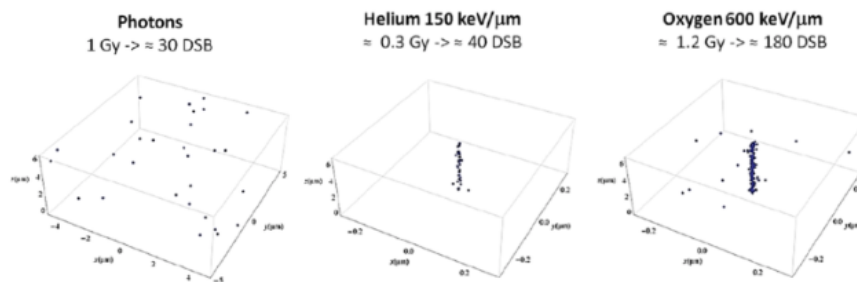


**Figure 1.3:** Different damage location of radiations with different LET. Heavier particles have higher LET and produce more localized damage and a higher number of DSBs.

This representation has been computed considering similar doses, i.e. considering similar energy released in matter. The idea of close damage is a key concept when talking about interaction between radiation and biological tissues, to clarify it, comparing three sample cases with increasing LET is useful:

- if dose is deposited through *infrared radiation*, its energy is going to increase thermal scattering in the tissue, but is not going to ionize atoms. Therefore the possibility to have either a SSB or DSB is very low.
- if dose is deposited through *gamma rays*, its energy is going to ionize atoms inside the tissue. But, as photons have a low LET, the ionization locations are unlikely to be close, and therefore the possibility to have DSBs is going to be low while a lot of SSB may be created.
- if dose is deposited through low energy *carbon ions*, its energy is going to ionize atoms inside the tissue. Considering that low energy carbon ions have a very high LET, they will not travel long and damage will be dealt in close spots, leading to an increased number of DSBs.

By the way a greater LET does not necessarily mean greater cell killing efficiency: in fact for really high values of LET a saturation is achieved and energy dealt to cells becomes of no use, as can be seen from figure 1.4.

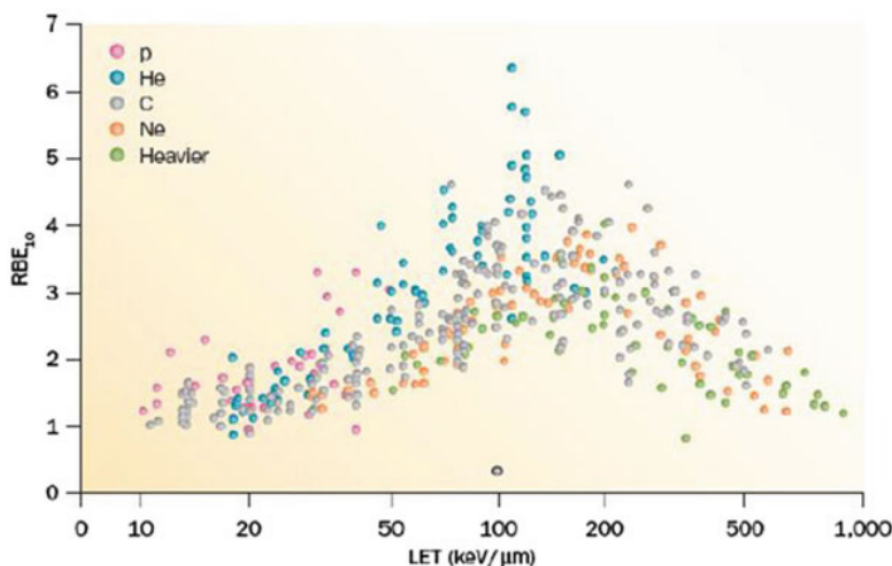


**Figure 1.4:** RBE versus LET from published experiments on *in vitro* cell lines. RBE is calculated at 10% survival; LET values are given as keV/μm in water. The different colours indicate different ions, from protons to heavy ions. Data points are extracted from the Particle Radiation Data Ensemble (PIDE) database ([www.gsi.de/bio-pide](http://www.gsi.de/bio-pide)) [2].

Another problem in treating tumours using radiotherapy is the higher radioresistance of cancerous

cells due to hypoxia. The OER has been found decreasing for increasing LET, therefore high LET particles can more efficiently treat tumours. Some models to calculate OER and its variance with LET exist, like explained in [11].

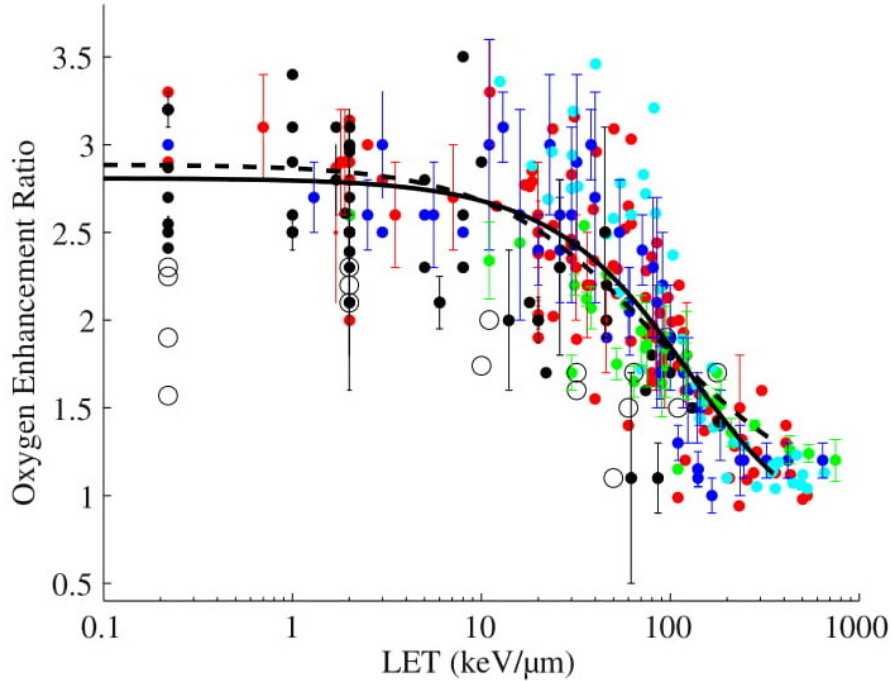


**Figure 1.5:** Taken from [11]: experimental data in literature for LET depending OER in vitro (filled circles) and in vivo (open circles) at 10% cell survival. Different colours correspond to different cell lines. Solid and dashed line indicate two different models.

### 1.4.3 Cost of the treatment

Hadrontherapy is not so spread, even though it has these advantages, because of its intrinsic *cost*: many studies and Markov simulations have been done to calculate cost and cost-to-efficiency ratio, and they do not all agree in their conclusions.

Here a comparison for capital price and price of different treatments and fractionings taken from [12] is used and Figure 1.6 is reported. Clearly conventional radiotherapy is economically advantageous, and this is the main reason why nowadays most cancers are treated using this technique.

	Particle facility			Photon facility	
	Combined carbon-ion and proton	Ratio to photon	Proton-only	Ratio to photon	
<b>Capital costs</b>					
Base case scenario	€ 138,600,000		€ 94,930,000		€ 23,430,000
Optimistic scenario (-20%)	€ 110,880,000		€ 75,944,000		€ 18,744,000
Pessimistic scenario (+20%)	€ 166,320,000		€ 113,916,000		€ 28,116,000
	Cost per fraction		Cost per fraction		Cost per fraction
Base case scenario	€ 1128	4.8	€ 743	3.2	€ 233
Optimistic scenario (-20%)	€ 1100	4.8	€ 724	3.2	€ 229
Pessimistic scenario (+20%)	€ 1156	4.9	€ 762	3.2	€ 237
<b>Operational costs</b>					
Base case scenario	€ 32,138,027		€ 21,800,383		€ 8,800,850
Optimistic scenario (-20%)	€ 25,710,421		€ 17,440,306		€ 7,040,680
Pessimistic scenario (+20%)	€ 38,565,632		€ 26,160,459		€ 10,561,020
	Cost per fraction		Cost per fraction		Cost per fraction
Base case scenario	€ 1128	4.8	€ 743	3.2	€ 233
Optimistic scenario (-20%)	€ 931	4.9	€ 613	3.2	€ 190
Pessimistic scenario (+20%)	€ 1325	4.8	€ 872	3.2	€ 276
<b>Lifecycle of a facility</b>					
	Cost per fraction		Cost per fraction		Cost per fraction
Base case: 30 years	€ 1128	4.8	€ 743	3.2	€ 233
5 years	€ 1837	5.6	€ 1213	3.7	€ 328
40 years	€ 1093	4.8	€ 719	3.2	€ 228
<b>No. of patients per year<sup>a</sup></b>					
Base case scenario	1810		1681		2287
Optimistic scenario (+20%)	2172		2017		2744
Pessimistic scenario (-20%)	1448		1345		1829
Pessimistic scenario (-30%)	1267		1176		1601
Pessimistic scenario (-50%)	905		840		1143
	Cost per fraction		Cost per fraction		Cost per fraction
Base case scenario	€ 1128	4.8	€ 743	3.2	€ 233
Optimistic scenario (+20%)	€ 940	4.8	€ 619	3.2	€ 194
Pessimistic scenario (-20%)	€ 1410	4.8	€ 928	3.2	€ 291
Pessimistic scenario (-30%)	€ 1612	4.8	€ 1061	3.2	€ 333
Pessimistic scenario (-50%)	€ 2256	4.8	€ 1485	3.2	€ 466
<b>Average time per fraction (particle)</b>					
	Cost per fraction		Cost per fraction		Cost per fraction
Base case: 18 min	€ 1128	4.8	€ 743	3.2	-
Optimistic scenario (-4 min)	€ 877	3.8	€ 578	2.5	-
Pessimistic scenario (+4 min)	€ 1379	5.9	€ 908	3.9	-
<b>Hours per day available</b>					
	Cost per fraction		Cost per fraction		Cost per fraction
Base case: 14 h/day	€ 1128	4.8	€ 743	3.2	€ 233
8 h/day	€ 1974	4.8	€ 1300	3.2	€ 407
16 h/day	€ 987	4.8	€ 650	3.2	€ 204
<b>Treatment room availability</b>					
	Cost per fraction		Cost per fraction		Cost per fraction
Base case: 95%, 98%, 98%	€ 1128	4.8	€ 743	3.2	€ 233
90% all facilities	€ 1191	4.7	€ 809	3.2	€ 253
<b>Treatment room utilization (particle)</b>					
	Cost per fraction		Cost per fraction		Cost per fraction
Base case: 98%	€ 1128	4.8	€ 743	3.2	-
90%	€ 1228	5.3	€ 809	3.5	-
<b>Energy costs</b>					
	Cost per fraction		Cost per fraction		Cost per fraction
Base case: 100 €/MWh/a	€ 1128	4.8	€ 743	3.2	€ 233
150 €/MWh/a	€ 1147	4.9	€ 749	3.2	€ 236
200 €/MWh/a	€ 1165	4.9	€ 755	3.2	€ 238
<b>Interest payment</b>					
	Cost per fraction		Cost per fraction		Cost per fraction
Base case: 5% over 20 years	€ 1128	4.8	€ 743	3.2	€ 233
5% over 25 years	€ 1089	4.8	€ 715	3.1	€ 228
5% over 30 years	€ 1063	4.7	€ 700	3.1	€ 224
No interest payment	€ 787	4.2	€ 516	2.8	€ 187
<b>T4 category photon treatments only [20]</b>					
	Cost per fraction		Cost per fraction		Cost per fraction
Base case: standard treatment	€ 1128	4.8	€ 743	3.2	€ 233
Weight factor 1.5	-	3.2	-	2.1	€ 350
Weight factor 2.9	-	1.7	-	1.1	€ 676
Weight factor 5.0	-	1.0	-	0.6	€ 1165

<sup>a</sup> Assuming an average number of fractions per patient (specific for each facility).

**Figure 1.6:** Comparison between classical radiotherapy and hadrotherapy cost [12].

## 1.5. Protontherapy and carbontherapy

In this work so far we have focused on comparison between photon radiotherapy and hadrontherapy, highlighting the advantages of the latter in terms of capability to kill tumoural cells and increase therapeutic index. But not all the hadrons behave the same when they are used to treat cancers, and some hadrons have some advantages over others. Here we will compare the two most common hadrontherapy approaches: protontherapy and carbontherapy

### 1.5.1 Facility and ballistics

It was already shown in Section 1.4.3 how expensive it is to accelerate carbon ions when compared to protons. This is due to the weight of the particle itself: heavier particles are harder to accelerate to an energy suitable for patient treatments. Therefore, looking from an economic perspective, proton facilities are preferred to carbon facilities as they are cheaper to build and maintain.

Moreover, considering the mass gap, it is easier to deflect proton beams over carbon beams, and therefore structures needed for therapies (such as gantries) are smaller, cheaper and easier to develop and use.



Nevertheless, thanks to their higher mass, carbon lateral scattering is less important, and it is therefore easier to save healthy tissues using these heavy ions.

### 1.5.2 LET, RBE and OER

Carbon ions, being heavier, have on average a greater LET when compared to protons of the same energy. As it has already been discussed before, this means that the track structure is more suitable to deal lethal damage to cells. From an experimental point of view, this can be seen looking at the RBE of the different hadrons, whose calculation need to take into account a large number of variables [13]. Historically, due to the intrinsic difference between proton and carbon beams, a RBE between 1.1 and 1.2 is considered when using protons, while for carbon ions the value taken varies between 2 and 5.

This means that carbon is far *more efficient* than proton when using for treatment, i.e. a smaller dose is needed and therefore should be preferred. Moreover carbon LET increases along the SOBP: it is greater in its plateau than at the beam entrance in the body. This means that the therapeutic index is greater using carbon therapy.

On the other hand, the fact that RBE varies this much may lead to errors when discussing treatment plans: protons lower and rather still along the SOBP RBE makes treatments easier to plan while carbon treatment effectiveness might depend on the RBE curve chosen.

Concerning hypoxia, carbon ions behave better than protons, as their experimental OER is far lower than protons one and close to two [2]. This means that carbon is more suitable than proton when treating hypoxic tissue.

In Figure 1.7 the RBE and OER for different ion beams is presented, and carbon advantages can be seen. Therefore carbon should be preferred over protons for radiation-resistant and hypoxic tumours.

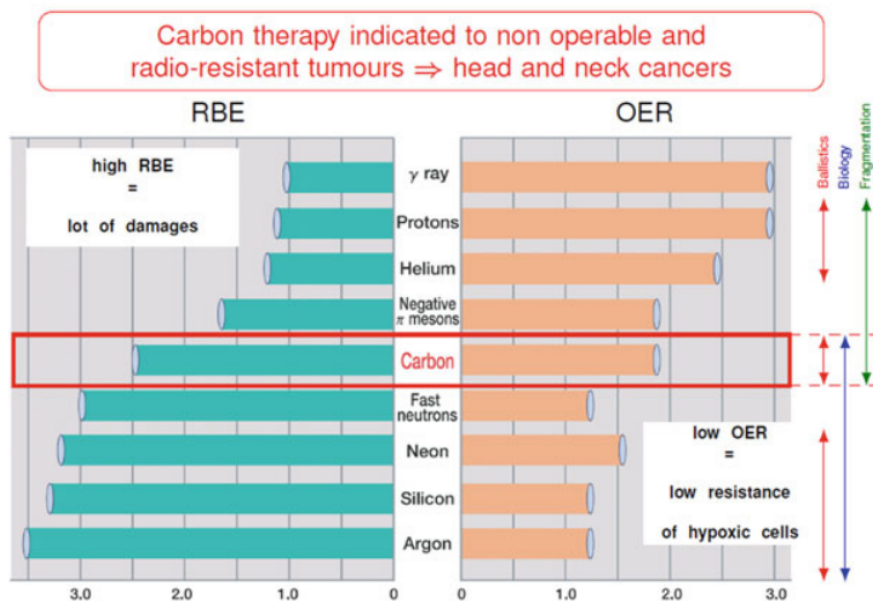


**Figure 1.7:** RBE and OER for different ion beams. Carbon is the ideal compromise to have a high LET and low OER beam with limited fragmentation problems [2].

Nevertheless both protons and carbon ions are considered valid treatments and are used nowadays according to single facilities disponibility.

## 1.6. Radiotherapy enhancement

This has been already discussed, carbontherapy is usually the best solution for radiotherapy, as it is able to treat successfully radio-resistant tumours. On the other side it is expansive and few centers exist around the world. From Figure 1.8 it is clear how in Europe most facilities use protontherapy, and only a few of them is equipped for dual ion (both proton and carbon therapy).

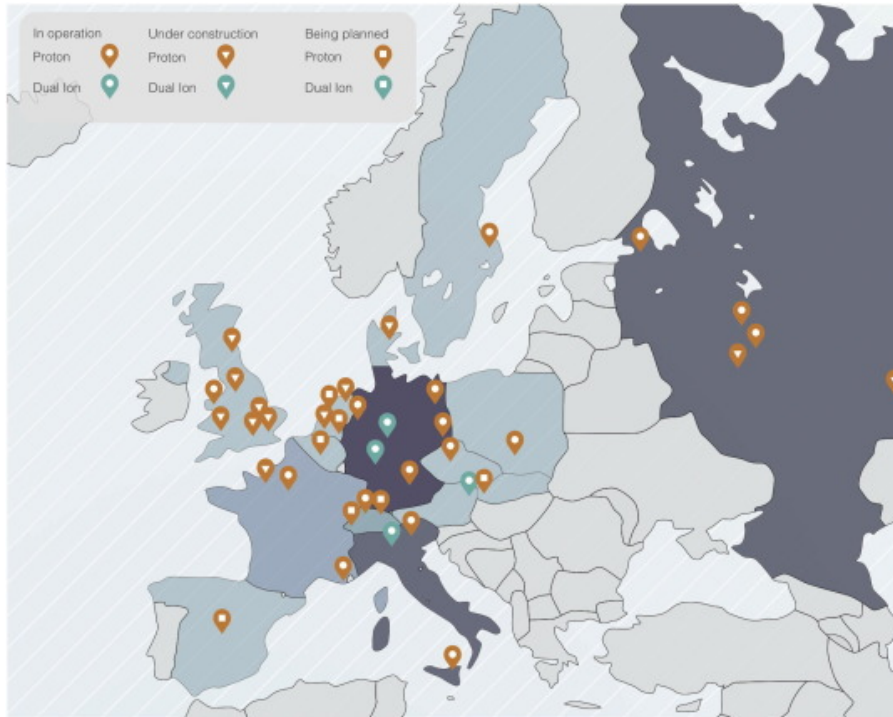


**Figure 1.8:** Map of working and planned hadrontherapy centers in Europe that will be working in 2021 [14].

Many *radiotherapy enhancement techniques*, both enhancement of conventional radiotherapy and hadrontherapy have been proposed over the years to solve this issue. Among these the most investigated exploit nanoparticles, drugs with radiosensitizers and induced nuclear reactions. In these therapies a drug, located in the tumoural zone, is used to enhance ionizing particles effectiveness.

Here a brief presentation of some famous radiotherapy enhancement will be presented. We will then focus the attention on the use of *Proton Boron Capture Therapy* (PBCT), that will be studied deeper in this work.

### 1.6.1 Radiosensitizing drugs

The effect of ionizing radiation on biological tissue strongly depends on the substances present inside the tissue itself. This has already discussed, for example, when the effect of *hypoxia* was studied: if oxygen concentration is below the usual ratio, the tumoural cells are more likely to survive to radiotherapy. Then, some drugs containing substances that enhance radiation effect might be used to improve therapeutic index [15].

---

An example of this is the use of *nitric oxide*: the introduction of an oxygen containing molecule inside the tissue might solve the problem of radioresistance due to hypoxia.

A different approach is the introduction of molecules that interact with proteins that usually fix DNA damage: if those proteins can be blocked, radiation effectiveness can be enhanced and tumour can be vanquished more easily.

G.E. Adams divided the radiosensitizers in five main categories [16,17]:

- suppression of intracellular-SH (thiols) or other endogenous radioprotective substances;
- radiation-induced formation of cytotoxic substances from the radiolysis of the sensitizer;
- inhibitors of post-irradiation cellular repair processes;
- sensitization by structural incorporation of thymine analogues into intracellular DNA;
- oxygen-mimetic sensitizers, for example the electron affinic drugs.

Out of these only the second refers to use of physical reactions or effects, whereas the other are studied more from a biological and chemical point of view.

## 1.6.2 Use of Nanoparticles

Another way to enhance radiotherapy is the use of *nanoparticles* [18]. Since 2004 good results have been reached using high-Z nanoparticles combined with classical radiotherapy, and tests have been done using fast ions as well, reaching an effective enhancement of biological efficiency. Gold nanoparticles have become particularly popular due to several advantages: biocompatibility, well-established methods for synthesis in a wide range of sizes, and the possibility of coating of their surface with a large number of different molecules to provide partial control of, for example, surface charge or interaction with serum proteins [19].

The idea behind the usage of nanoparticles is that those particles in combination with external radiotherapy (with both gamma and charged particles) significantly increase the secondary electron yield, compared to that of pure water, due to excitation of plasmons in the nano particle [19,20]: plasmons are excitations of delocalized electron in the material so the introduction of nanoparticles inside the tumours increase the generated free radicals and, consequently, the treatment lethality.

Nevertheless, some measurements about nanoparticles uptake [21] showed that there are no nanoparticles inside the cell nuclei, therefore this model needs to be revised (Figure 1.9).

Also some Geant4-DNA simulations [22], (discussed in [18]) reveal that physical effects play a minor role in the amplification of damage, as a very low dose enhancement or increase of dissociative electron attachment processes is observed. Thus, other effects, such as biological or chemical processes, may be mainly responsible for the enhanced radiosensibilization observed in biological experiments. However, more studies are needed to verify this hypothesis.

## 1.6.3 Induced nuclear reactions: the case of Boron Neutron Capture Therapy (BNCT)

So far we discussed hadrontherapy considering charged hadrons only, but a therapy using neutrons was proposed in 1936 and was firstly performed in a patient with a malignant glioma in 1951, using the

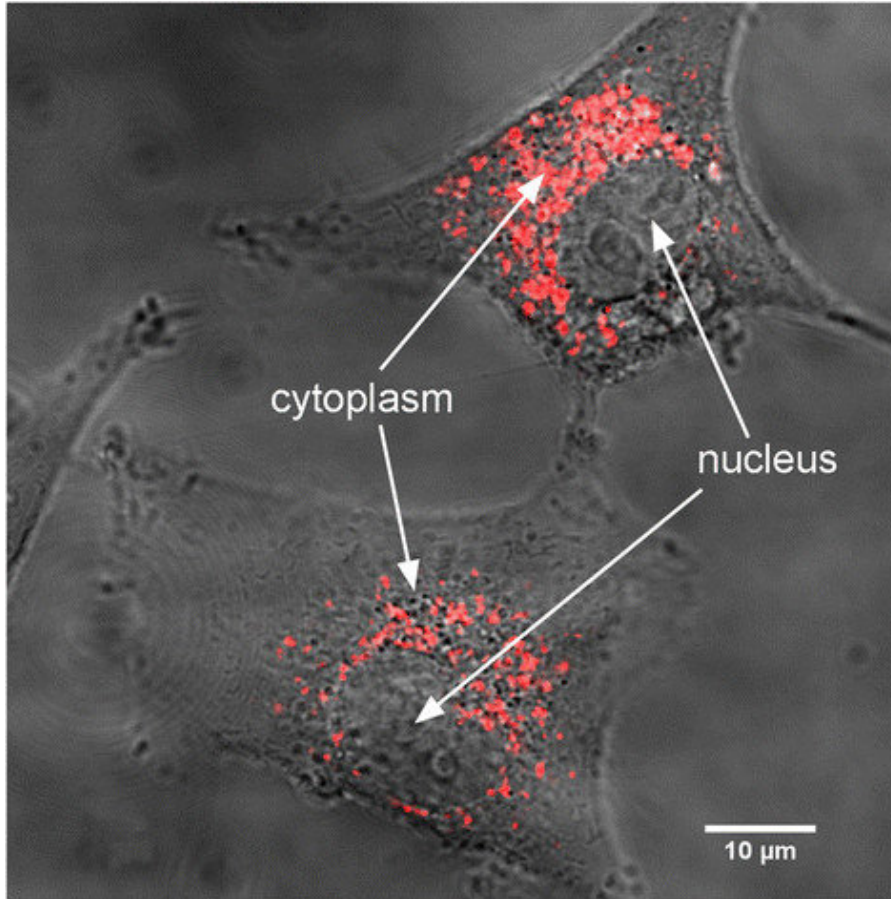


**Figure 1.9:** Merge image of the transmission and fluorescence images obtained by confocal microscopy of U87 cell loaded with GdBN-Cy5.5 (red) at a concentration of 0.6 mM incubated for 12 hours [21].

nuclear research reactor available at the Brookhaven Graphite Research Reactor. Hiroshi Hatanaka in 1968 re-instigated clinical application of BNCT in Japan using Borocaptate Sodium (BSH) by directly exposing the beam to surgically exposed intracranial tumour bed and reported with impressive results of achieving 58% of 5 year survival rate. Right now it is well developed and used in USA, Europe, Japan, Taiwan and Argentina [23].

In BNCT the occurrence of the following nuclear reaction is exploited:



Bringing to the production of low-energy lithium and helium nuclei.

The idea of BNCT is to insert a drug inside the tumour region containing boron (today the most used boron delivery agent is BSH  $\text{Na}_2\text{B}_{12}\text{H}_{11}\text{SH}$ ). If this molecule is uptaken by the cancerous cells, i.e. there is some boron inside cells, shooting neutrons reaction 1.1 can take place and heavy and high-LET particles that can lethal damage the cell are created. These particles travel less than the width of the cell itself before stopping.

The beam used for BNCT is made up of thermal neutrons (that have the highest cross section for boron capture), and if boron concentration is limited inside cancerous tissue, this therapy can strongly damage the tumour while limiting side-effects on healthy tissues.

The main limitations of BNCT are:

- neutron sources are hard to create and handle since they are not charged particles;

- deep-seated tumours can not receive a sufficient dose due to the limited depth of penetration of epithermal neutrons and, therefore, BNCT should be limited to more shallow tumours [24];
- boron *must* be located only in cancer tissue, or the treatment will burn healthy tissue and therapeutic index will be low.

### 1.6.4 The Proton Boron Capture Therapy

Proton Boron Capture Therapy (*PBCT*) is a new therapeutical approach firstly proposed first in [25]. It is similar to BNCT but wants to exploit the proton- $^{11}\text{B}$  reaction producing three alphas. The PBCT reaction is the following:



This reaction is referred to as *proton boron fusion* and it has already been studied for its applications in plasma fusion, as it has a relatively high cross section and is neutron-free. It has a Q-value of 8.7 MeV [1]. The breakup of the boron is not *prompt* in most of cases (as will be shown later in this work with TALYS analytical code [26]), but usually an unstable  $^{12}\text{C}$  is created thanks to a resonance at 675 keV [27]. This nucleus mostly decays  $\alpha$  emitting a first alpha particle, and then the  $^8\text{Be}$  decays  $\alpha$  as well, splitting in another pair of alpha particles.

When using protons with  $^{11}\text{B}$ , of course, also other reactions may occur. They will be discussed later in this thesis.

The experimental total cross section for p- $^{11}\text{B}$  reaction can be seen in Figure 1.10, EXFOR database [28].

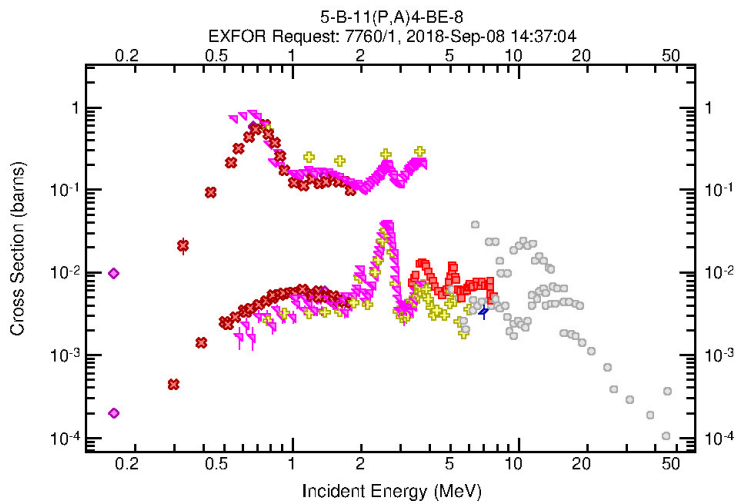


**Figure 1.10:** *Experimental data for the proton-boron fusion reaction (Equation 1.2). Data Taken from EXFOR database. Different colours correspond to different experimental campaigns.*

Here two curves can be seen: the one with higher cross section relates to the channel known as  $\alpha_0$ : after the carbon decay the  $^8\text{Be}$  is created in its fundamental state, while the latter relates to the  $\alpha_1$  channel, where the beryllium is created in one of its excited states. The upper curve in Figure 1.10 clearly shows a resonance pattern: cross section is peaked at proton energies about 675 keV where it reaches a maximum of 0.8 b. This could be a great advantage for the therapeutic use of this technique: if boron is located preferentially (but not exclusively) inside the tumour region, in fact, proton effect

would be enhanced where proton energy is low, i.e. inside the tumour, and a far lower enhancement should occur outside the SOBP, where healthy tissue is, improving therapeutic index.

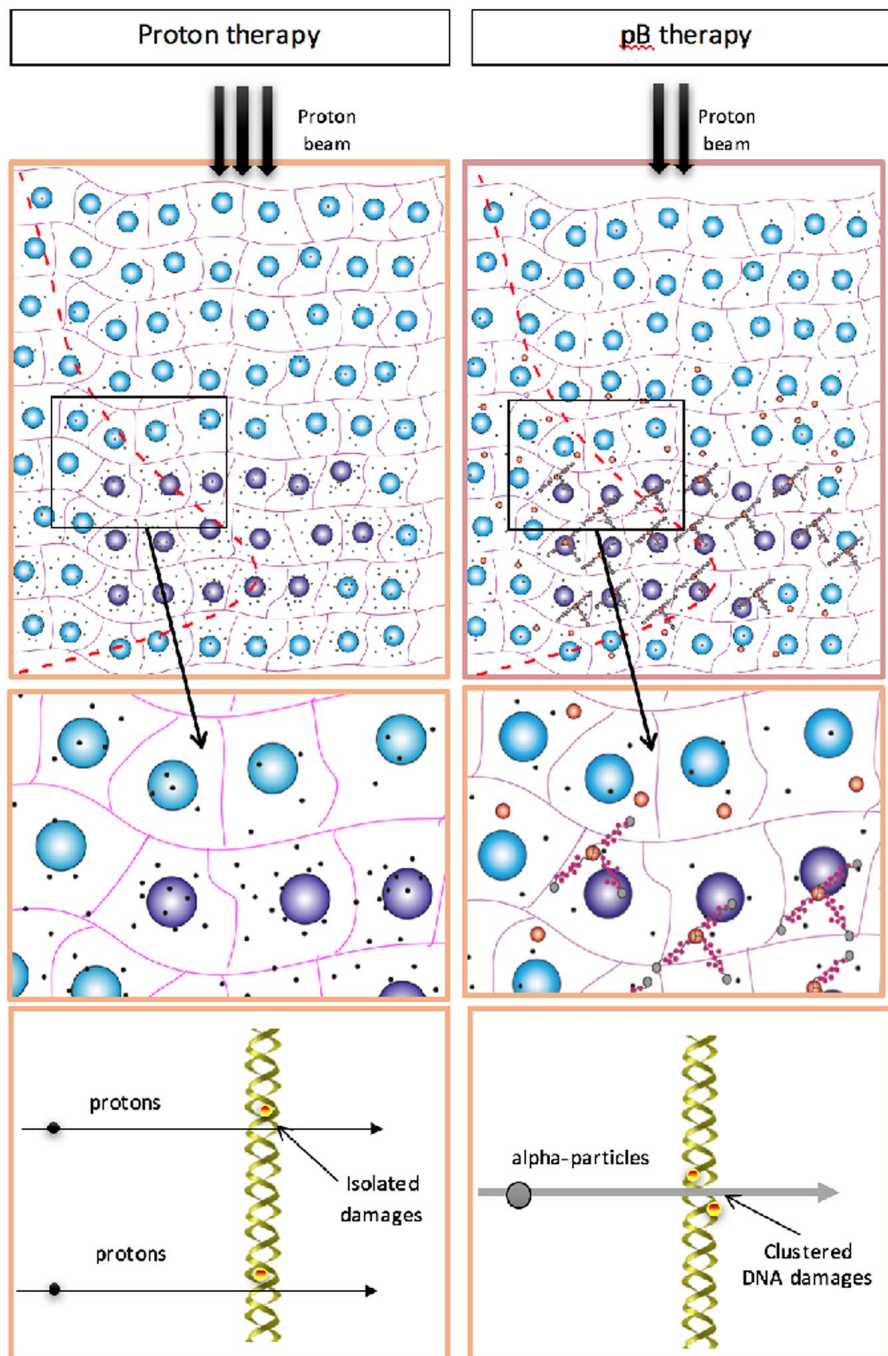


**Figure 1.11:** A schematic comparison between proton therapy and PBCT, If  $^{11}\text{B}$  is used localized damage is created only in the tumour region [1].

In Figure 1.11 [1] the idea of PBCT is schematically illustrated: boron is preferentially located in the tumour region that is treated using protons. When protons cross the tissue, some of them undergo reaction 1.2 and create three alpha particles. These alpha particles have a well known spectrum (depending on the channel) and a mean energy of 4 MeV and travel inside the tissue damaging cells. If the treatment is settled in order to maximize dose in the tumour region and minimize it outside (i.e. the plateau of the SOBP is where tumour is), the boron nuclei inside the tumour are the one more likely to react with the proton.

Some positive aspects of this approach when compared with other enhancement techniques are:

- a proton beam is easier to create and control than neutron beam.
- $^{11}\text{B}$  is the most common isotope of boron: the ratio between  $^{11}\text{B}$  and  $^{10}\text{B}$  is 0.8 to 0.2. This means that whereas for BNCT enriched boron needs to be used, in PBCT natural boron has an already good fraction of  $^{11}\text{B}$ ;
- the cross section of the PBCT reaction (Figure 1.10) has a higher cross section for low energies. This means that using a SOBP the effect due to boron presence would be not negligible only in the tumour region, and there would be less side-effect in presence of boron also outside the tumour;
- boron toxicity and delivery agents have already been studied for BNCT.

## 1.7. Physical quantities

Some physical quantities belonging mainly to nuclear physics will be used in this work, so here they will be briefly defined and described for their further use.

### 1.7.1 Cross section

Cross section ( $\sigma$ ) is a number describing *how likely* a given reaction may occur. Dimensionally it is a surface and usually in nuclear physics is measured in *barn* (b), where  $1\text{ b} = 1 \cdot 10^{-28}\text{ m}^2$ . Its calculation is important both in nuclear physics and subnuclear one and it is defined via the equation:

$$\frac{dN}{N} = -n_x \Delta x \sigma \quad (1.3)$$

where  $n_x$  is the numerical density of the target,  $\Delta x$  is the target thickness and  $\Delta N$  and  $N$  are, respectively, the number of particles of the beam that interacted and the total number of particles. This equation is defined for *thin* targets, i.e. when  $dN \ll N$ . The minus is because after the interaction there are less particles than before the interaction

It can be integrated to obtain a function for the number of particles in the beam after a width  $x$ :

$$N = N_0 e^{-n_x \sigma x} \quad (1.4)$$

Where  $N_0$  is the number of particles at  $x = 0$ . This equation is valid while  $x$  is still inside the target and can be used for thick targets as well.

### 1.7.2 Production Cross section

Let  $P_i$  be the set of processes a particle may undergo when reacting with another one, each with the cross section  $\sigma_i$ . Let  $p$  be one of the possible products for this reaction, i.e. a given particle. Every process will produce  $p$  with a multiplicity  $n_i$ , i.e. each process  $P_i$  will produce  $n_i$  particles  $p$ . Then, the production cross section for particle  $p$  will be defined as:

$$\sigma_p = \sum_i n_i \sigma_i \quad (1.5)$$

Note that this is not strictly a cross section as it can also be higher than the total cross section, but will describe the number of particles that might be created by given reagents, summing the contribution of all channels. It will be referred to as  $\sigma_p$  where  $p$  is the particle studied.

### 1.7.3 Multiple processes

Let us consider for example a set of  $n$  different processes  $P_i$ , for example hadronic processes. Let  $N_i(x)$  be the number of particles at depth  $x$  inside the target that will undergo the process  $P_i$ , and let  $N_{\text{tot}}(x)$  be the number of particles that have not interacted yet. Of course the following relation holds:

$$N_{\text{tot}}(x) = \sum_i N_i(x) \quad (1.6)$$

under the assumption that all processes are considered and that the detector is *big enough* for all particles to interact. Each process will follow Equation 1.3 with its own cross section and with total number of particles that have not yet interacted. In particular:

$$dN_i(x) = -N_{\text{tot}}(x)n_x\sigma_i dx \quad (1.7)$$

Defining now  $dN_{\text{tot}}$  as the difference between  $N_{\text{tot}}(x)$  after an infinitesimal width  $dx$ , it is going to be equal to  $\sum_i dN_i(x)$ . Then for all particles the relationship 1.3 holds with the cross section given by the sum of all different cross sections. Integrating that equation:

$$N_{\text{tot}}(x) = N_0 e^{-n_x(\sum_i \sigma_i)x} \quad (1.8)$$

Using this result in Equation 1.7:

$$dN_i(x) = -N_0 e^{-n_x(\sum_i \sigma_i)x} n_x \sigma_i dx$$

And, by integrating this last equation:

$$N_i(x) = \frac{\sigma_i}{\sum_i \sigma_i} N_{\text{tot}} + K_i$$

Where  $K_i$  is the integration constant. Considering now that the constraints are  $N_i(x \rightarrow \infty) = 0 \forall i$  and  $\sum_i N_i(0) = N_0$  these constants must be all equal to zero. Therefore the distribution of particles as a function of width when there are more processes possible but when only particles undergoing a given  $i$ -th process are considered is:

$$N_i(x) = \frac{\sigma_i}{\sum_i \sigma_i} N_{\text{tot}} \quad (1.9)$$



# Chapter 2

## Experimental Methods

The first experimental proof of PBCT was published by Cirrone *et al.* [1] and was the starting point for this thesis work. In this section, the experimental tools used to study PBCT will be briefly described.

### 2.1. Experimental facilities

Experiments on PBCT have been performed in two Italian facilities: Laboratori Nazionali del Sud (*LNS*) in Catania [29], and Centro Nazionale Adroterapia Oncologica (*CNAO*) in Pavia [30].

#### 2.1.1 Laboratori Nazionali del Sud - CATANA

Laboratori Nazionali del Sud (*LNS*) is one of the four national laboratories of *Istituto Nazionale di Fisica Nucleare* (*INFN*). It is equipped with a superconductive cyclotron able to accelerate ion beams from protons to uranium at energy levels up to 80 MeV/A. The pole has a 90-centimetre radius and the magnetic field inside can reach a value of 4.8 T. In order to achieve such intense magnetic field values, the superconducting cyclotron is equipped with two series of superconductive bobbins at Nb-Ti ( $\alpha$  and  $\beta$ ) immersed in liquid helium (LHe) at a working temperature of 4.2 K [31] [32].

Experiments have been performed at the *CATANA* (Centro di AdroTerapia ed Applicazioni Nucleari Avanzate) experimental room [29]: protontherapy facility equipped for ocular melanoma treatment [33] [34] [35].

A 62 MeV proton beam exits in air, through a 50  $\mu\text{m}$  kapton window placed at about 2.8 m from the isocenter. Just before the exit point in air there is a first *scattering foil* (Ta foil with 15  $\mu\text{m}$  in thickness). It constitutes the first element to increase the angular beam spread. After the first foil, the beam exits in air throughout a 50  $\mu\text{m}$  kapton windows where a 25  $\mu\text{m}$  foil of tantalum with a brass stopper of 4 mm in diameter is positioned. This scattering system (the two foils plus the brass stopper), is needed to obtain an optimal homogeneity of the final proton beam in terms of lateral dose distribution while minimizing energy loss. In Figure 2.1 there is a scheme showing how to obtain a flat field with a series of scatterers and a collimator. In Figure 2.2, on the left, the uniform beam profile is plotted together with a simulation, and on the right a photo of the brass stopper.

After the scattering system, a box hosts the *modulator* and *range shifter*. Modulator is a passive plastic wheel that, rotating, degrades the beam energy to obtain a SOBP; range shifter is a plastic block with a variable thickness that degrades the incident proton beam energy.

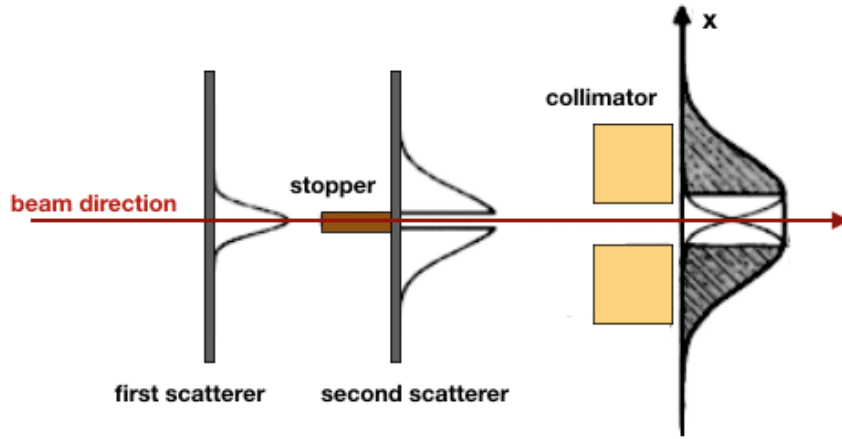


**Figure 2.1:** A scheme exhibiting the usage of multiple scattering foils and a collimator to obtain a uniform field suitable for patients treatment.

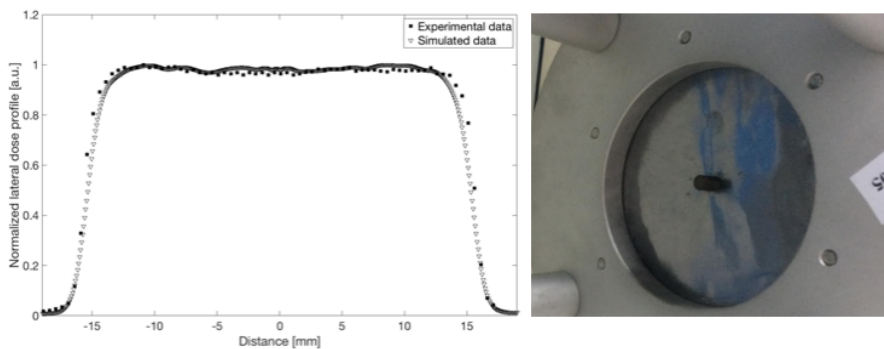


**Figure 2.2:** On the left, the measured CATANA beam profile at the isocenter with the simulated profile computed using hadrontherapy (see Section 4.5). On the right, a photo of a scattering foil with the brass stopper.

Two in-transmission *Monitor chambers* are used to provide an on-line control of the delivered dose and a micro-strip ionization chamber detector permits the on-line monitoring of the beam, called *MOPI* [36].

At the end of the beamline a 50 cm long brass tube with a final *collimator* is placed. The tube is needed to create a beam with negligible divergence.

All these elements have been studied in detail over the years and here only the main characteristics and goals of single elements have been reported. Part of the experimental room is reported in Figure 2.3.

A set of tools is present for the optimal centering of the patients, detectors and cellular samples during the experiments. At the isocenter a mirror, together with a light field, simulates the beam position in the transverse direction. In Figure 2.4 an example of this light field usage can be seen.

The experimental room is equipped with a system to perform beam quality control and dosimetry (both absolute and relative). The beam shape is measured by using a motorized *diode*, placed at the isocenter, that provides lateral dose distribution along two axis perpendicular to the beam line. The absolute dose is measured by using a Markus chamber [37] put in a motorized water tank with a resolution of 0.1 mm.

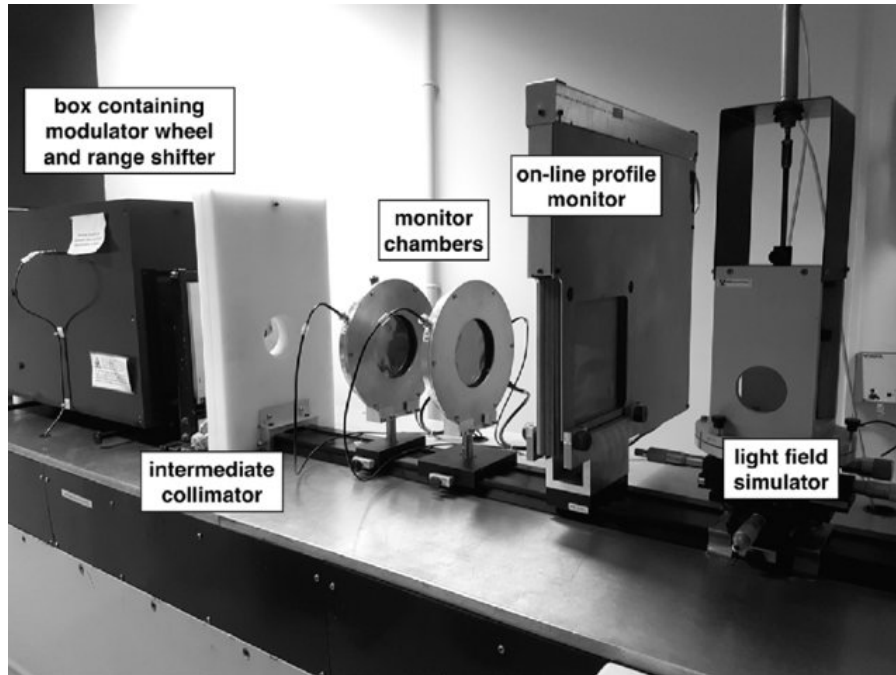


**Figure 2.3:** *Central section of the CATANA proton therapy beamline with some transport (collimators, modulators, and range shifters) and diagnostic (monitor chambers, on-line profile monitoring, and field simulator) [35].*

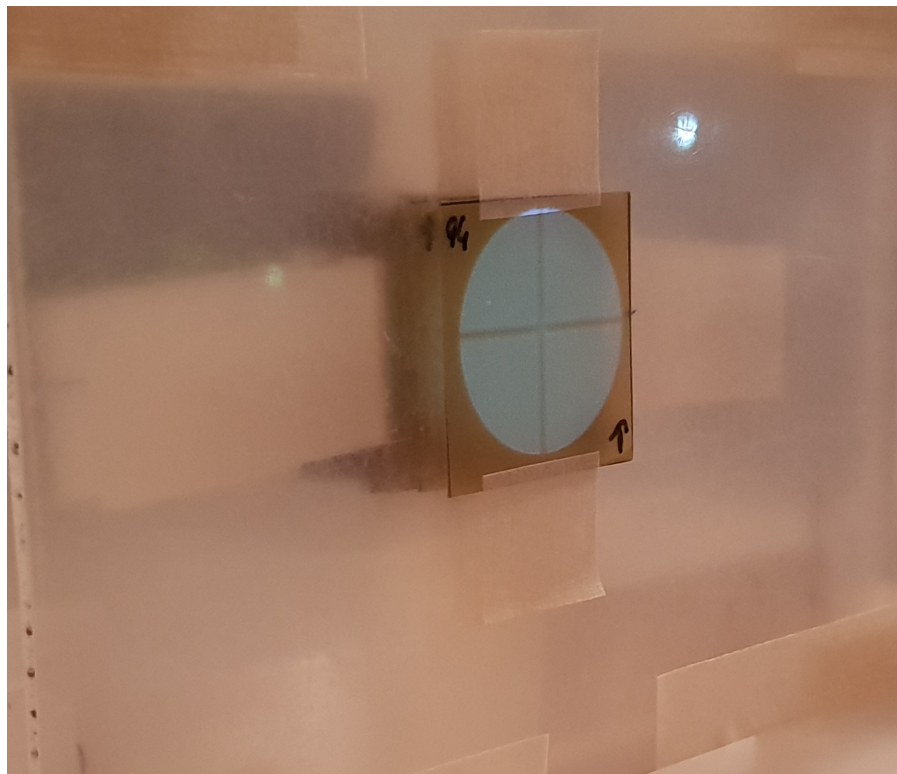


**Figure 2.4:** *The light field used to center the detector. Light simulates the trajectory of protons once the beam is switched on. Here a series of self-developing gafchromic films are used together with PMMA inert thickness to measure the SOBP profile.*

---

## 2.1.2 CNAO

CNAO *Centro Nazionale Adroterapia Oncologica* is a non-profit Foundation established by the Health Minister for the cure of radio-resistant or inoperable tumours making use of carbon ions and protons beams [30]. The hospital is situated in Pavia and is equipped with a 80 meter long synchrotron. The kinetic energy of particles used goes up to 250 MeV for protons and 480 MeV for carbon ions. The technique used for treatments is called *dose painting*: the beam is used like a brush moving with a precision of 200  $\mu\text{m}$  until all the prescribed dose is delivered. The beam is controlled in the plane perpendicular to the beam axis using electromagnets and on the beam axis changing its energy.

Quality controls are performed everyday, as the main goal of the center is to treat patients. Concerning radiobiological experiments, in CNAO a water tank with a self-moving support for flasks can be used to perform cell experiments in water at given positions of the SOBP.

## 2.2. Clonogenic assay

At today, the gold standard of the techniques to quantify the biological damage due to the ionizing radiation is the so-called *clonogenic assay* [38].

The *in-vitro* clonogenic assay is a cell survival assay based on the ability of a single cell to grow into a colony (a group of 50 cells). The assay essentially tests every cell in the population for its ability to undergo "unlimited" division. Clonogenic assay is a method able to provide a quantification of cell inability to reproduce after treatment with ionizing radiation [38].

In particular, for these experiments, 24 hours before irradiations cells were seeded in T25 flasks and were irradiated at subconfluence, i.e. cells were still growing when the irradiation began. Briefly after irradiation, cells were detached, counted by haemocytometer and seeded in a 6-well plate in triplicate at a density of 50-2000 cells per well, by plating an increasing cell quantity according to the dose delivered raising, in order to assay the Surviving Fraction (SF). Colonies were allowed to grow under normal cell culture conditions for two weeks and then were fixed with 50% methanol and stained 0.5% crystal violet. Colonies with more than 50 cells were counted manually under phase-contrast microscope and also with a computer-assisted methodology using Image J. The calculation of SFs in cells irradiated with protons were determined taking into consideration the plating efficiency (PE).

Cells survival as a function of dose is usually fitted by a linear-quadratic formula:

$$\frac{S(D)}{S(0)} = \exp(\alpha D + \beta D^2) \quad (2.1)$$

as can be seen from Figure 2.5.

This method enters a series of uncertainties on the survival fraction that need to be taken into account. Many of them are operator-related, and therefore a more experienced operator will more likely be more precise. The main possible uncertainties are:

- cell counting is statistical: often its precision is lower than 10%;
- if cells are not completely separated when plated, a single clone might originate from multiple cells that did not separate;
- clones are not easy to count.

Nevertheless this method is widely used and its limits are well known and described.

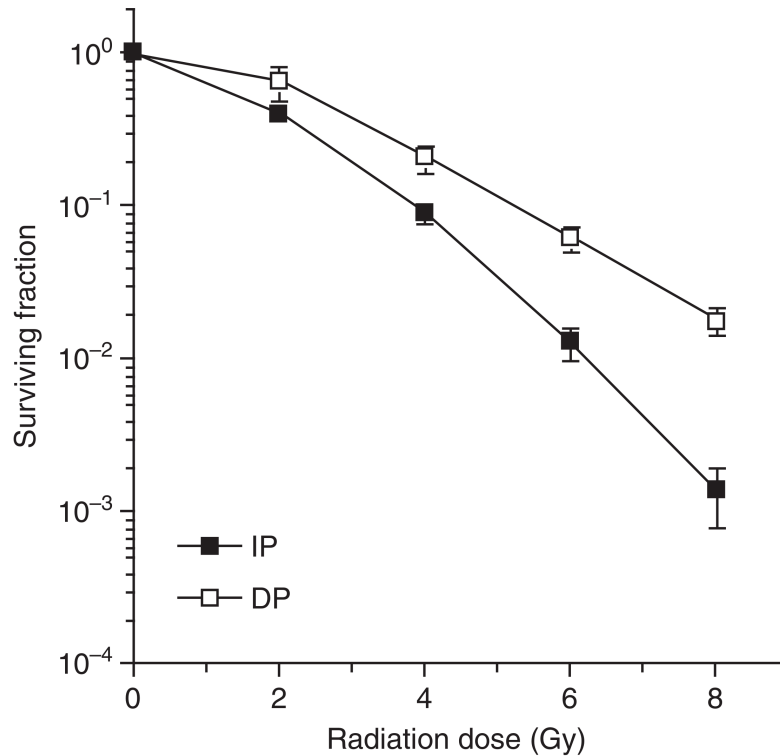


**Figure 2.5:** *Survival curves of Glioblastoma multiforma cells plated immediately (closed symbols) and delayed plated (open symbols) after irradiation. The linear-quadratic trend is noticeable [38].*

### 2.3. Chromosome aberrations with FISH approach

Chromosomal aberrations (CAs) are the microscopically visible part of a wide spectrum of DNA changes generated by different repair mechanisms of DNA double strand breaks (DSB) when cells are irradiated early in interphase. When both the strands of DNA break, a chromosome is left with *sticky* ends of unpaired basis. These ends might rejoin with other sticky ends, creating some aberrations. When a sticky fragment is created, it may:

- rejoin in their original configuration, i.e. no aberration is created;
- fail rejoining. This case leads to deletion in next mitosis;
- reassort in chromosomes that will be distorted at the following mitosis.

Two aberrations that might lead to cell death are the *dicentric aberration* and the *ring aberration*. In the former, two chromosomes break and rejoin together, creating a distorted chromosome with two centromeres and two fragments with no centromere. The latter forms when a break is induced in each arm of a single chromatid and the sticky ends reassemble to form a ring and a fragment (Figure 2.6) [39].

Considering then that radiation induces aberrations, and aberrations may lead to cell death, a measurement of aberrations might link cellular death to radiation damage. In particular, *complex* aberrations (there are at least three breaks in three chromosomes) are signature of high-LET particles.

The method of Fluorescence In Situ Hybridisation (FISH) [40] permit the measurement of chromosome aberrations. For every human chromosome there is a probe that makes it fluorescent in a different colour, making material exchange observable. When more probes are used, the method is referred to

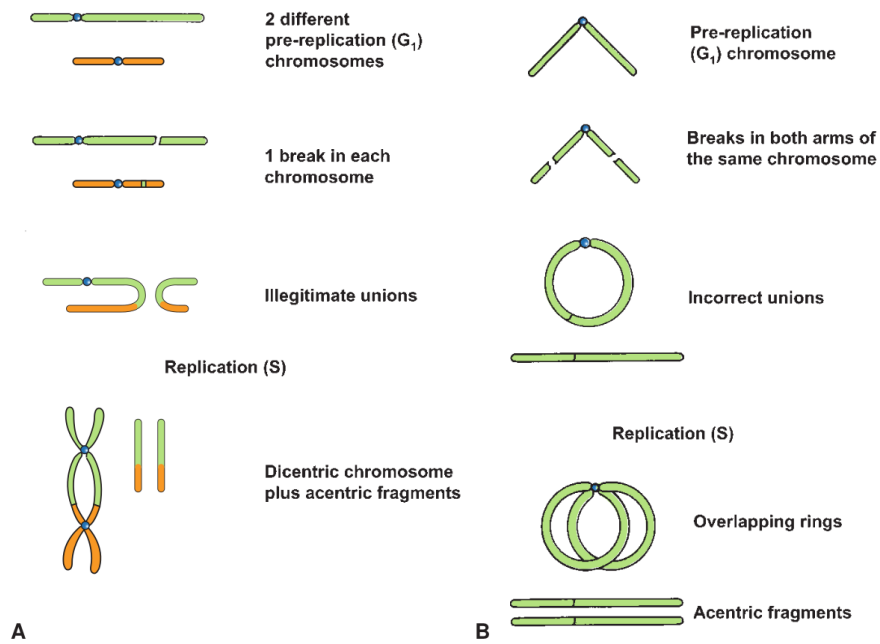
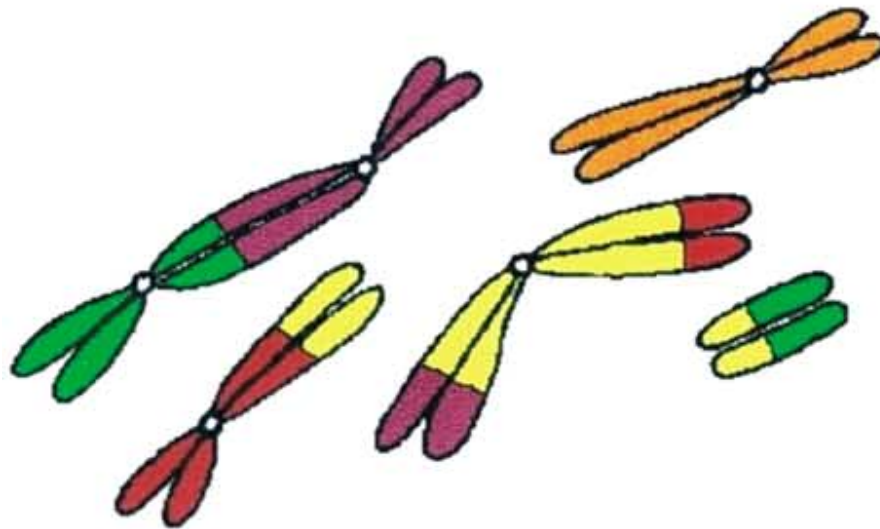


**Figure 2.6:** Steps in the formation of a dicentric (A) and a ring (B) by irradiation of prereplication chromosomes [39].

as mFISH (multicolour FISH). This last method is more reliable as it can recognize a larger number of aberrations (Figure 2.7).

In Figure 2.8 an example of aberration counting with mFISH technique is exhibited while testing PBCT effectiveness (see Section 3.1 for more details).



(e) **m-FISH painting**

**S&S: 2A, 2G, 2B, 3T**

**PAINT: *dic(BD)*, *t(Ce)*, *ace(be)*,  
*t-t(dEc)***

**Figure 2.7:** Representation of mFISH potentials: using different colours all aberrations can be counted [40].

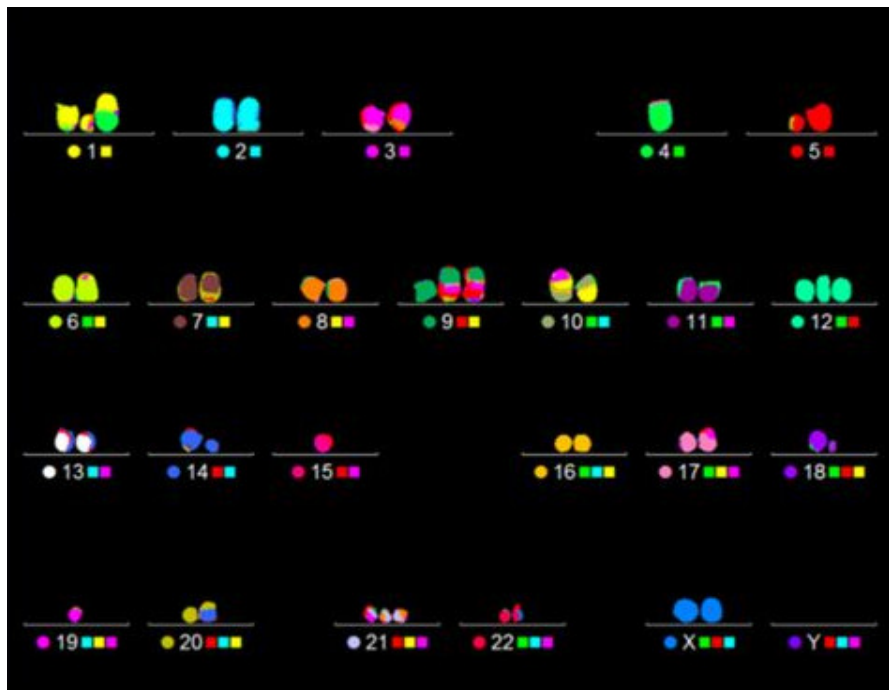


**Figure 2.8:** Analysis of proton irradiation-induced structural chromosome damage. Representative pictures of chromosome spreads from 4 Gy-proton irradiated cells treated with 80 ppm of  $^{11}\text{B}$  scored by mFISH analysis, exhibiting complex-type CAs [1].

---

## 2.4. CR39 detector

In order to try and measure the alpha particles yield a CR39 with a boron converter has been irradiated. A CR39 detector is a plastic made solid-state track recorder that is thermoset, cross-linked, totally amorphous and very sensitive to heavy-ion damage [41]. It is widely used for the study of alpha radioactive sources, cosmic rays and proton and neutron dosimetry.

When such as detector is placed in a mixed field, like the one of a therapeutic beam in air, it registers particles according to their LET: the more energy is deposited and the more chemical bounds are broken (and consequently a hole is created on the detector surface). A low-LET particle could be not able to deposit a lot of energy inside the plastic, and therefore could leave a hardly detectable signal of its passage. But if otherwise the particle is a high-LET one, then the track is going to be bigger, and the signal will be more visible. The dimension of the created holes can be easily correlated to the incident particle energy by using a calibration procedure. Once the detector has been irradiated signal reading is possible through a process called *etching*: the detector is held for a fixed time in an alkali solution that enlarges the holes left by particle passage. Etching procedure permits to detect and quantify the detector damage by using an optical microscope. This way it is possible to correlate the damage (express in term of holes) to the particle LET

This detector is ideal to use in a hadrontherapy experiment as it can be put in the beam axis without being too damaged as it is transparent to low-LET radiation.



# Chapter 3

## Experimental campaign

Part of this work was focused on an experimental campaign devoted to study the PBCT and its effectiveness. Here some of the experiments done will be briefly described.

### 3.1. First experimental proof

The first experimental proof of PBCT biological effectiveness was published in 2018 by Cirrone *et al.* [1]. Here the main results are reported.

Test of cell killing enhancement exploiting proton boron fusion have been done using the human prostate cancer line DU145, irradiated with graded doses at the middle position of the 62 MeV clinical SOBP using the proton beam at the CATANA room of INFN-LNS, described in Section 2.1.1. Two different concentrations of sodium borocaptate (or BSH,  $\text{Na}_2\text{B}_{12}\text{H}_{11}\text{SH}$ ), have been tested: 40 ppm (parts per million) and 80 ppm of  $^{11}\text{B}$ . A set of DU145 cells were grown and irradiated without BSH as well, as a control. The clonogenic survival fraction SF following irradiation with protons alone was best fitted to a linear-quadratic function of dose, i.e.  $\text{SF} = e^{-\alpha D - \beta D^2}$ , already presented in Equation 2.1. Data from proton irradiation in the presence of BSH exhibited a purely exponential behaviour as a function of dose. Least-squares fitting parameters are reported in Table 3.1, while clonogenic curve is reported in Figure 3.1.

	$\alpha$ [ $\text{Gy}^{-1}$ ]	$\beta$ [ $\text{Gy}^{-2}$ ]
X ray irradiation	$0.22 \pm 0.06$	$0.064 \pm 0.014$
Proton irradiation in the absence of BSH	$0.31 \pm 0.02$	$0.035 \pm 0.007$
Proton irradiation with 40 ppm $^{11}\text{B}$	$0.61 \pm 0.07$	—
Proton irradiation with 80 ppm $^{11}\text{B}$	$0.71 \pm 0.03$	—

**Table 3.1:** Calculated values for the  $\alpha$  and  $\beta$  parameters as obtained from the fitting of experimental data by the linear-quadratic model for radiation-induced cell killing are reported. Statistically equivalent to zero  $\beta$  values were found for proton irradiation in the presence of BSH [1].

Significant effect due to boron concentration was observed: a calculated DMF of  $1.46 \pm 0.12$  was determined at the 10% survival level ( $\text{DMF}_{10}$ ). BSH cytotoxicity was studied as well (Table 3.2) both in DU145 cells used for clonogenic assay and MCF-10A cells used for chromosome aberrations.

Cross section for proton boron fusion critically depends on the incident proton energy, as shown in

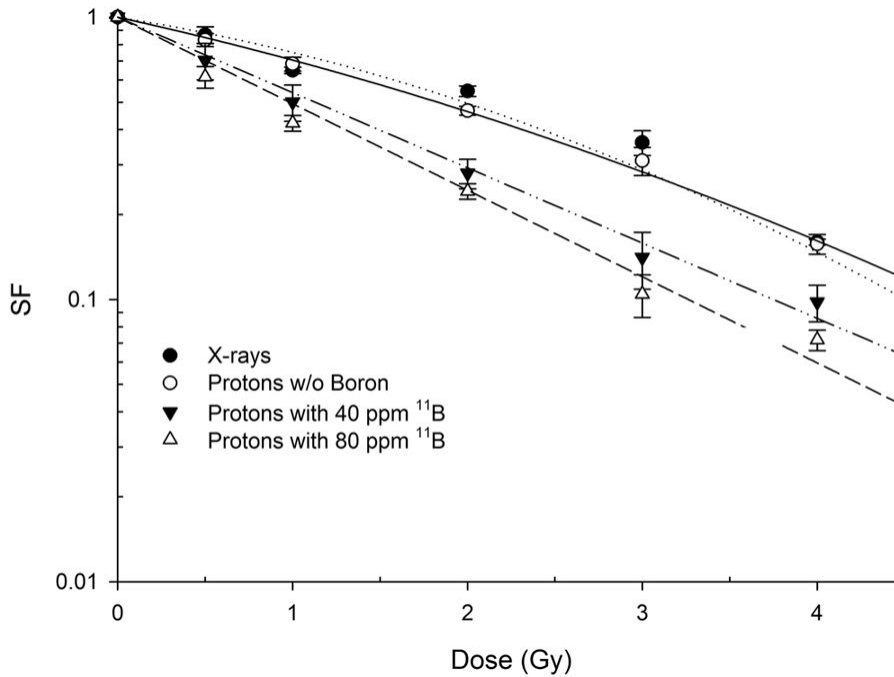


**Figure 3.1:** *Survival curves for the first experimental proof of PBCT at mid-SOBP [1].*

	Plating efficiency	Baseline CA frequency
No BSH	$0.58 \pm 0.02$	$0.027 \pm 0.003$
40 ppm $^{11}\text{B}$	$0.61 \pm 0.04$	$0.027 \pm 0.003$
80 ppm $^{11}\text{B}$	$0.60 \pm 0.04$	$0.023 \pm 0.003$

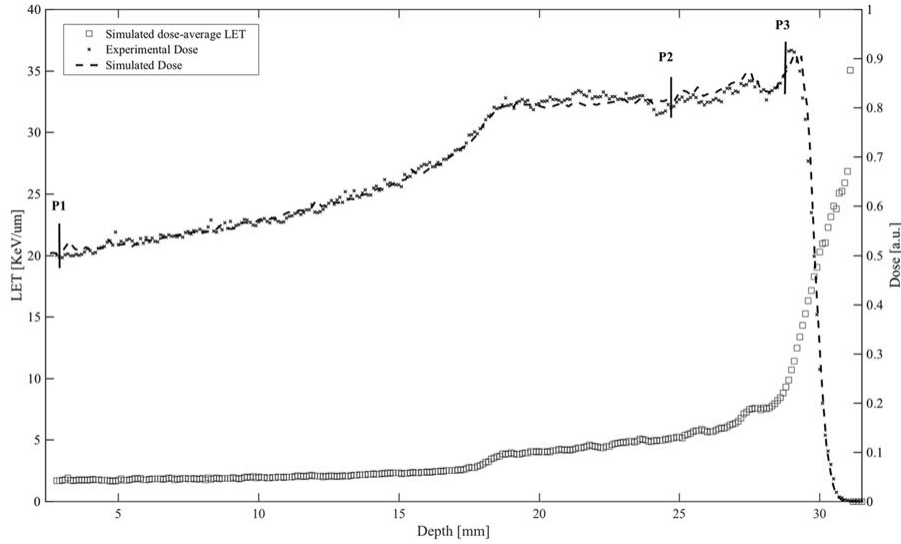
**Table 3.2:** *Plating efficiency (PE) values and total chromosome aberration (CA) yields in unirradiated DU145 prostate cancer cells (second column) and normal epithelial MCF-10A cells (third column), respectively, as a function of the amount of BSH. By definition, PE measures the survival of cells in the absence of radiation. Similarly, the recorded frequency of CAs in cells not exposed to radiation is referred to as baseline CA frequency. Data show lack of BSH-induced cyto- and genotoxicity at the used concentration [1].*

Figure 1.10; hence, its radiobiological effectiveness is expected to vary along the clinical proton SOBP. Enhancement of cell killing has been therefore studied in the presence of 80 ppm  $^{11}\text{B}$  in different positions of the SOBP (see Figure 3.2) .

Experimental data clearly show no effect of BSH at the entrance position (or P1). At mid-SOBP (P2 position) fitting parameters were  $\alpha = (0.31 \pm 0.02) \text{ Gy}^{-1}$  and  $\beta = (0.040 \pm 0.006) \text{ Gy}^{-2}$  for proton irradiation without BSH and  $\alpha = (0.65 \pm 0.02) \text{ Gy}^{-1}$  in the presence of 80 ppm  $^{11}\text{B}$ . At the distal end of the SOBP (P3 position) BSH appeared to be more effective with a DMF of  $1.75 \pm 0.13$ ,

Concerning chromosome aberrations, cancer cells are known to be genetically unstable, hence radiation-induced chromosome rearrangements would superimpose onto an elevated confounding frequency of baseline damage, and therefore they do not lend themselves to reliable assessment of radiation-induced DNA damage. Therefore, the non-tumorigenic breast epithelial MCF-10A cell line was chosen for scoring of radiation-induced CAs.

When comparing BSH treated cells with cells irradiated with protons in the absence of BSH, a higher yield of all CA types is found in the former, as shown in Figure 3.4. When comparing FISH and mFISH approach, the latter found a higher frequency because of its intrinsically greater sensitivity,



**Figure 3.2:** Cell irradiation along the proton SOB. Measured dose and calculated LET profile for cellular irradiation at different positions along the clinical proton SOB at INFN-LNS, Catania, Italy. Shown are the three depths along the SOB at which cells were irradiated and the corresponding calculated LET values (open squares). Dose profiles as obtained by direct measurement by Markus chamber and by Monte Carlo simulation [1].

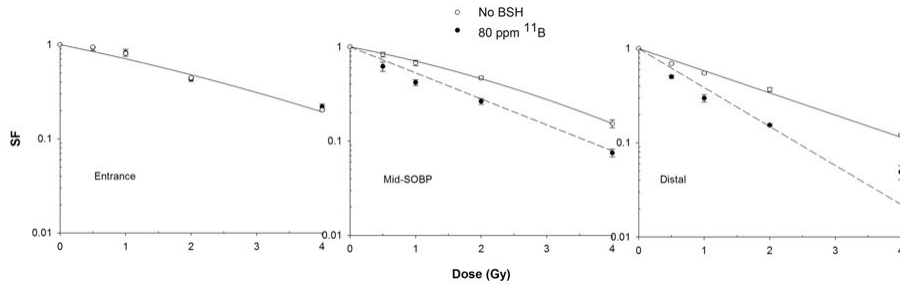


**Figure 3.3:** Clonogenic survival along the proton SOB. Data shown here refer to dose-response curves obtained at positions P1, P2 and P3 as indicated in Figure 3.2 along the clinical proton SOB. Enhancement of cell killing due to the presence of the boron compound (black circles) is null at beam entrance (highest proton mean energy) while reaching its maximum at the distal end of the SOB (lowest mean proton energies) [1].

as expected. Also boron-mediated enhancement of chromosomal damage is slightly amplified passing from conventional FISH scoring to mFISH analysis: the yield of CAs following 2 Gy of protons in combination with BSH increased from about 0.22 to 0.47 aberrations per cell compared to about 0.11 and 0.20. According to the assumption that protons are only slightly more effective than photons, the yield of CAs following x-rays was identical to that measured after exposure to protons in the absence of BSH.

A linear-quadratic function  $Y = Y_0 + D + D^2$  where the coefficient  $Y_0$  corresponded to the baseline CA frequency used to fit aberration data. Results are reported in Table 3.2. No statistically significant value for the parameter  $\alpha$  was found in the absence of BSH; on the other hand in presence of 80 ppm of  $^{11}\text{B}$  the value for  $\alpha$  and  $\beta$  found were  $(0.16 \pm 0.07) \text{ Gy}^{-1}$  and  $(0.03 \pm 0.02) \text{ Gy}^{-2}$ . DMF was calculated using the CAs number, in particular level set were 20 and 40 aberrations for 100 cells. The former resulted in a DMF of 2.1, while the latter was calculated as 1.6.

Even the result of complex-type aberration exchanges confirmed the presence of high-LET particles, as shown in figure 3.5. These results support the notion that the presence of BSH results in a significant dose-modifying effect on proton irradiation, increasing cell lethality and DNA damage, consistent with the action of the alpha particles produced by proton-boron fusion.

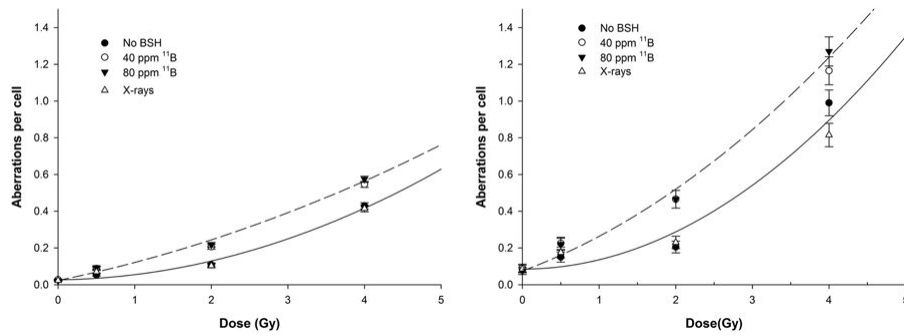


**Figure 3.4:** BSH-induced increased induction of chromosome aberrations following proton irradiation. The dose-dependent frequency of all chromosome exchanges scored by either conventional FISH painting (left) or m-FISH karyotyping (right) is shown for proton irradiation alone (black circles) and for proton irradiation in the presence of  $^{11}\text{B}$  at concentrations of 40 ppm (open circles) and 80 ppm (down triangles). X-ray data are also shown for comparison. In the interest of clarity, fitted curves are shown only for the highest boron concentration used (80 ppm, dashed line) and for irradiation with no boron compound (solid line). Data points correspond to the mean value measured in at least two independent experiments with standard errors of counts [1].

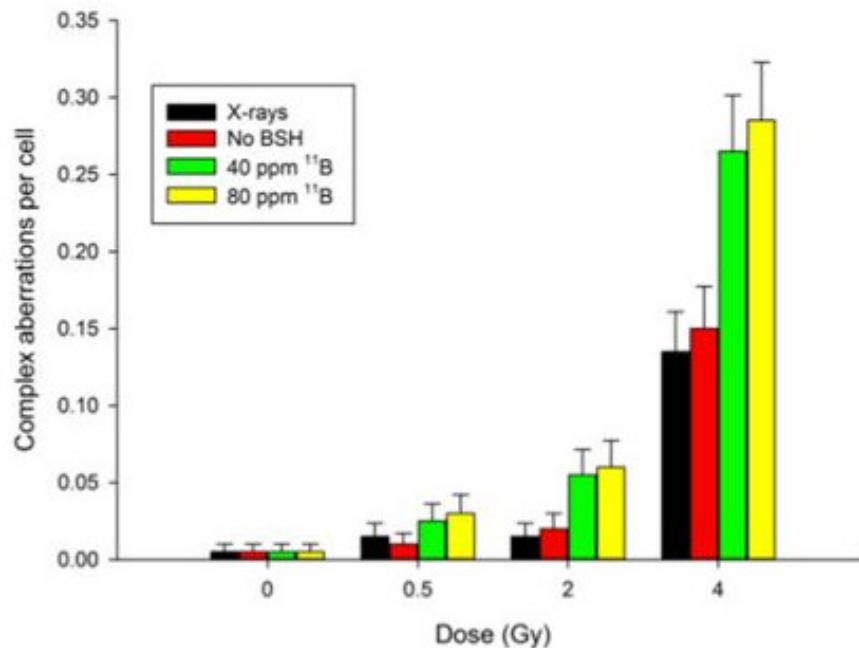


**Figure 3.5:** Induction of complex-type CAs with the mFISH method. A greater proportion of complex chromosome rearrangements was found in cells irradiated with protons and treated with BSH than in cells subject to proton irradiation alone [1].

## 3.2. Radiobiology at CNAO

A second experimental campaign was conducted at the CNAO proton therapy center to justify the independence of the biological effect from the experimental facility adopted. The main aim of this experiment was in fact to proof the repeatability of the effect and the independence of the neutron contribute (generally produced by a passive proton beam line like CATANA facility). Actually neutrons could react with  $^{10}\text{B}$  located inside cells, going through a BNCT-like reaction and creating high-LET alpha particles that might enhance proton lethality. Considering that in CATANA most of neutrons are created in the *passive* scattering system used for the SOBP creation, if this effect is responsible of the observed enhancement, such effect should not be detectable in a facility with an *active* different degradation energy system like in CNAO.

Moreover, the different released energy in the two adopted facilities (62 MeV at CATANA as respect to the 250 MeV at CNAO) could provide a quantification of a possible energy-dependence of the effect in a typical spectra of a SOBP obtained with an active beam scanning. Clonogenic assay of DU145 prostate cancer cells was conducted on biological samples irradiated along three position of a SOBP (entrance, mid and distal).

In Figure 3.6 survival curves are shown, and in Table 3.3 calculated fit parameters are exhibited.

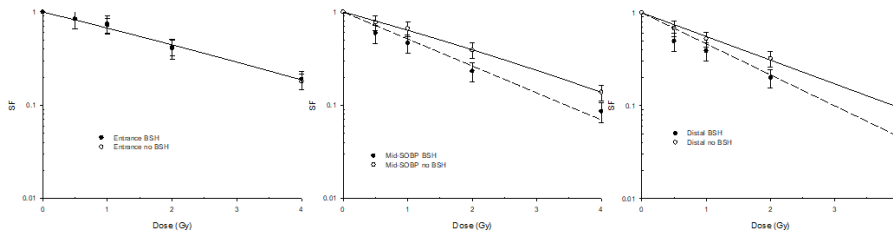


**Figure 3.6:** Survival curves for the entrance, mid-SOBP and distal points taken in CNAO experiment. These results are only preliminary and will need further analysis.

Position	$\alpha$ (BSH) [ $\text{Gy}^{-1}$ ]	$\beta$ (BSH) [ $\text{Gy}^{-2}$ ]	$\alpha$ (no BSH) [ $\text{Gy}^{-1}$ ]	$\beta$ (no BSH) [ $\text{Gy}^{-2}$ ]
Entrance	$0.39 \pm 0.07$	*	NA	NA
Mid-SOBP	$0.67 \pm 0.16$	*	$0.44 \pm 0.03$	$0.015 \pm 0.009$
Distal	$0.8 \pm 0.2$	*	$0.59 \pm 0.07$	*

**Table 3.3:** Fitted parameters for the survival curves taken at CNAO. NA means not available, and is present as for entrance position only BSH data fit have been performed. \* stands for not statistically significant (compatible with zero).

A  $\text{DMF}_{10}$  of about 1.31 in the mid-SOBP has been obtained in accordance to the results obtained at CATANA facility (see Section 3.1). These results look confirming the hypothesis of the enhancement due to a proton-boron fusion.

## 3.3. CR39 analysis

An experiment with a CR39 detector (see Section 2.4) has been done at CATANA facility of LNS. A CR39 has been equipped with a boron converter to try to produce some alpha particles exploiting the proton-boron fusion reaction. As a converter Boron carbonate ( $\text{B}_4\text{C}$ ) has been used. Boron carbonate

has been used instead of pure boron as it is easier to produce and use. Nevertheless, because of its toughness its depositing is almost impossible on the CR39 itself: it would be stressed and start cracking if the film is too thick. This was solved by depositing boron carbonate on another material and later put on the CR39.

For this experiment the detector used was a *three layers detector*: a  $(10 \times 10 \times 1)$  mm CR39 (a square in the transverse dimension) was equipped with a 500 nm PMMA, and above this layer 2  $\mu\text{m}$  of boron carbonate have been deposited. During the etching phase also the PMMA (with boron converter) layers is detached and removed from the detector itself. This setup permitted to deposit a relatively thick layer of boron carbonate without the stressing problem, nevertheless enters a material between the converter and the detector itself that might slow or stop some of the particles created. This is the reason why PMMA layer was so thin.

Irradiation has been done according to results obtained from simulation (Section 5.10). A low dose (1.46 Gy) has been delivered at beam entrance, without using water-equivalent PMMA sheets (Figure 3.7). This was decided to minimize the noise due to low energy protons, whose number would increase moving along the SOBP.

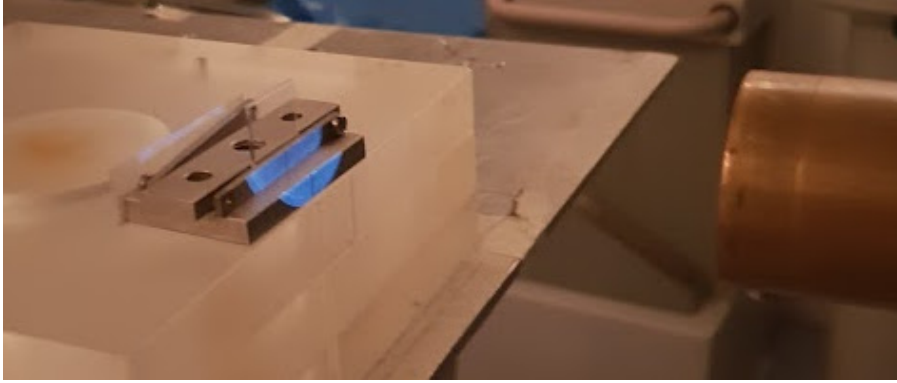


**Figure 3.7:** Irradiation of the CR39 detector with boron converter at CATANA facility. It was positioned right at the isocenter of the proton beam.

To analyze this detector, it has been etched for one hour (Figure 3.8), and then the detector was analyzed by using an optical microscope. Acquired images has been processed to compute the number of etching pits as a function of their area. Then calibration curves have been used to link holes diameters with alpha particles to obtain the yield of alpha particles with energy greater than 4 MeV.

The result of this analysis is exhibited in Figure 3.9. According to the calibration, alpha particles with energy greater than 4 MeV produce pits with diameter between 3  $\mu\text{m}$  and 15  $\mu\text{m}$ . The counts of these pits produce a number of alpha equal to:

$$N_{\alpha} = (6.58 \pm 0.17)10^5 \text{ per cm}^2$$

This result is important as it is the first test dedicated to quantify the alpha particles emitted in PBCT. The interpretation of this number will be done comparing it with results of the simulations in Section 5.10.

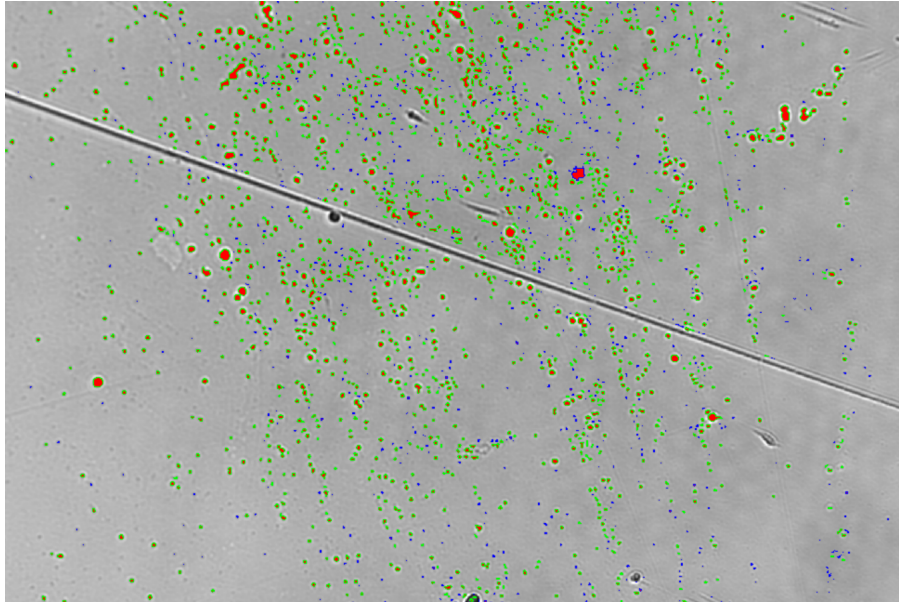


**Figure 3.8:** *An image of the CR39 detector after 60 min etching. The etching pits, linkable to high-LET particles passage, are visible.*

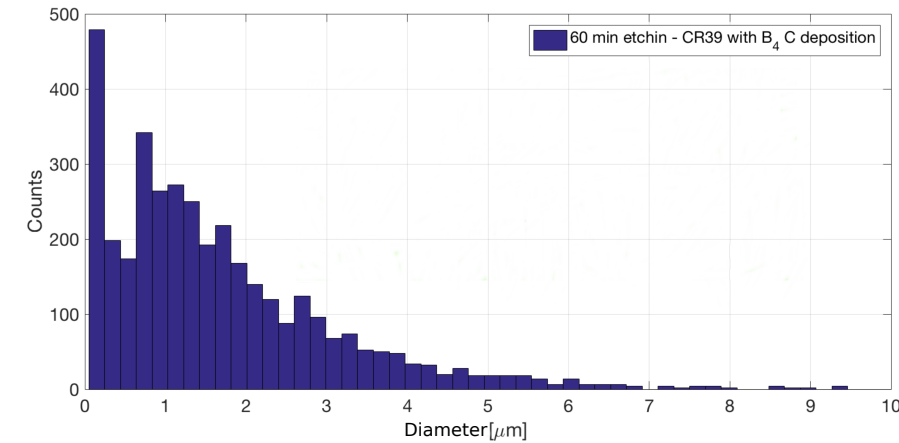


**Figure 3.9:** *The result of the etching analysis: counts as a function of pit diameter.*

### 3.4. Present and future perspectives: NEPTUNE

The results obtained studying PBCT, in particular the measurement of a so high biological effectiveness, aroused interest of Istituto Nazionale di Fisica Nucleare in this innovative technique, and in 2019 the project NEPTUNE (Nuclear process driven Enhancement of Proton Therapy UNravEled), funded by INFN, started. NEPTUNE is a three year project meant to study in details nuclear reactions capable to enhance proton therapy, such as PBCT. During these three years an exhaustive campaign should permit a deeper understanding of boron therapeutic effect both from an experimental and a modelling point of view. In particular this technique will be studied experimentally from three different points of view: imaging, microdosimetry and biological effectiveness.

Imaging focuses on assessing the distribution and kinetics of boron in cell cultures and mice models. Important tasks are the measurement of internalized  $^{11}\text{B}$  as a function of the administered BSH, and realizing of kinetic and cytotoxicity curves to determine pre-treatment time for optimal uptake. Also intracellular localization will be studied, as it provides insights on the cell-killing effects.

---

Microdosimetry will be studied all along the SOBP with detectors with tissue equivalent wall/converters unloaded and loaded with boron. Spectra will be taken in the same position of the radiobiological studies, to assess physical characterization of the radiation field at cellular dimensions. Tissue Equivalent Proportional Counters (TEPC), silicon telescopes and SiC devices will be used.

From the radiobiological point of view plans are to corroborate previous data and study radioresistant PANC-1 cells from high-mortality rate pancreatic cancer while using BJ fibroblast as normal cell reference. Cell death, chromosome aberrations and micronuclei will quantify proton-induced damage in cells exposed at mid-SOBP. Also other position along the SOBP will be studied to confirm whether proton boron fusion is the one responsible of the enhancement. Signature of high-LET radiation chromosome aberration study will be done, together with measurement of  $\text{H}_3\text{O}^+$ , recently identified as an alpha-particle chemical signature, measurements of ATR/ATM kinase ratio, colocalization of damage and mFISH study. Moreover bystander effects will be studied transferring irradiated cells onto unirradiated samples.



# Chapter 4

## Computational Methods

The main part of this thesis work was focused on the computational methods to model the PBCT observed effect.

Modelling has been done using different computational tools such as *Geant4* [42], *ROOT* [43] and *TALYS* [26]. *EXFOR* database [28] has been used as well. Specifically, an accurate validation of proton-boron fusion reaction cross section implemented inside the kernel of Geant4 Monte Carlo was performed. In this section, the main important adopted parameters as well as the general structure and philosophy of the entire Geant4 code will be described.

### 4.1. Monte Carlo methods

Monte Carlo methods were firstly theorized by the mathematicians Stanislaw Ulam and John von Neumann, and their study began in 1946 [44]. In unpublished remarks (dated 1983), Stanislaw Ulam confesses that the first idea of a Monte Carlo approach to a physical problem arose while he was playing solitaire. He realized that it would have been more efficient to estimate the fraction of winning decks just analyzing a hundred random plays and count the successful ones [45].

This was later recognized as the first Monte Carlo approach: when a problem is particularly hard to compute mathematically (or analytically) a statistical approach might lead to a faster (even if approximated) solution. Monte Carlo methods are these set of methods able to use random numbers to approximate the solution of a problem, and its usage is very common in different branches of science, also nuclear and particle physics.

The main steps that characterize a Monte Carlo approach are:

- a *set* of interesting variables, each with a set of possible values is chosen. Some will be *input variables* and others will be *output variables*;
- a *random number generator* decides the values of all the input variables;
- an *algorithm* computes the values of the output variables given the input variables.

The last two steps must be repeated a *sufficiently large* amount of times for the solution to be reliable.

Of course calculators are used for these problems given their innate speed in repeating algorithms. Nevertheless a problem arises when using processors to solve Monte Carlo problems: a random number generator does not exist. In its place, a pseudo-random number generator is used. This is a consequence of a processor nature: although it can compute billions of calculations per second it cannot generate a perfectly random number. A pseudo-random number generator is described mainly by its *correlation*

---

*length* and its *period*. A good number generator has a long correlation length and a long period. The reliability of the Monte Carlo method strongly depends on the random generator itself.

## 4.2. Geant4

Geant4 (GEometryANdTracking) is a toolkit for the simulation of the passage of particles through matter. Its areas of application include high energy, nuclear and accelerator physics, as well as studies in medical and space science [22]. It is a very versatile tool, and counts many functions and classes for the most different applications.

It is written in C++ language and it takes advantage from the object oriented software technology, which allows writing a clearer and more partitioned code. Geant4 is currently developed and managed by an international collaboration constituted approximately by one hundred members from Europe, North America and Japan. Usually, two updated versions of Geant4 are released every year. It follows exactly the Monte Carlo method structure described before, simulating random numbers to use as input and computing output variables.

It is not a *set of working programs*, but provides an environment the user must set in the best way to simulate its experiment. The environment is made of classes that can be grouped in two main different types: *initialization* and *action* classes. The former are invoked at the beginning of the simulation, while the latter are usually called repeatedly during the simulation.

The most important initialization classes are used to:

- create the experiment geometry;
- create the experiment physics;

while the most important action classes permit to:

- generate primary particles;
- set action at different levels of the simulation (run, event, track, step).

These aspects of a simulation creation are well described in Geant4 manual [46], and here only a brief explanation concerning how they could be used (and without focusing on commands) will be given.

It is better to introduce some notations peculiar to Geant4 simulations: a *step* is the object describing a particle between two *processes*, like interactions or transportation in a different volume, the collection of steps for a given particle is called *track*, the collection of tracks started from the same primary generation is called *event* and the collection of events with the same geometry setup is called *run*.

### 4.2.1 Geometry

Geometry in Geant4 is the set of all objects particles might interact with, i.e. both sensitive detectors and inert volumes. Only one instance of the geometry is saved along a run, and it is created at the beginning of the simulation. Geometry is created inside a Geant4 simulation in a tree-like structure: a main volume exists, called the *world volume*, and every other volume must be defined inside another one, in a daughter-mother relationship.

---

Geometry is defined through three different steps: the solid, the logical volume and the physical volume, and every step adds some details on the object needed for the simulation.

*Solids* are the geometrical structure of the object. A lot of pre-defined solid constructors can be used, like boxes, tubes, spheres, trapezoid and so on [46]. All constructors need some dimensions in order to build the solid. Solids can also be imported from external project softwares.

*Logical volumes* add some characteristics to the solid, like the material, temperature, electromagnetic field and sensitivity. Concerning material, it can be taken from NIST database [47] as it is, or can be manually built using elements. Also elements can be retrieved from the database or be built using isotopes (if different isotope ratio is needed), and the same structure is for isotopes that can be defined through the number of protons and neutrons. When defining a material and associating it to a solid to create a logical volume, some features must be given, like the density and the temperature. Internally Geant4 then calculates some quantities important for the simulation, such as the ionization potential and radiation length.

*Physical volumes* are the placing of logical volumes in a mother volume. A physical volume adds to the logical one a position (with respect to the mother volume) and a rotation.

## 4.2.2 Physics models

Physics models can be divided in three main parts: *particles*, *processes* and *cuts*. A physic model is set at the beginning of the simulation.

Before introducing these concepts it is necessary to describe how Geant4, as a Monte Carlo method, can simulate a physical process. Assuming a particle is inside a volume<sup>1</sup> that volume has a given *material*, and therefore the simulation will know the numerical density of all different isotopes, the number of electrons, ionization potential and so on. In this condition, a mean range for each possible process can be calculated. Therefore a particle in a given object may undergo a list of different processes, such as hadronic interaction, electromagnetic interaction or transportation. For each process a range can be sampled according to specific probability distributions depending on the object characteristic (material, temperature and so on) and particle type and energy. Once all ranges are simulated, Geant4 chooses the lowest one, deciding which process the particle will undergo. Therefore the particle state is evolved (i.e. direction, velocity and energy are upgraded and secondaries are created) and the tracking continues. This process is repeated as long as there are particles to track. A particle is not tracked anymore when it stops and cannot do anything while still or exits the world volume.

This method to choose what process the particle will undergo is adopted for all the *hard processes*, i.e. processes where energy trade among reagents is located in an exact region in the spacetime, such as hadronic processes, photoelectric effect, Compton effect and so on. But if continuous processes or processes with really high cross section were treated this way, the simulation would become really computational power hungry. To solve this, *soft processes* are treated in a statistical way and does not compete with hard processes. Multiple soft scattering and Coulomb interaction are treated this way.

*Particles* are the list of objects that may be tracked by Geant4. Each particle is associated with a list of properties such as mass, charge, strangeness and so on. Particles can be created exploiting the

---

<sup>1</sup>even the world volume is a volume, particles cannot be tracked outside the world volume and tracking stops whenever a particle reaches one of its borders

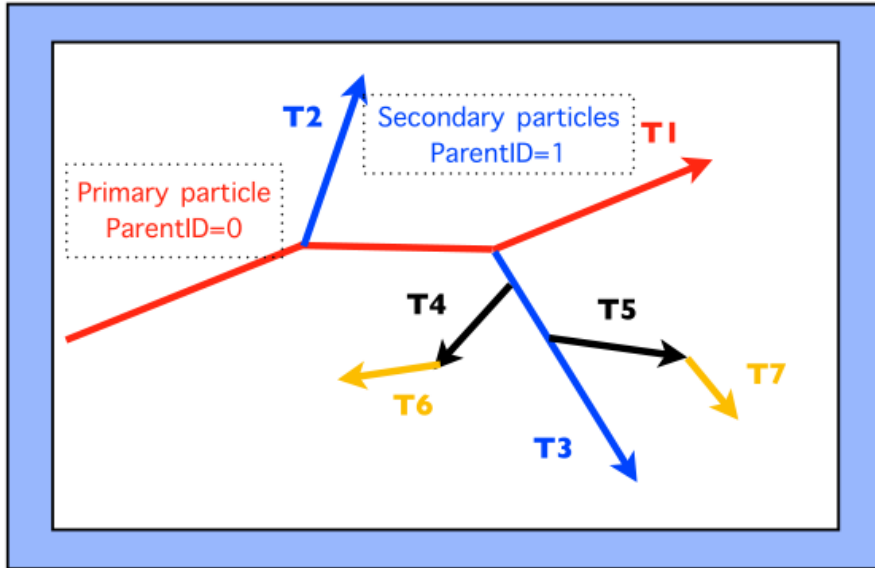


**Figure 4.1:** An example of Geant4 tracking routine. A primary particle ( $T1$ ) undergoes a different process at every step, according to sampled ranges. Sometimes secondary particles are created and later tracked [48].

PDG database [49].

*Processes* are the list of actions particles can go through. A process must be associated to a list of particles, and it is described by:

- the list of particles that can carry on this process;
- the list of isotopes that can activate this process, i.e. this process can happen when a particle crosses a given material;
- the cross section for the process as a function of the particle energy;
- the list of particles produced by this process and their spectra;

*Cuts* are threshold parameters in range for secondary particles creation. If a particle travels less than the cut, that particle is not tracked and its energy is released at the creation location. This operation allow to speed up simulation while saving computational power.

Usually physics is loaded in a *modular* way. Different modules are used for different processes and different particles. The group of all these modules is called *physicslist* and its application will be deeply studied in this work. Different modules are used for different processes: a module might describe Coulombian processes, another will describe hadronic interactions, and another one decays. If the simulation is reliable, all the *important* processes must be entered through a specific module.

Usually also the single modules use more than one model depending on the process, the particle nature and its energy. In Figure 4.2 an example of this can be seen: Liège intranuclear cascade is a hadronic module, and it uses different models for different reactions.

### 4.2.3 Primary generators

As the experiment involves passage of particles through matter, a primary generator is needed in order to set the characteristics of the simulated particles. The user must create a specific class where to set:

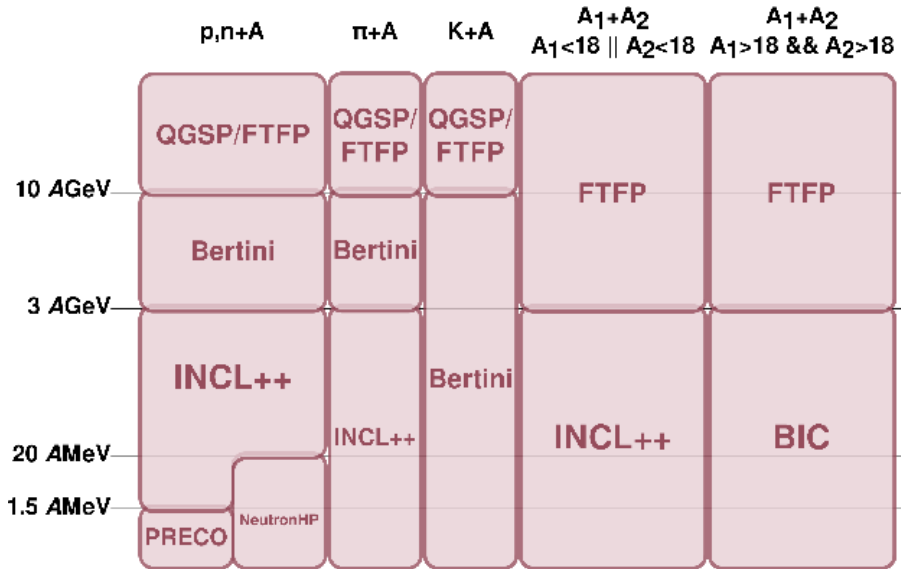


**Figure 4.2:** An example of multiple models usage inside a given physics list. According to a particle nature and energy, different models are used to compute physical quantities such as cross sections or spectra [50].

- particle type (a lot of particles can be chosen like stable and unstable leptons, all hadrons in PDG database [49], many ions and also a fictitious particle, named the geantino, that does not interact with anything along its flight);
- particle energy (or momentum module);
- particle direction;

and many other secondary characteristics. All these features can be set equal for all the simulation or randomized in every event. A specific class also allows the user to select a non point-like source for particles: they might be shot from a volume, or its surface, or a beam-like source, with random position and direction for each new event. Also energy and position spectra can be given as input to obtain the correct randomization for particles features.

#### 4.2.4 Simulation outputs

There are many ways to interact with the simulation. Usually outputs are saved in *text files*, *binary files* or *ROOT histograms*. During a simulation, all the features can be saved, for example particle position, energy, type and so on. The interaction with ROOT allows to save directly an histogram ready for further analysis. This way only mono- and bi-dimensional histograms can be saved. Many standard methods allow the user to open files and save histograms in a multi thread safe way. Saving proceeds mainly in two ways: *sensitive detectors* and *user actions*. Sensitivity is a characteristic set to a logical volumes that makes the detector sensible, i.e. some properties are saved every time a particle crosses it; while user actions allows the saving at different levels: an action (i.e. writing in a text file) can be repeated for every run, event, step, track and so on.

### 4.3. ROOT

ROOT is a modular scientific software toolkit. It provides all the functionalities needed to deal with big data processing, statistical analysis, visualisation and storage. It is mainly written in C++ but integrated with other languages such as Python and R. [51] In this work ROOT has been used mainly

---

to plot and compare functions and histograms, save graphs and data, and fit them.

ROOT fitting uses by default a chi-squared minimization method but a maximum likelihood can be used as well for low-statistics histograms [52]. ROOT interface easily allows the user to fit data using default functions, such as polynomial, exponential or gaussian or a complicated user defined function. Parameters boundaries can be set, and suggested parameter range can be set as well to help the program find the optimal values. Minimization of the parameters is computed in a stochastic way.

## 4.4. TALYS

TALYS is software for the simulation of nuclear reactions. Many state-of-the-art nuclear models are included to cover all main reaction mechanisms encountered in light particle-induced nuclear reactions. TALYS provides a complete description of all reaction channels and observables, and is user-friendly [53]. The main parameters that have been calculated by an analytical approach are:

- cross section for every channel,
- spectra of ejected particles,
- spectra of recoiled nuclei,

and this can be repeated over a large number of energies given as input.

TALYS works on the assumption that a nuclear reaction can be seen as a chain of nuclei forming after the emission of a light particle. When, for example, the reaction proton on  $^{11}\text{B}$  is given as input, the calculation for cross sections and spectra works as follows:

- the total energy of the compound nucleus (if energy is high enough for a compound nucleus to form) is calculated according to the proton energy and the eventual excitation energy of the target  $^{11}\text{B}$ . This energy will be compatible with an excitation level of the compound nucleus, either in the discrete or continuous region;
- the compound nucleus de-excite itself emitting particles. The probability to emit a given particle is calculated according to physical models. De-excitation may produce a new nucleus in an excited state;
- the created nuclei de-excite like the compound nucleus, emitting particles. This process repeats until all possible nuclei are in a ground state or isomer;
- The total yields for different channels are summed up to compute cross section (both inclusive and exclusive) and spectra.

Different physics models are used for different energetic regions (Figure 4.3). These models have all some free parameters that are fitted according to experimental nuclear data, and for some data (such as discrete levels) databases like RIPL (Reference Input Parameter Library for Calculation of Nuclear Reactions and Nuclear Data Evaluations) [54] are used.

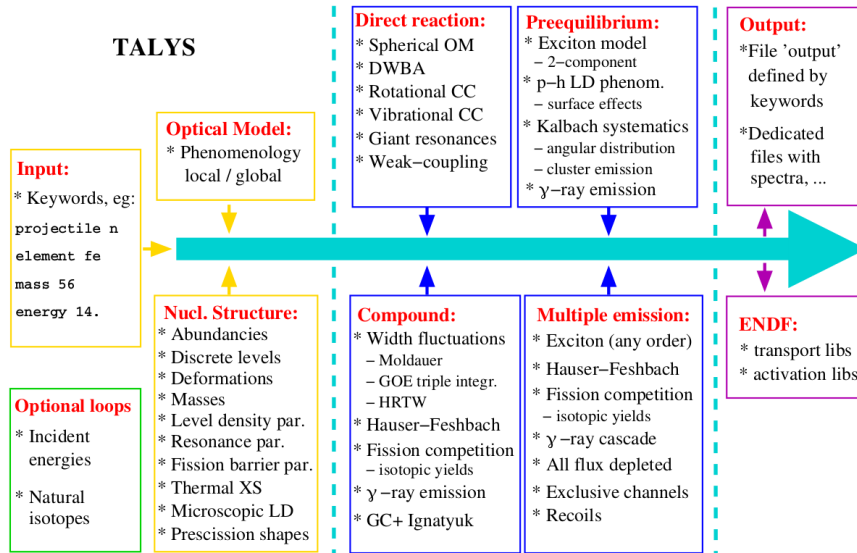


**Figure 4.3:** Nuclear models in TALYS for the calculation of physical quantities by using different approaches [55].

## 4.5. Hadrontherapy

Hadrontherapy is an official Geant4 advanced example and here it will be briefly described as it has been used widely in this work [56].

Advanced examples are a set of examples that can be found inside Geant4 installation the user can look at to find how Geant4 can be used in a real experimental simulation. Hadrontherapy has been used in this work because it simulates some hadrontherapy lines, including CATANA (Section 2.1.1), where some experiments have been done. Building an application starting on this example permits to reproduce in a reliable and validated way the experimental conditions in which data have been taken, and therefore help understanding the physical processes behind the effect registered.

### 4.5.1 Geomtery

In Hadrontherapy through some simple macro commands different lines can be simulated. In particular, today available lines to simulate are:

- CATANA passive proton beam line,
- passive carbon beam line of INFN-LNS synchrotron,
- a laser-driven beam line with a Faraday Cup.

Considering CATANA in particular, each element of the experimental beam line is simulated in detail. In Figure 4.4 a sketch of the geometry is reported.

### Modulator

The modulator rotation in Hadrontherapy is simulated through a loop in different runs: the interface asks the user to set a number of events to be simulated for *every step of the modulator*, i.e. if the user sets 1000 particles the simulation will run 1000 particles with the modulator in a given position, then rotate the modulator of one degree and simulate another 1000 particles. This will be repeated 360

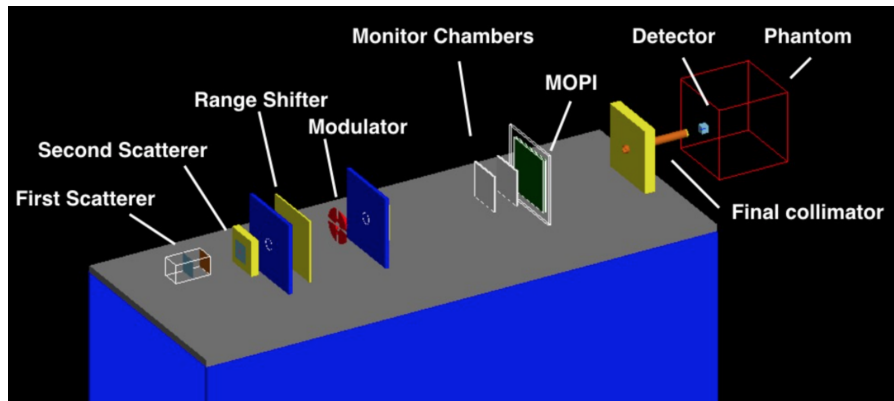


**Figure 4.4:** An image showing hadrontherapy simulating CATANA line in all its parts. It can be obtained running Hadrontherapy in Geant4. Different elements have been labelled according to their description in Section 2.1.1

times, until the modulator is once again at its starting position.

## Detector

Besides the beam line, this application permits to simulate a water tank after the transport line with a voxelized detector inside. A voxelized detector is a sensitive detector divided in boxes (that are called voxels), and every voxel works as a different detector. The user can set its overall dimensions and also the voxel dimensions, with the constraint that the detector must be fully coverable in voxels, i.e. their dimension must be exact divider of the detector ones.

This structure permits the study of the beam in different points along the SOBP: if voxels are chosen to be vertical slices of the detector, i.e. planes perpendicular to the beam direction, the user can study how the beam changes while entering in the simulated water tank.

The voxelized detector inside Hadrontherapy permits to retrieve information about the particles at different levels: energy, particle type, position, direction, and so on along the SOBP. By default a file containing dose for every voxel is saved, but some algorithms permit also dose averaged  $LET$  (for every particle and mean one) estimate in every voxel.

In Figure 4.5 an example of the SOBP simulated with Hadrontherapy can be seen. This graph is obtained plotting the output of this application.

## 4.5.2 Primary Generator

The simulation starts with protons generated in vacuum before the first scattering foil. Particles momentum is randomized according to beam characteristics: position and direction are randomized in a gaussian way and same happens for particle energy. Parameters has been set up according to a long validation process that lead the simulation to realistic fit the experimental data [56].

## 4.5.3 Physics

Hadrontherapy can easily load *physicslists* with different modules. The standard *physicslist* uses the following modules, and their full description can be found in Geant4 *physicslist* reference manual [50]:



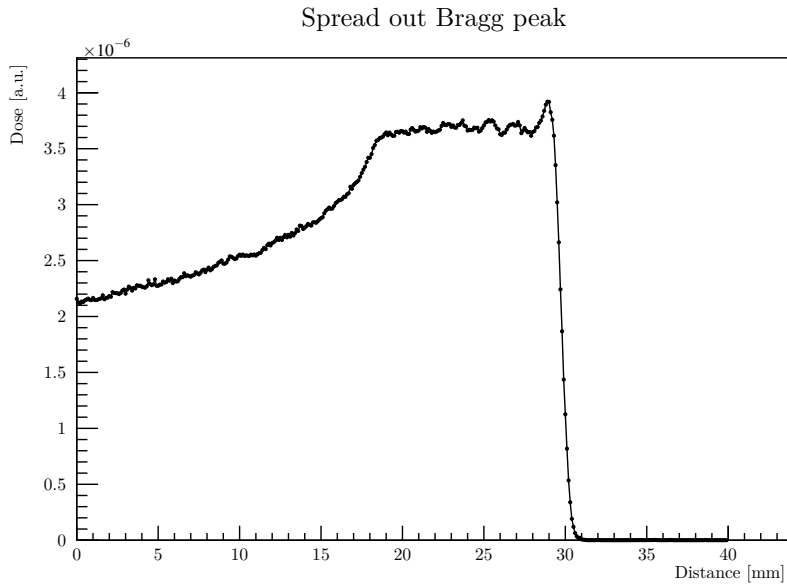


**Figure 4.5:** *Simulated SOBPs with hadrontherapy. It can be easily obtained by plotting one of the output files of the application.*

- G4DecayPhysics for unstable particles decay;
- G4RadioactiveDecayPhysics for the decay of radioactive ions;
- G4IonBinaryCascadePhysics for interactions between ions;
- G4EmExtraPhysics for electromagnetic processes;
- G4HadronElasticPhysicsHP for elastic interactions between hadrons;
- G4StoppingPhysics for nuclear capture of particles with negative charge;
- G4HadronPhysicsQGSP\_BIC for hadronic inelastic interaction;
- G4NeutronTrackingCut to enter neutronic cuts;

the user can also select another *physicslist* with different modules.

## 4.6. Hadr03

Hadr03 is one of the extended examples in Geant4 and it was developed to check the hadronic cross section for different *physicslists*. It was used to compute the proton-boron fusion cross section loaded in Geant4. That cross section was later compared with experimental one and the one calculated by TALYS.

The idea of this application is to calculate the cross sections using the mean path of the particle before its interaction. To compute analytically this mean value the Equation 1.4 must be used. It was described as the number of particles after the width  $x$ , but can be interpreted as distribution of the track lengths. Therefore, the mean of this variable can be computed by integrating this function and dividing it by the number of simulated particles:

$$\bar{x} = \frac{1}{N_0} \int_0^{\infty} N_0 e^{-n_x \sigma x} dx = n_x \sigma$$

---

and knowing the mean path the cross section can be estimated as:

$$\sigma = \frac{1}{\bar{x}n_x} \quad (4.1)$$

this is the purpose of this example: the user can study a hadronic interaction computing the mean free path.

Note that Geant4 groups processes in categories: for example, the process *hadronic inelastic interaction* will be the sum of all hadronic inelastic processes, and therefore this is the one that can be computed using this example, not single hadronic inelastic channels.

### 4.6.1 Geometry

Geometry of Hadr03 is really simple: a box of a material chosen by the user. Also box dimensions can be set. In order to calculate cross sections, this box should be *semi-infinite*, i.e. all particles should interact inside the box and no transportation process to the *out of the world* region should occur. If this happens, the cross section is going to be biased.

### 4.6.2 Primary generator

The user should set the particle that will be generated and its energy depending on the cross section study. Particles are then generated on the box surface with momentum direction perpendicular to the face itself. They are generated on one face to maximize the material before reaching the geometry border, and their position is randomized because each particle is meant to be independent from the previous and from the following one. Nothing would change if all particles were shot from the same place, but randomized point help the visualization.

### 4.6.3 Physics

Physics must be set by the user, as the purpose of this application is exactly to study different physics models. The only constraint is that there should be no *AlongTheStep* process loaded: a process statistically treated that does not have an exact point for interaction cannot be studied using this example, and its presence would bias the study of standard *PostStep* processes happening at given points in space.

### 4.6.4 Output

As this example goal is to calculate hadronic cross section, some quantities are printed on the terminal for every process at the end of the simulation:

- the mean free path  $\bar{x}$  with its uncertainty;
- the massic free path  $\bar{x}_m$  (the mean free path multiplied by the density of the medium) with its uncertainty;
- the total cross section (the cross section multiplied by the numerical density of the medium, equal to the slope of the exponential in Equation 1.4) with its uncertainty
- the cross section with its uncertainty;
- the reference cross section loaded inside Geant4 (depending on the *physicslist* used)

---

Moreover some quantities correlated to different reactions are printed:

- the list of nuclear reactions with their yield and Q-value without counting the number of gamma at each reaction;
- the list of generated particles with their mean, minimum and maximum energy;
- the overall momentum balance to check for errors.

These data get corroborated by some histograms as well:

- kinetic energy of all scattered particles;
- kinetic energy of all gamma rays;
- kinetic energy of all neutrons;
- kinetic energy of all protons;
- kinetic energy of all deuterons;
- kinetic energy of all alphas;
- kinetic energy of all nuclei;
- kinetic energy of all mesons;
- kinetic energy of all baryons;
- Q-values of different reactions occurred;
- momentum balance for every event;
- atomic masses of produced nuclei;

In Figure 4.6 an output example can be seen.

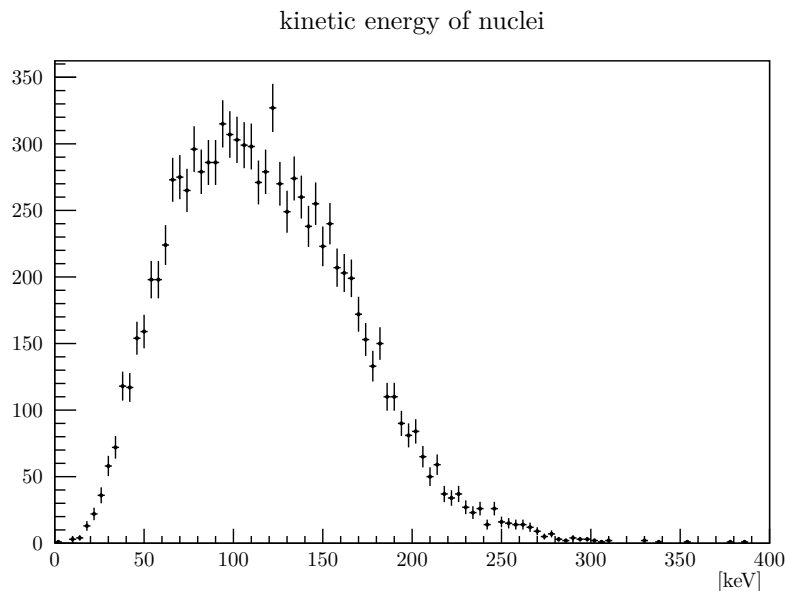


**Figure 4.6:** An example of Hadr03 output: distribution of kinetic energy for all nuclei generated. Here 10000 protons with an energy of 10 MeV were shot in a box of  $^{98}\text{Mo}$ .



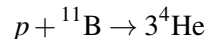
# Chapter 5

## Computational results

Here the results obtained in this work thanks to computational tools described before will be discussed and analysed. Sometimes the process that leads to these results was a *trial by error* process, but here only the last and best working version of the programs will be presented.

This section is divided in *phases*: first some preliminary issues are presented, then programs written are presented and discussed together with their results, and if needed also validation of the method is computed. The goal of this work is to achieve some primitive results on *modelling* of PBCT technique, i.e. understanding *if, how* and *why* it may work.

This means, practically, to find out whether proton-boron fusion is really the one responsible for lethality increment due to boron introduction as found in Section 3. Here this reaction is reported for clarity:



An example of what could be done to achieve this goal is:

- compute the right cross section for alpha particles creation and implement a simulation tool with it;
- compute the right energetic spectrum for alpha particles and implement a simulation tool with it;
- study the effect of other generated particles thanks to the presence of  ${}^{11}\text{B}$ ;
- study the effect of generated particles thanks to the presence of  ${}^{10}\text{B}$ ;
- fully simulate experiments in a reliable way;
- compute the realistic LET increase due to alpha particles presence;
- compute DMF using models relying on LET.

This work focused mainly on the first point, but nevertheless touched the others.

### 5.1. EXFOR

EXFOR [28] is a database created and kept updated by the *Nuclear National Data Center* (NNDC) and groups experimental data of nuclear reactions. The interface allows the user to freely access to data using simple constraints on the nuclei and the physical quantity studied. Information can be given about the target, the reaction channel, the products created and the energy. The database

---

contains cross sections, differential cross sections, angular distributions, production yields, secondary particles correlations and many other quantities.

Here it has been used to obtain alpha particles cross section, plotted in Figure 1.10.

## 5.2. The ${}^8\text{Be}$ problem

When comparing simulations and analytic calculations to reality, the case of  ${}^8\text{Be}$  must be taken in account: sometimes the computer finishes his result telling the user that one of the output particles is a nucleus of  ${}^8\text{Be}$ . In physical experiments like the one described in Section 3, by the way, this nucleus is never seen because it decays really fast. Lifetime can be found in literature [57]:

$$\tau = 0.97_{-0.19}^{+0.32} \cdot 10^{-16} \text{s}$$

so it instantly decays in a pair of  $\alpha$  particles. This nucleus is approached in different ways in Geant4 and in TALYS.

In Geant4 its treatment depends on the *hadronic physicslist* used: according to the developer manual [46] Geant4 does not track particles with lifetime lower than  $10^{-15}$ s, so it should never create these particles but create directly a pair of alphas, but some hadronic models create these nuclei. This means that the user has to manually interpret them as a pair of alphas: in fact, for example, in *energy span* program described in Section 5.4 tracks are destroyed after the first interaction, so the eventual  ${}^8\text{Be}$  will not decay and will not be counted correctly as a pair of alpha.

TALYS treatment is different: it does not consider at all of  ${}^8\text{Be}$  decay and registers it like any other recoiled nucleus, therefore its decay must be taken into account manually.

## 5.3. TALYS application

TALYS has been used to obtain a reference cross section for alpha particles production. The following input was given, in order to obtain cross sections and spectra, as well:

```
1 #
2 # General
3 #
4 projectile p
5 element b
6 mass 11
7 energy CATANA_energies
8 #
9 # Output
10 #
11 channels y
12 filechannels y
13 outspectra y
14 outcheck y
15 outdiscrete y
16 recoil y
17 filerecoil y
18 filespectrum n p d t h a
```

We will briefly describe any of these commands:

- 
- `projectile p`: to set up the projectile to be a proton;
  - `element b`: to set up the target material to be boron;
  - `mass 11`: to set up the target mass number to be 11;
  - `energy CATANA_energies`: to set up incoming protons energies: the file `CATANA_energies` is a file containing a list of energies where every row is a different energy going from 0.1 to 62.5 MeV with steps of 0.1 MeV each. With this command, TALYS will calculate cross sections and spectra for every step written in that file;
  - `channels y`: to switch on channels: when this command is active the program calculates and output all exclusive reaction channel cross sections, like for example (p,p) or (p,n);
  - `filechannels y`: to switch on saving of channels cross sections in different files: all exclusive reaction channel cross section is saved in a different file as a function of energy with name `xsNPDTHA.tot`, where  $N$  is the number of neutrons in the outgoing channel,  $P$  stands for proton,  $D$  for deuteron,  $T$  for tritium,  $H$  for  $^3\text{He}$  and  $A$  for  $\alpha$  particle. These particles are the only *ejectile particles* treated in the outgoing channel by TALYS. Other particles are referred to as *recoils*;
  - `outspectra y`: to switch on saving of ejectile spectra: for each different energy a different file named `spNPDTHAEYYYY.YYY.tot` is written, where  $Y$  is the energy of the incoming particle. It contains the incident energy and 6 columns, with the spectra per outgoing particle type;
  - `outcheck y`: to switch on some numerical checks along the calculation;
  - `outdiscrete y`: to switch on the output of cross sections to each individual discrete state;
  - `recoil y`: to switch on recoil study: when this command is active the program calculates and output data about recoiled nuclei;
  - `filerecoil y`: to switch on saving of recoil spectra in different files: for every incoming particle energy and for every; recoil a different file is saved with name `recZZZAAAspecYYY.YYY.tot` where  $Z$  is the atomic number of the recoil,  $A$  is its mass number and  $Y$  is the incoming particle energy;
  - `filespectrum n p d t h a`: to switch on spectrum of all ejectiles, a new file will be written for every outgoing particle and every incoming particle energy with name `XspecYYY.YYY.tot` where  $X$  is the ejectile and  $Y$  is incoming particle energy;

Looking at the commands given to TALYS it can be understood that calculations were concerning both cross sections study and spectra one. The complete description of all these commands, together with the description of all commands TALYS can receive as input, can be found in TALYS manual [55].

About cross sections, they have been read and studied *channel by channel*: any reaction with given products had a given cross section that could be read in a file written thanks to `filechannels y` command. This allowed both the study of single channel cross section and particle production cross section.

The spectra, moreover, can be useful to calculate radiobiological quantities that can try to interpret experimental results. One of the limitation of TALYS is that spectra cannot be bound with reactions: the reaction cross section is available, the particle spectra is available, but spectra due to specific reactions cannot be computed. Therefore while alpha production cross section can be computed through sum of single channels, spectrum cannot be computed starting from single reactions but need to be taken *in toto*.

In later sections a small validation of TALYS calculations will be done and the results of this application will be described and discussed.

---

## 5.4. Energy span

Energy span is a Geant4 based application starting from a modified version of the Hadr03 extended example (described in Section 4.6). It uses Geant4 to simulate events and obtain histograms related to the *physicslist* used and ROOT to analyse those data.

### 5.4.1 Cross section uncertainty

In Hadr03 the cross section is computed through a mean of track lengths. Looking at the laws defining cross section, track lengths are not supposed to be distributed in a way such that all values float around a mean value, but they are sampled according to an exponential distribution, shown in Equation 1.4. Therefore using only its mean value to compute the cross section, the uncertainty calculated as the dispersion of the sample is going to be high and not reliable. Knowing the shape of the track lengths distribution, fitting is a more accurate way to estimate the cross section and its uncertainty.

This issue has been solved adding a histogram with track lengths that is later fitted using a ROOT macro, and the numerical density has been added as an output of the Geant4 simulation, as it is needed by the ROOT macro to compute the cross section. This way, the cross section obtained has a reliable uncertainty, and the convergence is achieved also with a smaller number of events simulated. Besides, by fitting the curve, the problem of the semi-infinite detector can be solved: if the detector is not big enough to make all the particles interact, even though some computational power will be wasted, the cross section will not be biased. In Figure 5.1 an example of a fitted histogram is reported.

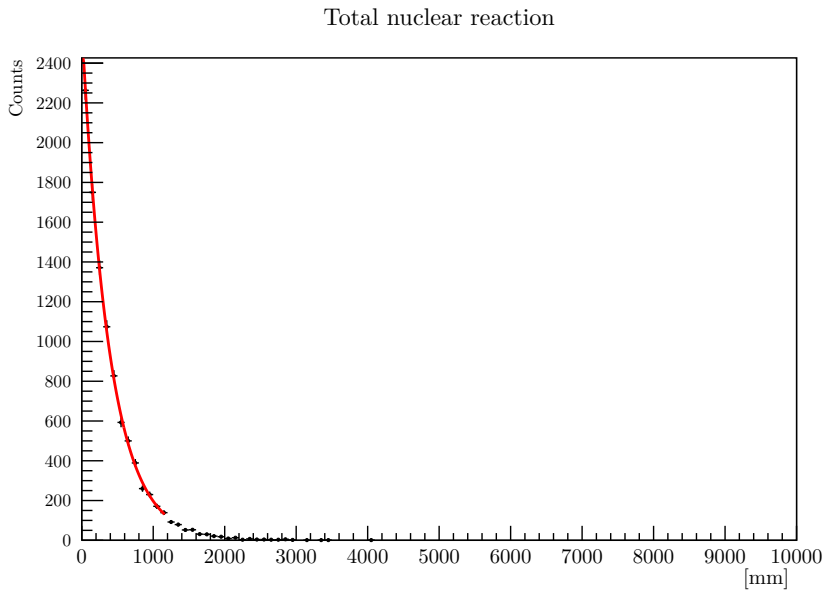


**Figure 5.1:** Example of an exponential fit of track length to compute the cross section. As will be clarified later, this really is just a projection of a bidimensional graph, where counts are function of track length and incoming proton energy (here 140 MeV).

### 5.4.2 Process cross section

As described before, Hadr03 computes cross sections for *group of channels*. This means that for hadronic inelastic processes the cross section computed does not refer to single channels, like having a given particle as an ejectile. This does not permit an easy comparison with TALYS calculations, and makes it hard to understand how the proton-boron fusion is loaded inside Geant4 and therefore



which hadronic model is the best and whether it is realistic or not. Some outputs have been therefore added to the simulation and later analysed.

In particular the concepts explained in Section 1.7.3 have been exploited. If the only process available is the hadronic inelastic, and there are more channels available, then the distribution of the track lengths, when fitted, will give the sum of the cross sections of all available channels of hadronic inelastic processes. In order to obtain the cross section for a given channel, also the number of events undergoing that exact channel is needed. Thus, if  $\sigma$  is the fitted cross section,  $N_i$  is the number of particles that have undergone the channel  $P_i$  and  $N_{\text{tot}}$  is the total number of particles that did a hadronic inelastic process, the cross section of that channel can be obtained as:

$$\sigma_i = \frac{N_i}{N_{\text{tot}}} \sigma \quad (5.1)$$

this can be seen substituting the expression for  $N_i$  given in equation 1.9.

Therefore, to obtain cross section for a given hadronic inelastic channel, at first only inelastic hadronic reactions must be loaded (i.e. only that module is present inside the *physicslist*), then the number of particles undergoing a given process is saved and later used together with the track lengths histogram to compute single channels cross sections, easy comparable with TALYS application results.

### 5.4.3 Fixed energy

Hadr03 works with a fixed energy: an energy value is chosen and the cross section is computed for that incoming particle energy in the laboratory frame. It would be faster to have a program giving the cross section as a function of energy, without needing to restart the program for every energy point chosen. Then some deep modifications of the application kernel have been implemented in the energy span application we have developed. In particular, the possibility to change energy along a single run has been entered, through the command `\energySpan\setEnergySpan` able to activate a routine to study different energies at fixed distance one from the other. For example, if the following line is included in a macro:

```
1| \energySpan\setEnergySpan 1 10 MeV 10
```

Program will span the energies between 1 and 10 MeV with 10 steps, i.e. the energy of the incoming particle will be set to 1 MeV for the first particles, then will be changed to 2 MeV and up to 10 MeV. The number of particles simulated for each energy depends on the number of total particles set: if the simulation is set to run for a given number of particles  $N$ , the energy will be changed every  $N/N_{\text{steps}}$  particles, so that more or less the same number of particles will be simulated for each energy.

Because of this upgrade, also the outputs of the simulation need to change:

- the histogram of the track lengths becomes a bidimensional histogram, where the number of events is a function of track length and energy of the incoming particle. By slicing this histogram the unidimensional histogram needed for cross section computation can be obtained;
- the number of particles undergoing a given channel becomes a histogram, where the number is a function of incoming particle energy. By using the bin contents of this histogram the number of particles undergoing a given reaction can be obtained.

In Figure 5.2 some output histograms can be seen: both the bidimensional and a unidimensional one. These are the main outputs of the *energy span* Geant4 application.

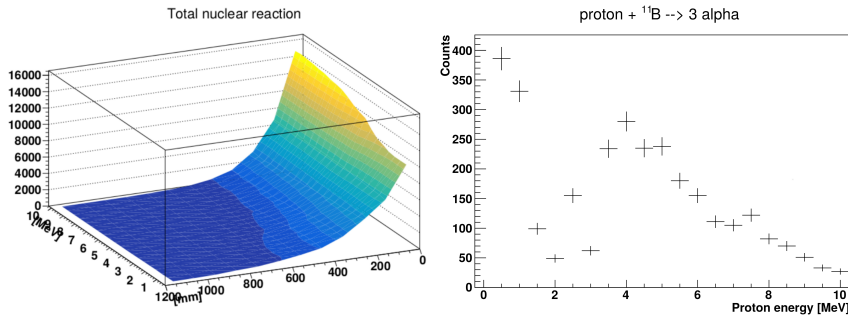


**Figure 5.2:** Example output of the Energy span application. In the unidimensional histogram counts for a given channel are a function of incoming particle energy, while in the bidimensional one counts for all channels are function of the incoming particle energy and track length.

Moreover, of course, the ROOT analysis program has been changed to work with these data for varying energy, and produce a graph of the channel cross section as a function of incoming protons energy.

#### 5.4.4 Different cross sections

The analysis program can work in two ways to compute different types of cross sections for debug and analysis.

In the *single channel mode* the standard cross section is calculated. The program for every energy point slices the bidimensional track length histogram and fit it to compute the sum of cross section for that energy and the total number of interaction (obtained through integration), and then loops among the unidimensional histograms until he finds the one with the title equal to the channel studied. Then uses Equation 5.1 to compute the cross section for every energy. This routine is repeated until a graph with cross section as a function of incoming particle energy is created.

In the *production mode* the production cross section is calculated. The routine is exactly like the one in single channel mode, the difference is that while in the latter the loop stops after the channel is found, in this mode the loop does not end but keeps on running until all histograms have been analysed. This is because in this mode we are not asked to set the reaction, but a particle that is going to be studied. Also some aliases can be used (for example to solve the beryllium problem explained in Section 5.2 i.e. considering a  $^8\text{Be}$  like a pair of alpha particles). In order to compute the product cross section, the program sums the bins of histogram describing a reaction where the particle has been produced, each multiplied by the multiplicity of the particle in that given reaction, and then, according to Equation 1.5 computes the production cross section for a given energy as:

$$\sigma_p = \frac{\sum_i N_i n_i}{N_{\text{tot}}} \sigma \quad (5.2)$$

where  $N_i$  is the bin content and  $n_i$  is the multiplicity.

### 5.5. Hadrontherapy with CR39

Another Geant4 application has been written, and this was based on the Hadrontherapy example, described in Section 4.5. It has been written to simulate the optimal number of protons and the optimal position to try and see a good amount of alpha particles using the CR39 detectors described in Section 2.4. Hadrontherapy example was used as the experiments were performed in CATANA facility, and that example already simulates all the elements of the beam transport. The geometry

---

has been changed, removing the voxelized water tank with the detector and entering the CR39. The material of the detector is already defined in NIST database while PMMA and boron captate (with the stoichiometric ratio of 2.5 to 1) have been defined manually.

The default geometry shows a CR39 detector with PMMA and boron captate, but the type of the detector can be easily changed (i.e. entering different inert material before or after the converter) with the simple command `CR39/CreateType n` where  $n$  is a number referring to different detectors. Also the thickness of material in front of the detector itself, and the detector size itself can be changed through the use of other commands such as `/CR39/CR39Size` or `/CR39/BoronCarbonateWidth`. The application internally builds the CR39 with physical constraints (the transverse dimensions of the boron carbonate layer, for example, must be equal to the ones of the CR39), allowing to easily change parameters.

The detector sensitivity is built to simply save in an external text file all the particles reaching the CR39. This way, after the simulation, the number of alpha particles can be computed (as will be described later) and compared to the signal noise (taken as the number of protons with energy below 5 MeV).

Moving the detector along the beam axis and inserting water depth before allows to study which position of the SOBP is the best to see some alpha particles due to boron presence.

## 5.6. TALYS results

Results obtained with TALYS application (described in Section 5.3) are showed and discussed here. In particular, even if this program allows a deep study on many reactions with a lot of different particles in a biological environment, the reaction of protons on  $^{11}\text{B}$  is the one that has been studied so far, as it is the one considered responsible of the increased DMF experimentally found.

### 5.6.1 Alpha production cross section

Alpha particles production cross section is one of the outputs of the application, and this output can be seen in Figure 5.3 where all channels are present. In that plot the dominant channel for alpha production for low energies is the  $\alpha + {}^8\text{Be}$  channel, nevertheless its cross section goes to zero at about 80 MeV, and for energies higher than about 12 MeV other channels open up, and the total production cross section does not decrease as the channel one. Other channels include the *prompt breakup* in three alpha particles (mostly negligible), and creation of alpha with lighter particles like protons or neutrons, and creation of  ${}^8\text{Be}$  with, for example, ejection of a triton and a proton. These channels have not been reported in the legend for clarity.

This graph has been obtained considering the multiplicity of single reaction channels and taking into account the *beryllium problem* (Section 5.2).

The calculation of this cross section permitted a *validation* of TALYS, computed comparing experimental data available and TALYS calculations. But these data are calculated differently: whereas TALYS production cross section has been calculated considering the contribution of all channels producing at least one alpha particle (or a  ${}^8\text{Be}$ ), experimental data available only refer to the  $(p,\alpha)$  channel. TALYS validation has been therefore done considering only  $(p,\alpha)$  channel *cross section* (in green) and without entering the multiplicity factor instead of total alpha production cross section, i.e. comparing the *channel cross section* instead of the production cross section exhibited in Figure 5.3.

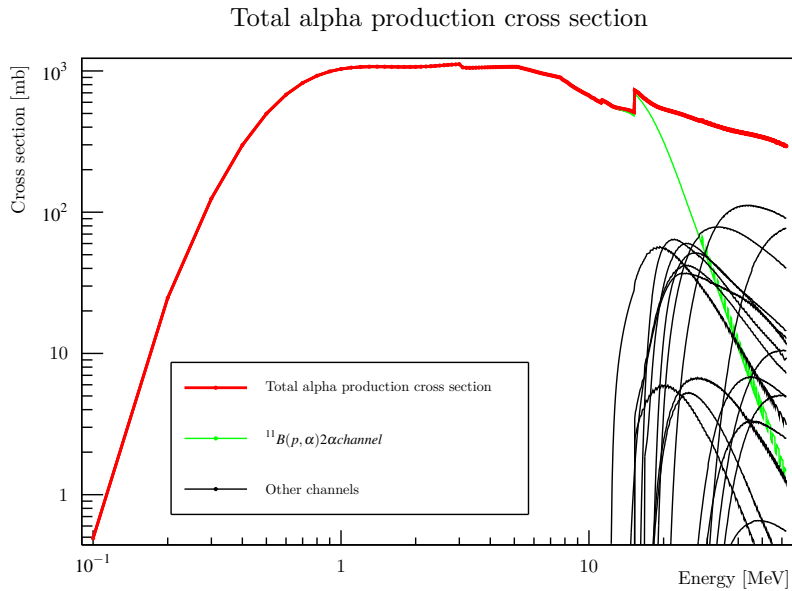


**Figure 5.3:** Alpha production cross section calculated using TALYS. Up to 12 MeV only the proton-boron fusion creates alpha particles, while for higher energies other channels open up.

In Figure 5.4 all experimental data available (also reported in Figure 1.10) are plotted together with  $(p, \alpha)$  channel cross section.

- the two channels of experimental data ( $\alpha_0$  and  $\alpha_1$ ) do not need to be taken both into account: the  $\alpha_1$  with lower cross section is negligible. Therefore, for TALYS validation, it is better to use only the higher one and erase lower data, as they are at least a factor 5 smaller than the higher ones;
- TALYS calculation below 1 MeV is poorly reliable as it does not include the resonance cross section at about 675 keV. This resonance is particularly important for PBCT application and therefore must be taken into account somehow;
- above 3.85 MeV experimental data mess up: the two channels are not distinguishable anymore and cross section is really far from TALYS one;
- between 1 and 3.85 MeV TALYS cross section is slightly higher than experimental one.

An estimation of *how poorly* TALYS describes this reaction has been done choosing to neglect data below 1 MeV as TALYS does not calculate very well in this range, and data above 3.85 MeV as experimental data are not reliable. Then an integral of the cross section has been computed and the two integrals have been compared. The region chosen for the integral can be seen in Figure 5.5.

For integral computing, closest data have been linearly fit. Integration results are:

$$\begin{aligned} \text{TALYS integral} &= 1020 \text{ MeVmb} \\ \text{experimental integral} &= 460 \text{ Mevmb} \end{aligned}$$

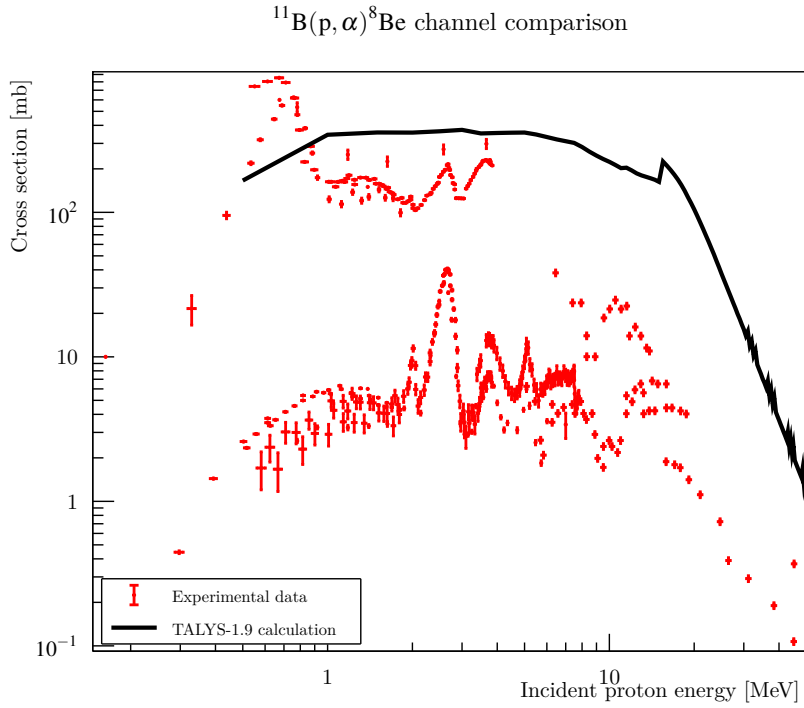


**Figure 5.4:**  $(p, \alpha)$  cross section calculated with TALYS and experimental data. The two channels refer to different excitation of the  $^8\text{Be}$  and are called  $\alpha_0$  (the higher) and  $\alpha_1$  (the lower), and the latter can be neglected. Below 1 MeV TALYS description is not reliable, while above 3.85 MeV experimental data are not clear anymore.

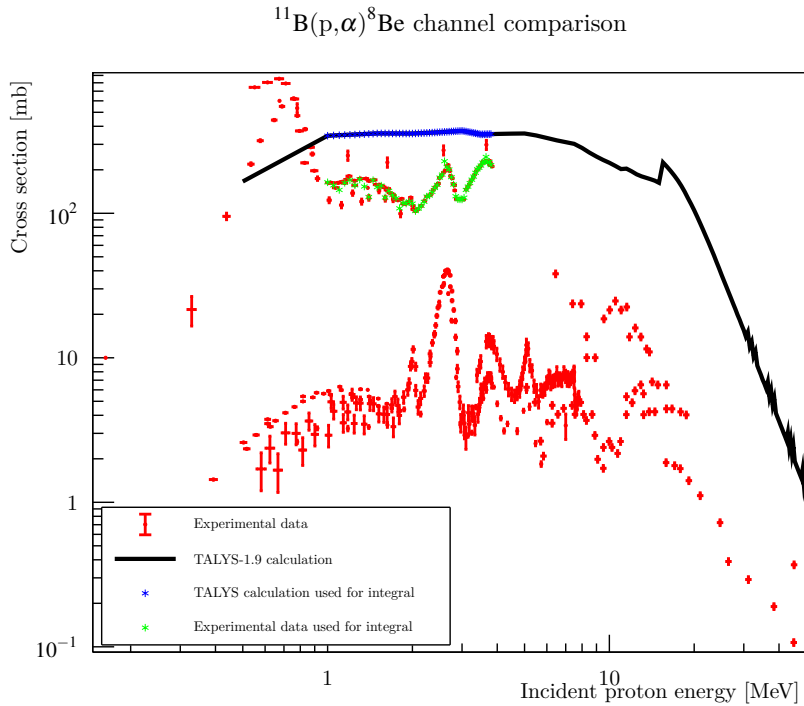


**Figure 5.5:** Data and calculations used for integral computing (see the text for more details).

## 5.6.2 Alpha spectrum

The spectrum of outgoing alpha particles has been computed as well and it is shown in Figure 5.6. As stated before, while for cross sections the total production can be computed as the sum of single channels ones, the spectrum needs to be taken as is and cannot be deconvoluted in its primary sources. Alpha particles spectrum is presented in a bidimensional histogram where cross section is shown as a function of alpha particles energy and incoming proton energy. Calculating then the projection of this histogram along the proton energy axis the alpha spectrum for protons with a fixed energy can be seen.

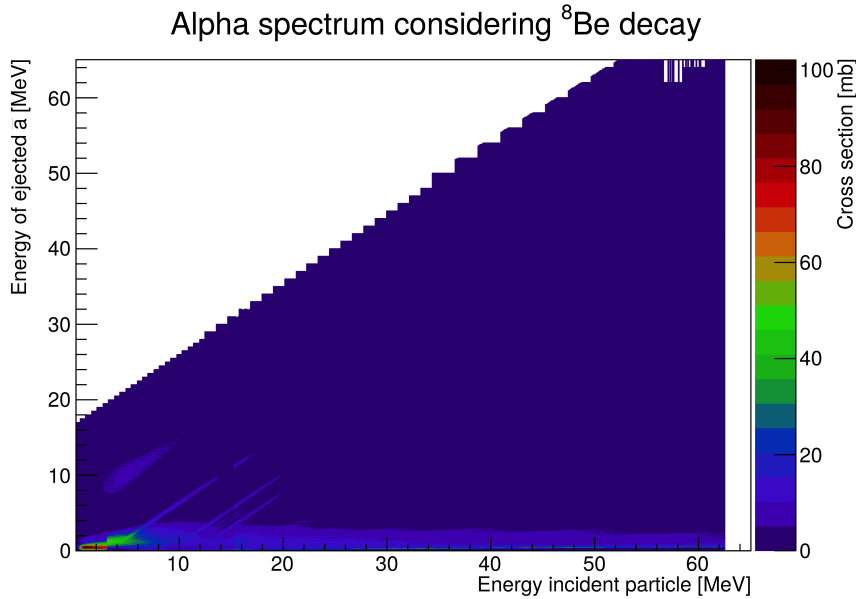


**Figure 5.6:** *The spectrum of alpha particles generated with protons on boron. See the text to understand how  $^8\text{Be}$  has been treated.*

$^8\text{Be}$  has been treated in a naive way to be included in this graph: instead of sampling the energy distribution for its breakup, the Q-value was neglected and alpha particles created shared half of the energy of the beryllium. Moreover, a rebinning operation was necessary to make the graph readable: TALYS creates some standard energetic bins that, while plotted, tend to create some blank space among them. Data have therefore been rebinned uniformly.

It can be seen that TALYS sampling creates some spots where spectrum changes a lot (like for example for proton energy equal to 3 MeV as can be seen in Figure 5.6). Moreover, from TALYS perspective, it is clear how *relatively high energy* alpha particles are created only in the  $(p, \alpha)$  channel: in fact for energies higher than 12 MeV alpha spectrum is peaked for really low energy alphas, while below a peak can be seen for slightly more energetic particles.

Integration of this spectrum for fixed proton energy permitted to check if it was compatible with the cross section found in the last section. If everything has been done correctly, the integral should give the production cross section. This test has been done and the result can be seen in Figure 5.7: the two estimates are more or less equal, despite some small differences probably due to approximations and rebinning.

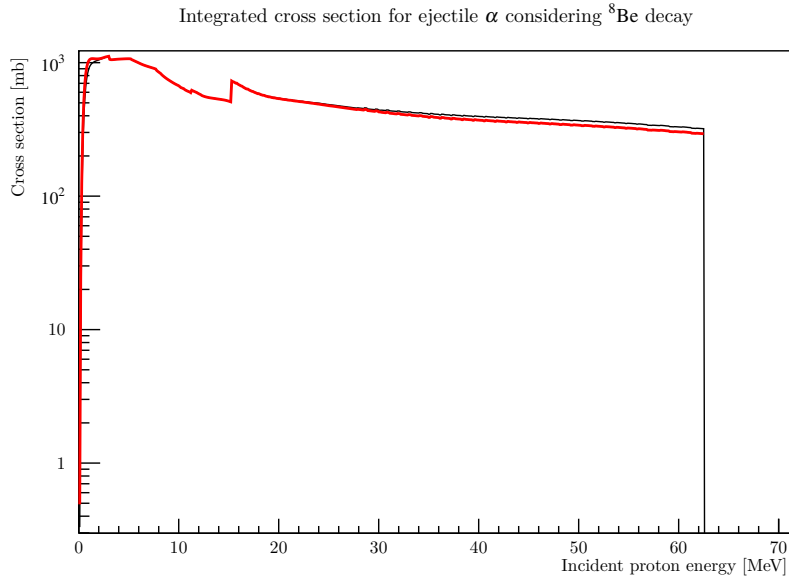


Figure 5.7: Comparison between integrated spectrum and standard cross section calculation.

### 5.6.3 Other particles

The calculations presented for alpha particles have been repeated also for the other particles created thanks to  $^{11}\text{B}$  presence. This was done because killing potential enhancement could be due to other high-LET particles created, and not only alpha particles. For example, in Figure 5.8 the cross section for the production of the isotope  $^6\text{Li}$  is shown, while in Figure 5.9 the particles spectrum can be seen. This has been done for *every particle* produced by the interaction of proton with boron, and data are waiting for further analysis.

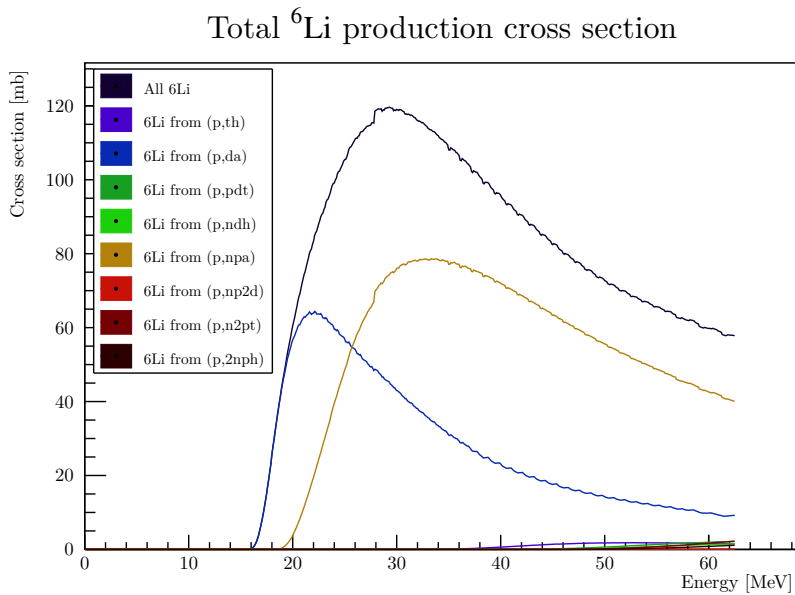


Figure 5.8: Cross section for  $^6\text{Li}$  production with proton- $^{11}\text{B}$  reactions through various channels.

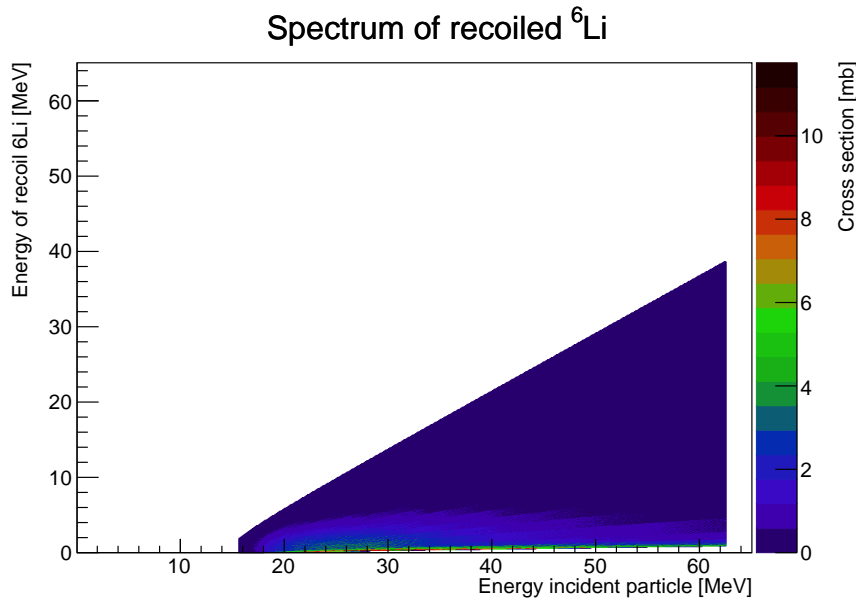


Figure 5.9: Spectrum of produced  ${}^6\text{Li}$  through various channels.

### 5.6.4 Future perspectives

Other work can yet be done using the program written. First, the alpha spectrum should be fixed considering a more realistic split of the  ${}^8\text{Be}$ , and then it should be interpreted, understanding which spectra are calculated by TALYS. Then these spectra should be compared to data in literature, as it has been done with cross sections: a validation approach may lead to understanding if TALYS is reliable also for calculating energetic spectra or not. This validation routine will have to take into account all alpha generating reactions as TALYS spectra do not divide data according to different channels.

Moreover all particles created should be studied, both from interaction with  ${}^{11}\text{B}$  and interaction with other nuclei present in the experimental flask, such as  ${}^{10}\text{B}$ , oxygen, hydrogen, carbon and so on. This may reveal a non neglectable cross section for high LET particles different from the alphas meant to enhance protontherapy. Nevertheless the enhancement could be due to the interaction between a *generated particle*, like a neutron obtained from interactions between protons and water, and an isotope like  ${}^{10}\text{B}$ , and so on. Also these reactions should be studied with TALYS and compared to experimental data to check whether their effect is neglectable or not.

## 5.7. Cross section

The *goal cross section* was taken as the alpha production cross section to introduce inside Geant4 to simulate the experiments where PBCT has been studied. This cross section relied mainly on *experimental data* and on *TALYS calculations* where experimental data were not available or not reliable. In particular, the  $\alpha_0$  channel of experimental data was taken below 3.85 MeV, while above TALYS calculation has been used, as displayed in Figure 5.10.

It is hard to couple this cross section with an uncertainty: experimental data have a mean uncertainty of the order of 1.2%, and are therefore very precise. Nevertheless, they do not completely agree and even for close energies data taken from different experimental campaigns look not compatible. Therefore an estimate of the uncertainty of this cross section should be higher than the 1.2% readable in



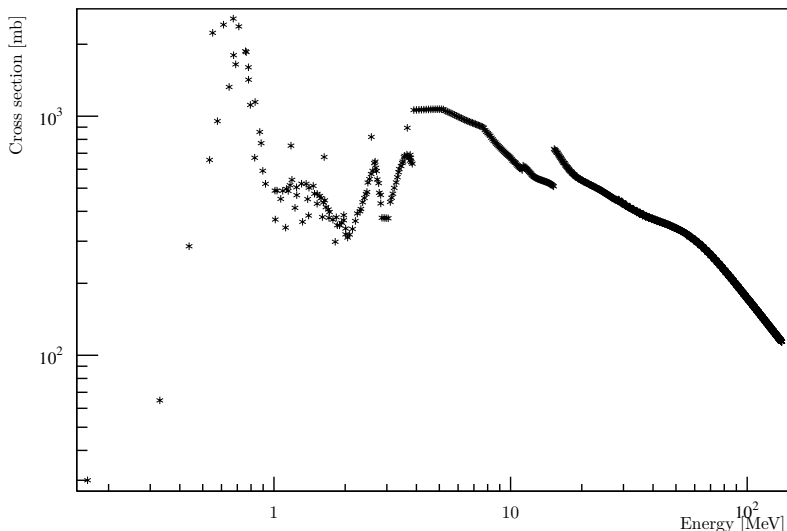


**Figure 5.10:** *Goal alpha production cross section made up of experimental data where available and TALYS calculation elsewhere.*

each reference. Concerning TALYS, its modelling of course enters some errors, as can be seen from its validation (Figure 5.5), where a difference of about a *factor 2* was noticed when comparing experimental data and TALYS calculation.

This means that the cross section estimate is just an *order of magnitude* of the cross section, as there are not enough tools to do a better estimate.

## 5.8. Physicslists study

The main part of this work focused on the study of *physicslists* inside Geant4, and it was done thanks to the Energy span application we wrote. First, a validation of this application was necessary.

### 5.8.1 Energy span validation

An *internal validation* was done in order to check if the method described in Section 5.4 actually works.

The check has been computed using Hadr03, described in Section 4.6. In order to do that, cross section of *inelastic hadronic processes* has been firstly computed using standard Hadr03 example for different energies, and then it was computed using the *energy span* routine described before. All these tests have been run using proton on  $^{11}\text{B}$  and the same *hadronic physicslist*. The result of this check is shown in Table 5.1. For low energies differences can be seen because the Hadr03 example was not changed at all (only the right material and *hadronic physicslist* were selected), and the semi-infinite detector was not really semi-infinite and therefore cross section computed was biased. This test has been run using 10 thousands particles for every energy in each approach.

Then, looking at Table 5.1 one can notice that energy span results are close to Hadr03 one. Looking at that application, one can see that its estimate is *really close* to what is loaded in Geant4 libraries (as shown at the end of each run), meaning that the estimated cross section is close to loaded one

Energy [MeV]	Hadr03 [mb]	Energy span [mb]	Difference [mb]	Diff %
5.0	32.5	29.6	2.9	9.0
7.5	96.0	98.6	-2.5	2.6
10.0	202.5	197.4	5.1	2.5
12.5	325.7	328.9	-3.3	1.0
15.0	425.1	426.9	-1.8	0.4
17.5	491.2	490.4	0.8	0.2
20.0	502.5	495.9	6.6	1.3
22.5	487.3	490.6	-3.3	0.7
25.0	473.1	461.4	11.7	2.5
27.5	448.8	445.1	3.6	0.8
30.0	429.8	432.0	-2.1	0.5
32.5	416.5	427.6	-11.2	2.7
35.0	402.3	413.8	-11.6	2.9
37.5	384.8	389.4	-4.6	1.2
40.0	375.3	365.9	9.4	2.5
42.5	362.4	356.2	6.2	1.7
45.0	348.6	336.8	11.9	3.4
47.5	333.4	327.3	6.1	1.8
50.0	318.3	315.5	2.7	0.9
52.5	311.1	310.8	0.2	0.1
55.0	294.4	291.9	2.5	0.9
57.5	292.2	287.6	4.6	1.6
60.0	279.7	269.6	10.1	3.6
62.5	275.3	273.3	2.0	0.7
65.0	270.0	269.4	0.6	0.2

**Table 5.1:** Comparison between cross section obtained using Hadr03 application and Energy span, used as validation for the written application.

within statistical uncertainty. Thus energy span routine calculates the same correct cross sections as well, with a systematic error that is below 5%. Considering the number of particles simulated, the two tools for cross section estimations are compatible.

## 5.8.2 Physicslists in Geant4

Physics modules use different models to try and describe its experiments. They can be found in the path:

```
1| geant4-install/include/Geant4/
```

where all Geant4 classes headers can be found. Their builder is the one starting with the string `G4HadronPhysics`. When using Geant4-10.04p02 version, they are the following:

- INCLXX
- NuBeam
- FTF\_BIC
- QGS\_BIC
- QGSP\_BIC

- 
- FTFP\_BERT
  - QGSP\_BERT
  - Shielding
  - QGSP\_BIC\_HP
  - FTFP\_BERT\_HP
  - FTFQGSP\_BERT
  - QGSP\_BERT\_HP
  - FTFP\_BERT\_ATL
  - FTFP\_BERT\_TRV
  - ShieldingLEND
  - QGSP\_BIC\_AllHP
  - QGSP\_FTFP\_BERT

Models overlap in these *physicslists*: in particular, studying the reaction for energies below 100 MeV it was clear how only *four* different models showed different results. Here these models are briefly described. For a more complete description of *physicslists*, the physics reference manual should be consulted [50].

*Binary cascade model*, referred to as BIC, is a model where interactions are between a primary or secondary particle and an individual nucleon of the nucleus. Propagating of particles in the nuclear field is done by numerically solving the equation of motion. The cascade terminates when the average and maximum energy of secondaries is below threshold. The remaining fragment is treated by pre-compound and de-excitation models.

*Bertini intranuclear cascade model*, referred to as BERT, includes excitons, a pre-equilibrium model, a nucleus explosion model, a fission model, and an evaporation model. The main idea is that as in particle-nuclear collisions deBroglie wavelength of the incident particle is comparable (or shorter) than the average intranucleon distance, hence a description of interactions in terms of particle-particle collisions is justified. The steps of this model are summarized as follows:

- the space point where the particle enters the nucleon is selected uniformly over the projected area of the nucleus;
- path length for the projectile is selected according to total cross sections and region-dependent nucleon densities;
- momentum of the struck nucleon, type of reaction and four-momenta of the reaction products are determined;
- cascade proceeds;
- if allowed by Pauli exclusion principle and the energy of the particle is above a threshold, products are transported;
- a non-equilibrium model describes the event after the intra-nuclear cascade.

*Liège Intranuclear cascade model*, referred to as INCL, is a model created to improve the quasi-classical treatment of physics without relying on too many free parameters [58]. At the beginning of the run, momenta and positions of nucleons are determined, with density profiles based on the Hartree-Fock-Bogoliubov calculations. Nucleons then move in a static potential well, and cascade is modeled by

---

tracking the nucleons and their collisions.

*ParticleHP*, referred to as AllHP, is a model using some pre-loaded evaluated libraries like the ENDF6 [59] to determine cross sections between hadrons and spectra of outgoing particles. As this library lead to the best results, its description will be deepened in the next section.

As there are only four models for these energies while there are seventeen different *physicslists* that a user can choose from, more *physicslists* will give the same results as they use the same model in this range of energies for this reaction. This has been proven. In particular, the *physicslists* that give the same results are:

- *INCLXX*
  - INCLXX
- *Bertini cascade*
  - NuBeam
  - FTFP\_BERT
  - QGSP\_BERT
  - Shielding
  - FTFP\_BERT\_HP
  - FTFQGSP\_BERT
  - QGSP\_BERT\_HP
  - FTFP\_BERT\_ATL
  - FTFP\_BERT\_TRV
  - ShieldingLEND
  - QGSP\_FTFP\_BERT
- *Binary cascade*
  - FTF\_BIC
  - QGS\_BIC
  - QGSP\_BIC
  - QGSP\_BIC\_HP
- *ParticleHP*
  - QGSP\_BIC\_AllHP

In Figure 5.11 an example of these *physicslists* output can be seen in alpha production cross section, done thanks to the *energy span* application written. Also the goal cross section discussed before is here reported. In this figure all 17 HPLs has been drawn but as one can easily observe only four can be distinguished because they superimpose each other.

From this figure one can see that no *physicslist* is close to the goal cross section, and therefore there is no model in Geant4 capable to describe this reaction *sufficiently good*, and validation is not possible with these models.

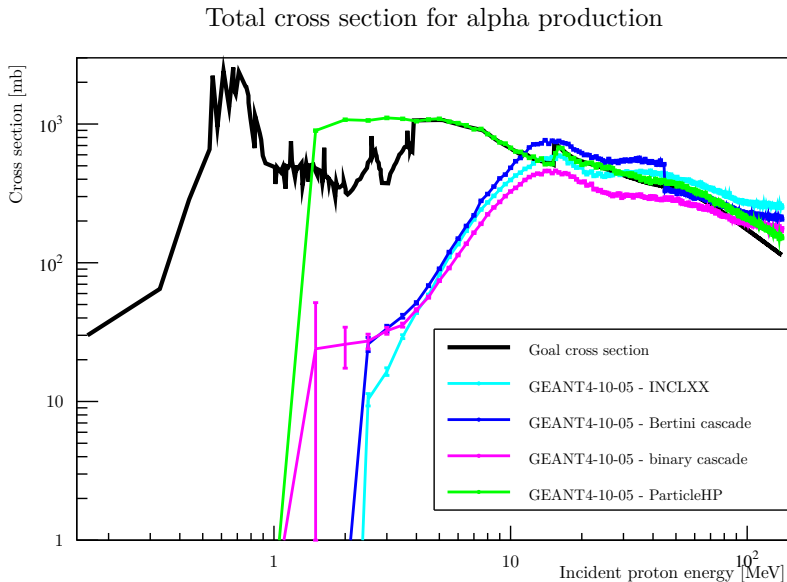


Figure 5.11: A comparison between all Geant4 Hadronic models and goal cross section.

### 5.8.3 ParticleHP

From Figure 5.11 it is clear how, among all possible models, the closest one to cross section is the *ParticleHP*. This model will be the starting point for a reliable description of what happens in PBCT.

ParticleHP is an evolution of the NeutronHP model written in the last decade that adds a description for charged particles. HP stands for *High Precision*, and this model uses experimental cross sections and evaluated calculations to compute cross sections and spectra. It is deeply different from all the others: most of them calculate cross section every time a process may occur while high precision does not calculate cross sections but reads them from a library. This permits to use complicated models without making the simulation too long to run (even if when it is used simulations are slightly longer compared to the use of other *physicslists*). The libraries used are the ENDF-6, and for protons the library used is the *TENDL library*, where TENDL stands for Talys Evaluated Nuclear Data Library. For incoming protons no experimental data are used, but only analytical calculations. This is why this library is the closest to the goal cross section: it uses data produced through calculations done by TALYS, like the goal cross section. Nevertheless, some problems arise when this model is used:

- When TENDL libraries have been written, no data below 1 MeV have been added. This was done because TALYS itself does not describe well what takes place below that energy;
- goal cross section is far different from TALYS one below 4 MeV as it was built using experimental data;

in particular, ParticleHP does not describe well the 675 keV resonance.

These problems have been solved changing the TENDL libraries, creating a *new version of ParticleHP*, able to describe this reaction according to the *goal cross section*. How it has been modified can be found in Appendix A. Before seeing modified version, let us describe how this model works. In particular, there are *two* different run modes, that can be chosen defining an environment variable, named `G4PHP_DO_NOT_ADJUST_FINAL_STATE`. In both cases, the information read from the libraries are mainly three: the cross section, the yield for the creation of a given particle and the angular-energy correlation spectra for the outgoing particles.

If the variable is set to *zero* (or is not set), the *adjust final state routine* is run through the simulation. The cross section is the one read from the libraries, and if the process *hadronic inelastic interaction* is

called (i.e. the simulated range, sampled according to cross section just read, is shorter than all other ranges) an outgoing channel particle is selected, according to particles yield and its energy is sampled according to the spectra read. Selection of particles continues until the *baryonic number* is violated, and adding a last particle there would be more baryons in the outgoing channel than the ones in the incoming channel. Then this last particle is removed, and the last baryons that do not form nuclei in the outgoing channel are set to form a nucleus to keep the baryonic number conservation. This process allows a *small* violation of the baryonic number, i.e. a process with a missing neutron in the outgoing channel is considered a good process (this is mandatory because otherwise it would be impossible or, at least, too much computational time consuming, to conserve both baryonic number and energy just sampling particles).

If it is set to *true*, the *adjust final state routine* is not run. This means that after the process is selected, particles yield and their energies are sampled according to data and not conserving the baryonic number. If libraries contain well written data (as it is), the baryonic number will be conserved *on average*, and some nonsense reactions may occur. This means, for example, that while three alphas will be produced on average, there will be some cases where proton on boron produces only one alpha particle and nothing else, and other cases where 5 alpha particles are produced. In Figure 5.12 this fact can be seen: most reactions do not conserve baryonic numbers, they are conserved only *on average*. This mode does not permit the study of *channel cross section*, many non-physical channels open up, but permits study of *production cross section*.

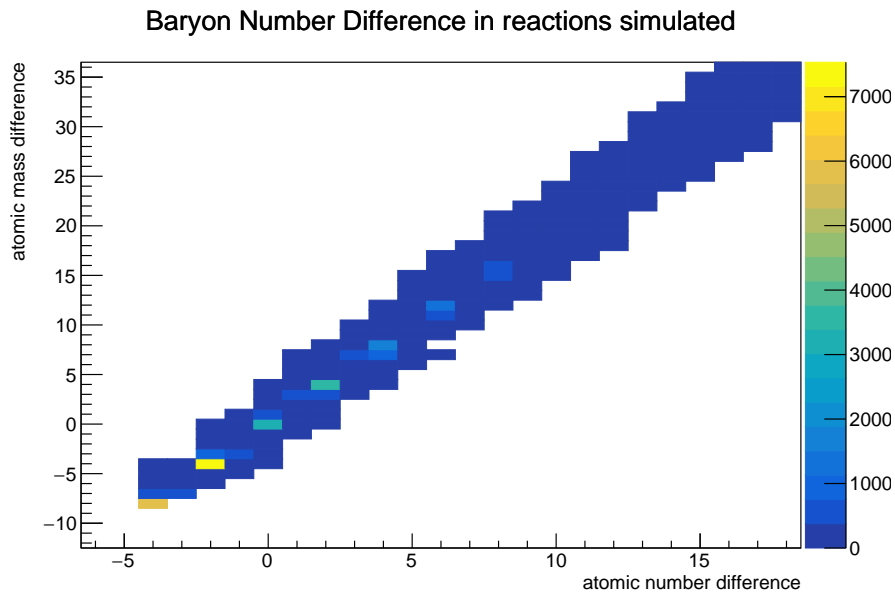


**Figure 5.12:** *Baryonic numbers conservation when adjust final state routine is deactivated. Most of these reaction do not conserve neither Z or A baryonic number.*

A similar relation holds for particle energy: in the *adjust final state mode* energy is conserved in almost all reactions, while if the environment variable is set to *true* energy is not conserved event by event but only *on average*, just like baryonic numbers.

While the latter mode looks hard reliable, because far from physics itself, it is the best mode to use when using incoming charged particles: in fact, as no experimental data are used for these reactions, simulation may not work in the *adjust final state mode*. This is suggested in the physics manual itself [50]. In our simulation, it was clear how the first mode could not be used, as for energies higher than 10 MeV to conserve baryonic number the simulation tried to build a neutron-only nucleus. This nucleus is not only non-physical, but interrupts the simulation as is not among the particles loaded in

this *physicslist*, and therefore cannot be created or tracked, and its creation leads to a *segmentation fault* of the application. Then the second mode has always been used, even though single channels were not reliable.

After modifications to TENDL libraries, a far better agreement was achieved considering cross section has been introduced *by hand*, as can be seen in Figure 5.13. With this model, in fact, the reaction cross section is really close to the goal cross section, and finally also the 675 keV resonance can be simulated. The differences still present in this model are attributable to the fact that:

- for high energies, the model ParticleHP overlaps with the model *BIC* as the *physicslist* used was the QGSP\_BIC\_AllHP. This can be easily changed, but is not a priority of the study discussed in this work;
- in the resonance zone, experimental data are not coherent, as different experimental campaigns report different cross section values not always compatible. Simulated result relies on a *linear interpolation* among data inserted in the *physicslist*.

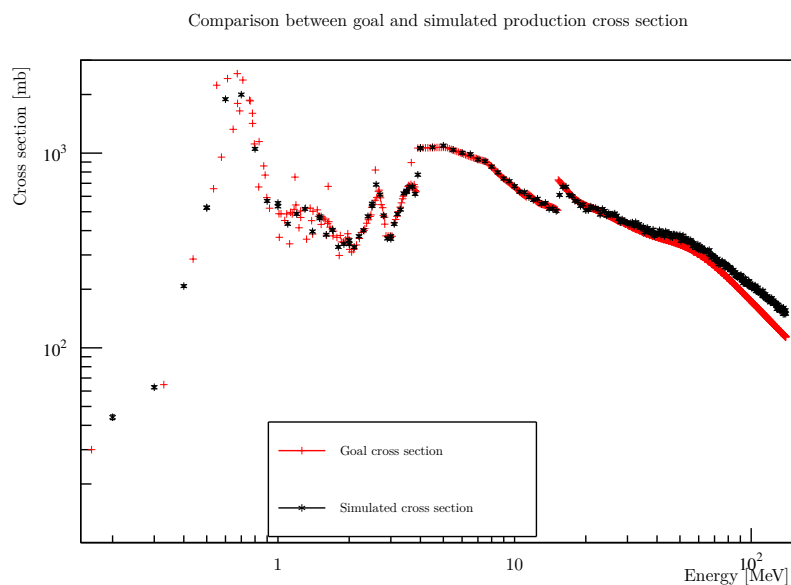


**Figure 5.13:** Comparison between upgraded ParticleHP and goal cross section. See the text for more details.

## 5.8.4 Future perspectives

About future perspectives, in order to simulate in the best possible way the effect of PBCT using a modified version of the ParticleHP model, the following modifications should be accounted:

- an *evaluation* of the experimental cross section should be done to solve compatibility issue between experimental data. If the goal cross section were clearer, even simulations would be more reliable;
- the spectra of alpha particles should be studied and fixed if not correct, analogously to what has been done with cross sections;
- the alpha particles should be produced *in bunches* of three alpha particles for microdosimetry interpretations, or the decay of the  $^8\text{Be}$  should be studied as well to grant reliable bunches of particles;
- other reactions with proton on boron should be studied and fixed if not having the correct cross section or spectra;
- other important reactions with different reagents should be studied.

Nevertheless, this *physicslist* should be used to compute effectively the alpha yield and LET due to boron presence thanks to the Hadrontherapy application, permitting a more precise estimate of radiobiological quantities.

## 5.9. Semi-analytical analysis

As the validation of Geant4 hadronic models was not possible because there was not any *physicslist* which could describe well the reaction cross section, a semi-analytical analysis was one of the first results obtained with the applications written for this work. In particular, a mixture of Geant4 and TALYS calculations permitted to evaluate the yield of alpha particles produced in a radiobiology experiment and the LET modification due to alpha created thanks to  $^{11}\text{B}$  presence. This was done before the modifications to ParticleHP model considering that Geant4 was not capable to estimate correctly the alpha generation due to  $^{11}\text{B}$  presence. This work has already been published [60].

This analysis started from the standard Hadrontherapy Geant4 application with only a few modifications: the whole transportation line has been simulated in a realistic way using one of the *physicslists* suggested<sup>1</sup> and the water-only detector has been divided in 400 vertical voxels perpendicular to the beam axis and with a depth of  $100\ \mu\text{m}$ . This length has been chosen as it is the typical length of cells. Then, an output has been added to the simulation: in a text file the energy of every proton entering a given voxel was saved. This way a protons spectrum along the beam axis could be computed. The result can be seen in Figure 5.14.

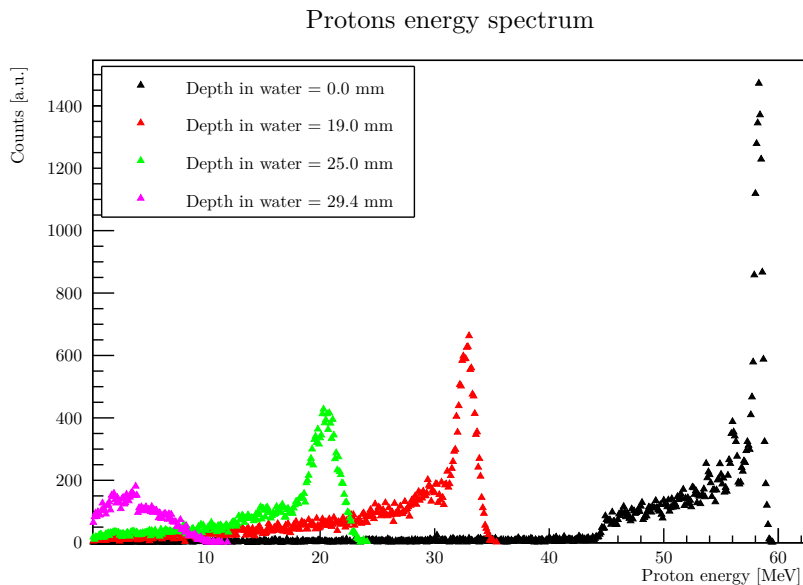


**Figure 5.14:** Simulated spectra of protons obtained using hadrontherapy application. As depth increases, protons become less and less energetic.

Here it is easy to see how the spectrum at the entrance is widened because of the modulator (and also of the air), and how moving along the SOBP the number of protons decreases as well as their energy. This is of course caused by the interactions of protons with matter.

Reliability of the simulation can be confirmed considering the fact that simulated SOBP is really similar to measured SOBP, and therefore *physicslist* used is a good choice. Of course a multiplicative

<sup>1</sup>this has been chosen because these *physicslists* and their results have been long validated in literature.



factor needs to be taken into account as only about a million protons have been simulated while with a clinical beam and a dose of 2 Gy about  $10^{12}$  protons are used.

Knowing protons spectra, and considering the goal cross section as the best estimate for the cross section, an estimate of the alpha yield can be computed. By the way some physical quantities are needed to be able to describe the experimental data. Here they are presented, and their usage will be clarified later:

- *width of the voxel*: this is a parameter set for simulation, in this case it was  $d = 100\mu\text{m}$ ;
- *physical dose deposited*: this depends on the experiment itself. Here, for example, the 2 Gy experiment was the goal, so in this case it was  $D = 2\text{Gy}$ ;
- *density of the medium*: this depends on the experiment itself, but its value must be set in the simulation too. Considering the experiment was done using water equivalent PMMA sheets and simulation was done with water, in this case it is  $\rho = 1000\text{kg m}^{-3}$
- *boron density*: this depends on the experiment that is meant to be simulated. Here the higher concentration experiment was simulated, therefore the value taken is  $C_B = 80\text{ ppm}$ ;
- *boron atomic mass*: this is a constant of nuclear physics, here the value taken is  $M_B = 10.811\text{ g/mol}$ ;
- *Avogadro number*: this is another constant of chemistry, and its value is  $N_A = 6.022 \cdot 10^{23}$ ;
- $^{11}\text{B}$  *fraction*: this is a property of natural boron, here the value taken is  $f = 0.8$ ;
- *Collimator hole surface*: this depends on the collimator used for the experiments, here the collimator used had a radius of  $r = 4.5\text{ mm}$ ;
- *Flask surface*: this depends on the flask where cells were deposited, in this experiment a T25 flask has been used so the value taken is  $S = 2500\text{ mm}^2$ ;

With these values, the two outputs of the simulation (the protons spectra and the simulated dose) and the goal cross section, an estimate of alpha yield can be done. However, before it is necessary to comprehend the multiplicative factors to include: let us consider for instance to have the mean number of alpha particles that are generated according to the simulated proton spectra. The number of alphas will be multiplied then by a factor  $F_G$  accounting for geometry and a factor  $F_D$  accounting for dose. These factors can be calculated as follows:

$$F_G = \frac{S}{\pi r^2} \qquad F_D = \frac{D}{D_S}$$

where  $D_S$  is the simulated dose in that voxel.  $F_G$  is necessary because during the experiment the sample has been uniformly irradiated, therefore multiple irradiations have been done. The number of irradiations is equal to the ratio between the flask surface and the beam surface.  $F_D$  is necessary because during the experiment the dose deposited was 2 Gy for each position along the SOBP, and simulated particles would deposit a lower dose. The value  $D_S$  is read from the simulated SOBP in the chosen voxel.

Now let us discuss how to calculate the alpha yield. The equation to use is Equation 1.3. It is important to compute the numerical density of  $^{11}\text{B}$  in water. It can be calculated using chemistry and physics definition as:

$$n_x = f \frac{C_B \rho N_A}{M_B} = 3.56 \cdot 10^{24} \text{ atoms/m}^2 \qquad (5.3)$$

Knowing these numerical constants, the alpha yield for a given voxel can be computed. The procedure is the following: first the dose is read from the simulated SOBP and the factor  $F_D$  is calculated. After that, histograms information can be used: every bin of the spectrum histogram is multiplied by

the corresponding bin in the cross section histogram. This means that the two histograms must be created such that they have the exact same binning. The results of this operation are summed and then multiplied by the numerical density and the multiplicative factors. The equation used is:

$$N_{\alpha} = F_G F_D \sum_i p_i \sigma_i n_x d \quad (5.4)$$

This gives the number of alpha particle in every voxel where  $p_i$  is the content of the  $i$ -th bin of the spectrum in that voxel and  $\sigma_i$  the cross section for the  $i$ -th bin. This equation permits an estimate of how many alpha particles are created in a voxel thanks to  $^{11}\text{B}$  presence.

Note that spectra have been obtained considering a water-only phantom, and are therefore realistic only if the number of protons interacting with boron is neglectable compared to the total number of protons. This is due to the mixture between simulated spectra and analytical (or experimental driven) cross sections: in this calculation the simulated spectrum at depth  $d$  does not depend on the number of protons that had an alpha-producing interaction before  $d$ . This is an approximation, but if the number of interactions is neglectable (and it will be shown), then the argument holds and the yield estimate is be reliable.

The result of Equation 5.4 when the goal cross section is used can be seen in Figure 5.15, where the alpha yield has been presented together with the simulated SOBP to help understand the meaning of water depth. This means that according to these calculations alpha yield does not increase along the SOBP (as theorized by Cirrone *et al.* in [1]), going against experimental data. This is due to the fact that alpha particles created from *all* proton- $^{11}\text{B}$  channels are considered, not only the  $(p,\alpha)$  channel. A comparison with another number, for example the total proton number used to reach that dose, might help understanding this yield. This number can be seen in Figure 5.16 where the simple total number of protons is presented.

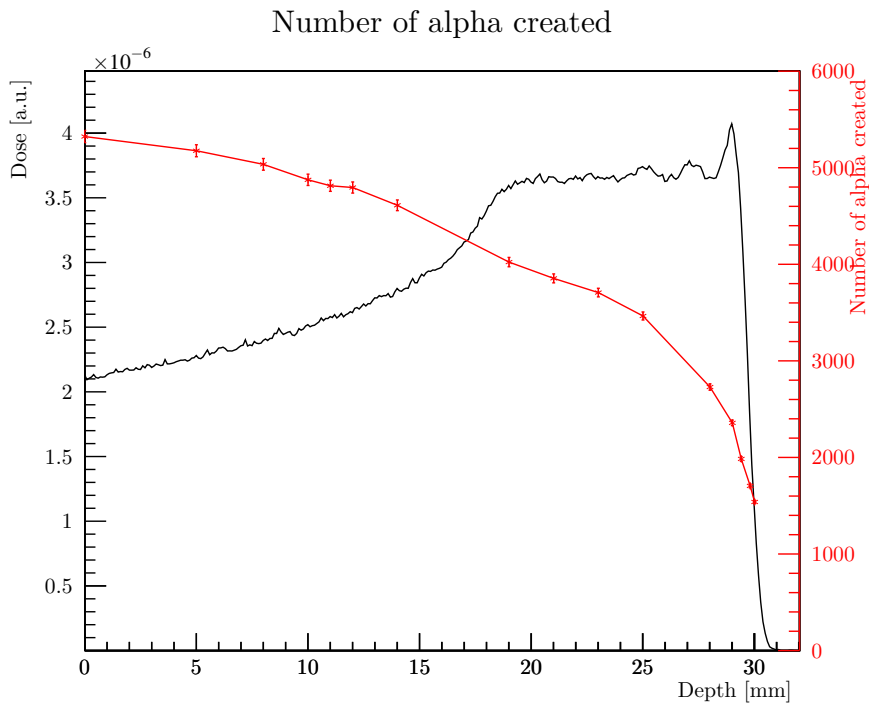


**Figure 5.15:** Total alpha yield generated in a voxel thanks to  $^{11}\text{B}$  presence in a simulated experiment with 2 Gy dose.

Comparing these graphs it is clear how the alpha yield is neglectable compared to proton yield and also their contribution to LET will be (this will be better explained later): alpha particles produced

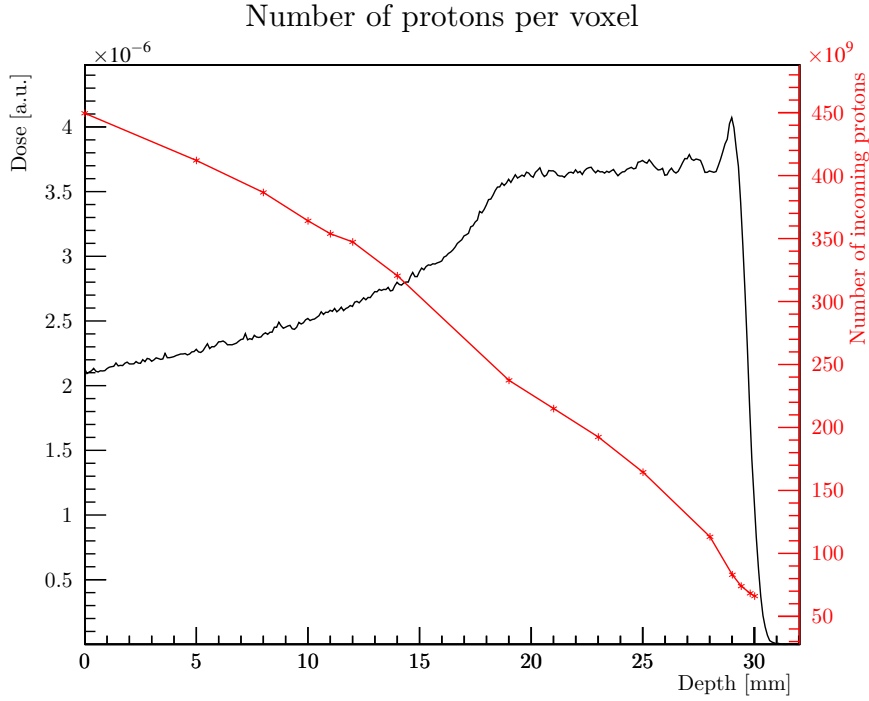


**Figure 5.16:** Number of protons reaching a given voxel as a function of water depth in a simulated experiment with 2 Gy dose.

are about  $10^4$  while protons are about  $10^{11}$ .

Although this alpha yield is neglectable, to be able to fully reject the hypothesis of a DMF increase due to LET increment, a LET estimate must be accomplished. So a model to calculate *mean LET* will be presented, together with a model to *estimate DMF* knowing the mean LET.

For LET estimation both the alpha particles yield and their spectrum are necessary. A first approach to this estimate focused only on the yield: knowing that the particles generated thanks to proton-boron fusion have a spectrum with mean energy of about 4 MeV, the spectrum has not been computed, but all alphas were considered to share that energy. For coherence sake, on the other hand, only alphas produced through split in three alphas could be considered, so the alpha yield has been estimated once again considering only the part of the goal section due to this reaction. The result can be seen in Figure 5.17. From that graph it is clear how the alpha number due to that reaction is almost exclusively concentrated in the distal position, as theorized in [1]. This is a consequence of the fact that cross section is non neglectable only for low energy protons.

LET has been defined in Section 1.3 for a given particle, but it can be calculated also when there are more types of particles. This method can be used both to describe LET of different particles and LET of particles with different energy and, therefore, different stopping power. In particular, the *dose-averaged LET* will be used here as it allows a better prediction of medical quantities when using proton beams. This method has been taken from [61]. Dose averaged mean LET in a point  $z$  can be calculated as:

$$\overline{\text{LET}}_d(z) = \frac{\sum_i \int_0^{\infty} S_i^2(E) \varphi_E^i(z) dE}{\sum_i \int_0^{\infty} S_i(E) \varphi_E^i(z) dE} \quad (5.5)$$

where  $S_i$  is the electronic stopping power for the  $i$ -th particle, and  $\varphi_E^i$  is the local fluence spectra of particle  $i$  with energy  $E$ .

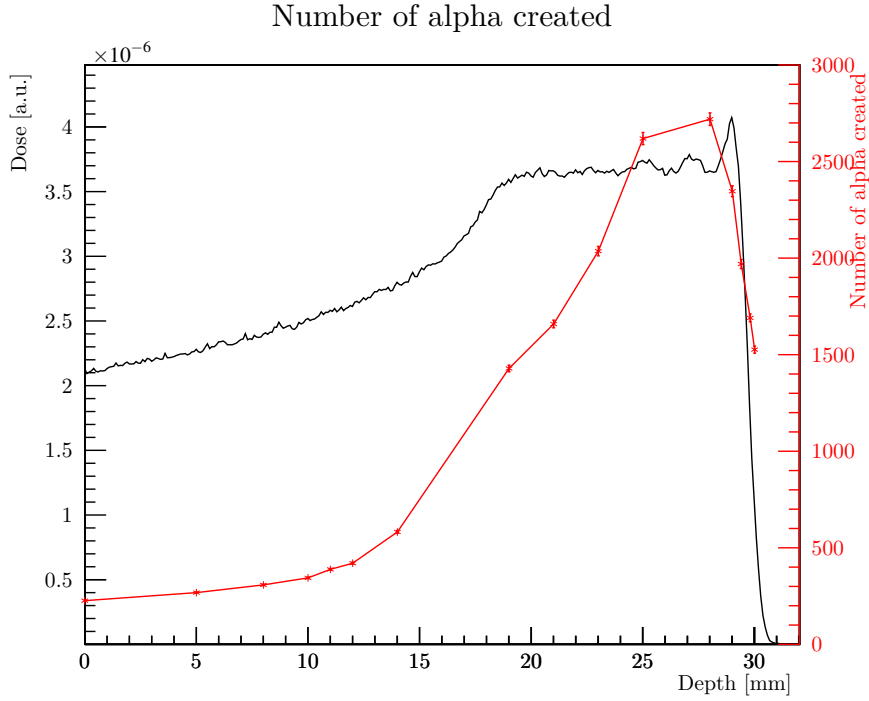


**Figure 5.17:** Alpha yield considering only proton boron fusion.

A well-validated method to calculate average LET in Geant4 is using the formula:

$$\overline{\text{LET}}_d(z) = \frac{\sum_i \sum_j N_j^i e_j^i S_j^i}{\sum_i \sum_j N_j^i e_j^i} \quad (5.6)$$

where  $i$  is an index over the particle types and  $j$  is an index over the energy bins. Here  $N_j^i$  is the number of particles in the  $j$ -th energy bin of  $i$ -th type,  $S_j^i$  is  $dE/dx$  and  $e_j^i$  its energy deposited. The idea of this equation is to compute a *weighted mean* of the LET, where weight is the number of particles multiplied by the energy released in that voxel by a single particle.

What to use as  $dE/dx$  is crucial: using slightly different numbers may lead to far different LET estimates. This number has been taken differently for protons and for alpha particles. First let us discuss what the *ideal* number to input is. If we had information about every step and therefore every interaction of every single particle, a dose averaged LET might be calculated by using the energy deposit at the end of the step and the length of the step itself. This approach is the one computed by Hadrontherapy application when the LET output is selected. But, as alpha generation yield was not included inside Geant4 yet, this approach could not be followed.

What was done was an estimate on the energy released by single particles. If on one hand a high-energy proton enters the voxel, knowing the Bragg peak profile, we well know that it is not going to deposit a large amount of energy, and therefore its energy outside the voxel will be close to the energy it had entering. This means that also the stopping power, that is a function of the proton energy, will be similar all along the proton flight inside the voxel. Therefore a good estimate is the *stopping power*.

If on the other hand a low energy proton or an alpha particle enters the voxel, it might not be able to reach the other side of the voxel, and may stop inside it. This means that a good estimate of the  $dE/dx$  term can be done using the concept of *range*: the mean path a particle flies before stopping.

If the range is shorter than the voxel width, the term  $dE/dx$  can be computed as the total energy divided by the range (and so considering the energy decrease linear).

An approximated approach has been used to ease calculations. The goal of this calculation was to compare estimated cell survival with the experimental one. Thus three position has been used, as cells were located in those positions during the radiobiology experiment. At these depths the simulation was used to compute the spectrum of the primary protons, but only the integral of the spectrum (the proton fluence) and its mean has been used for LET estimate. The mean LET has been calculated considering *all* protons had the same energy (the mean one) and *all* alpha particles shared the energy of 4 MeV.

Alpha particles with this energy have a range of about 27  $\mu\text{m}$  [62], and therefore below the voxel width (that is 100  $\mu\text{m}$ ), so the  $dE/dx$  has been estimated as:

$$\left. \frac{dE}{dx} \right|_{\alpha} = \frac{4 \text{ MeV}}{27 \mu\text{m}} \approx 150 \text{ keV } \mu\text{m}^{-1}$$

On the other hand, protons energy loss has been considered neglectable (and so the stopping power has been used) in the entrance and mid-SOBP positions, while the range has been used (similarly to alphas) in the distal point.

These calculations allowed an estimate of the dose averaged LET with and without the contribution of alpha particles generated thanks to proton boron fusion. LET is not strictly a radiobiological quantity, but some models can link LET to the measured experimental quantity, i.e. the DMF. The model used is the *Micro Kinetic Model*, known as MKM [63].

Interaction between radiation and cells can be considered in terms *lesions induced*. The cellular survival fraction is equal to the probability that the number of lethal lesions is zero in the cellular nucleus. When the distribution of lesion number in the nucleus is assumed to be the Poisson distribution, the survival fraction,  $S$ , is calculated as follows:

$$S = e^{-\langle L_{\text{nucl}} \rangle} \quad (5.7)$$

where  $\langle L_{\text{nucl}} \rangle$  is the cellular population averaged number of lesions in the nucleus.

Then in the MKM model the cell nucleus is partitioned into microscopic-sized domains, and the energy of the domain is calculated as the sum of single event energies as:

$$z = \sum_i z_i$$

and  $z_i$  are calculated using experimental driven models (microdosimetry). Then the number of lesions is calculated as the sum of lesions in all domains.

Number of lesions is assumed to be a linear-quadratic function of deposited energy:

$$L_{\text{nucl}} = \sum_{\text{nucl}} (Az + Bz^2) \quad (5.8)$$

where the parameters  $A$  and  $B$  depend on the cell type. Assuming then a Poisson distribution for the event number of the domain, the population-averaged number of lesions can be calculated as:

$$\langle L_{\text{nucl}} \rangle = (\alpha_0 + \beta z_{1D})D + \beta D^2 \quad (5.9)$$

where  $\alpha_0$  is  $nA$  with  $n$  number of events and  $\beta$  is  $nB$ . The parameter  $z_{1D}$  is the single event mean dose, and it is calculated as:

$$z_{1D} = \frac{\int_0^\infty z^2 f_1(z) dz}{\int_0^\infty z f_1(z) dz} \quad (5.10)$$

where  $f_1(z)$  is the probability density of  $z$  deposited by single energy deposition events of the domain.

Using this MKM model the experimental DMF can be translated in LET and therefore compared to calculations. The result is summarised in Table 5.2.

Position mm	LET (protons) $\text{keV } \mu\text{m}^{-1}$	LET (also alpha) $\text{keV } \mu\text{m}^{-1}$	LET (needed) $\text{keV } \mu\text{m}^{-1}$	DMF (experimental)
Entrance (5.0)	1.30	1.30	3.66	$1.2 \pm 0.4$
Mid-SOBP (21.0)	2.29	2.29	9.53	$1.4 \pm 0.4$
Distal (29.8)	11.70	11.70	33.92	$2.0 \pm 0.7$

**Table 5.2:** Comparison between LET values. In the second column the LET of primary protons only (simulated with hadrontherapy), in the third column the LET with calculated alpha yield (see the text for more details), in the fourth column the LET needed, according to MKM model, to explain experimental DMF, exhibited in the fifth column.

It is clear how the alpha yield has absolutely *no role* in the calculation of mean LET. This was already evident before, as there is about one alpha particle every billion protons, and therefore even if their LET is much greater, the effect on average will be neglectable. This result can be enlightened by plotting together these LET values and simulated SOBP profile, like in Figure 5.18, confirming how far calculated LET is from the one needed to explain experimental values.

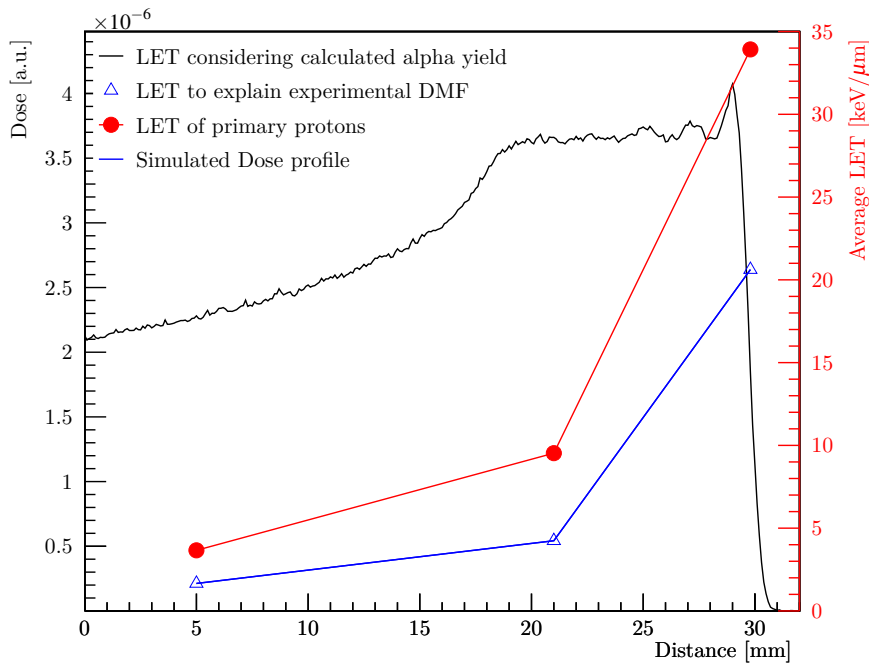


**Figure 5.18:** comparison between LET values. LET due to protons only perfectly superimpose to LET calculated considering also the contribution of alpha particles calculated. Both these values are far from LET needed (according to MKM model) to explain experimental data.

## 5.10. CR39 simulation

As described in Section 3.3 part of this work was focused on the usage of a CR39 with a boron converter to try and measure some alpha particles created thanks to the presence of  $^{11}\text{B}$ . Before the actual experiment the system has been simulated, as described in Section 5.5.

In the simulation all the physical dimensions of the system (such as the detector shape or the converter thickness) have been taken equal to the actual one, and the only thing changed was the position of the detector and, therefore, the water thickness before the detector itself. Two approaches were possible: on one hand Geant4, with its upgraded particleHP *physicslist* describing proton boron fusion could estimate the alpha yield in the detector itself, accounting also for energy loss due to PMMA presence, on the other hand the proton spectrum could be used like in the semi-analytical estimate (Section 5.9) to compute the number of alpha. Although Geant4 is more accurate, a validation process for different processes caused by boron presence is not finished yet, as more reactions must be studied. Therefore the second method was considered more reliable, and the alpha yield was calculated using the proton spectra and the cross section described in Section 5.7. This entered an approximation: protons spectra are different in the converter and in the CR39 itself. This effect has been neglected assuming the spectrum at CR39 was the same that reacted with boron in the converter. This is justified by the fact that PMMA layer is really thin compared to other lengths of the system.

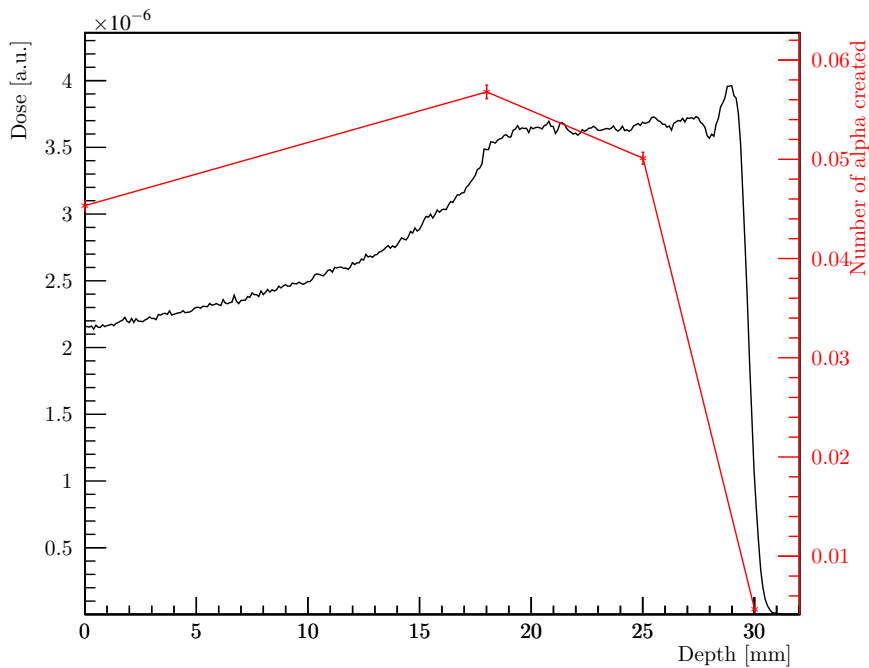


**Figure 5.19:** The alpha yield calculated as a function of depth, plotted with the simulated SOBP.

This computational approach has different main goals:

- to understand the best position for the SOBP;
- to understand the best number of protons to shoot;
- to understand whether alpha spectrum agrees with calculations.

For the former purpose, a simple study of the alpha yield has been done, comparing it to *noise protons*, i.e. protons with energy below 5 MeV that might be confused with alpha particles in the analysis. This

---

unambiguously showed that entrance position was the best: although proton boron fusion reaction is really unlikely, boron can create alpha particles as well thanks to the opening of other channels according to TALYS calculations. Moreover in the entrance position the yield of slow protons is really low, when compared to other positions analysed. The alpha yield can be seen, exhibited together with SOBP, in Figure 5.19, where about 1 million protons have been simulated.

For dose estimation it was chosen to try and produce about least  $5 \cdot 10^4$  particles to have a non-negligible probability to see some in the CR39 detector. The number of this particle was estimated using the *simulated SOBP*: Figure 5.19 shows that there are about 0.045 alpha particles produced at the entrance when a dose of about  $2 \cdot 10^{-6}$  Gy is used. A dose of about 1.5 Gy then corresponds to about  $4 \cdot 10^4$  alpha particles. This value was chosen.

According to the experimental analysis described in Section 3.3, more alpha particles (about a factor 15) entered the CR39 detector. This effect is probably due to the fact that this simulation did not account for alpha particles produced by all channels (i.e. interaction with all isotopes present such as  $^{12}\text{C}$  or  $^{16}\text{O}$ ). Some further simulations will try to account for this effect and explain experimental data.



## Chapter 6

# Conclusions

In this work PBCT has been presented and a step further has been performed towards a full interpretation of the physical processes occurring by means of state-of-the-art simulation codes. The experimental data show a clear and statistically relevant enhancement of the proton therapy lethality thanks to BSH presence, but no confirmation on the origin of this enhancement has been obtained with the simulations.

Simulation approach has been studied in a deeper way and although the uncertainty is still very high (and as mentioned only an order of magnitude study can be done) there are yet about *five orders of magnitude* of difference between the simulated yield of alpha particles and experimental results when the LET is studied with the semi-analytical approach. This shows, indubitably, that a *more complex* approach is needed to explain experimental data, accounting for example for *energy deposit bursts* that might instantly kill a cell or biological effect like the *bystander effect*.

Nevertheless, simulations are still improvable, as so far they do not account for alpha particles spectra and for reactions different from proton boron fusion. Work is still needed to understand what occurs when protontherapy is performed in presence of boron, and NEPTUNE project will probably cover part of this work in the next three years.



# Appendix A

## TENDL libraries

Here a brief description of *how* TENDL libraries are written and, therefore, we modified them, will be given. The work has been done using the most recent TENDL libraries available so far, the *G4TENDL1.3.2*, downloadable from the site <http://geant4.web.cern.ch/support/download>. This is not meant to be a complete description.

When opening the libraries directory, besides finding a `readme` file and a text file containing the history of those libraries, five different directories can be found. Those directories refer each to one incoming particle that can be simulated using the ParticleHP hadronic model. Those particles are alpha, deuteron, He3, proton and triton. Every directory shares the same structure, therefore here only one will be described (the `proton` directory), but the structure would be the same if another directory were studied. Neutrons can not be found in these libraries as the high precision neutron model uses ENDF libraries instead of TENDL ones.

In the proton directory there are two subdirectories: elastic and inelastic. The elastic directory is an empty directory, and probably will be implemented in further versions of the library, that so far can simulate inelastic interactions only. Opening the inelastic folder, there is another `readme` file, a `CrossSections` directory and a set of directories whose name is an `F` followed by two figures. The numbers go from 01 to 36 and every directory refers to different reactions, as will be clarified later.

### A.1. CrossSections

The `CrossSection` directory contains a set of text file (in a binary format), one for every different isotope that the proton might interact with. For example, the file `5_11_Boron.z` is a binary file that once translated into the original text will contain data referred to the inelastic interaction between protons and  $^{11}\text{B}$ . These file have a structure that can be understood looking at ParticleHP source code. In particular, the `5_11_Boron` file looks like shown in Table A.1.

Those words and numbers are to be interpreted as follows: first the keyword `G4NDL` is needed to recognize that this is a file of ND (Nuclear Data Library) written for Geant4 code. If this word is missing, a different routine is run to read this file. Then the following word, here `TENDL-2014` is the keyword of the library itself, in this case it is TENDL and 2014 is added as this is the year this library has been written in. After that, two following numbers are just dummy (here the two zeros), and then the last number, here 45 is the first number important for the simulation, as it gives the number of points that will be read from this file. In fact, after that number, there is a set of exactly 45 couples of numbers, the first one here is  $(1.000000e+06; 3.487870e-01)$ . These numbers give the *energy* for the incoming

G4NDL  
TENDL-2014

	0				
	0				
	45				
1.000000e+06	3.487870e-01	2.000000e+06	3.588650e-01	3.000000e+06	3.830200e-01
4.000000e+06	4.514080e-01	5.000000e+06	4.903260e-01	6.000000e+06	5.358611e-01
7.000000e+06	5.586960e-01	8.000000e+06	5.707080e-01	9.000000e+06	5.823310e-01
1.000000e+07	5.865010e-01	1.100000e+07	5.983040e-01	1.200000e+07	6.287950e-01
1.300000e+07	6.302471e-01	1.400000e+07	6.296161e-01	1.500000e+07	6.261740e-01
1.600000e+07	6.246161e-01	1.700000e+07	6.184400e-01	1.800000e+07	6.114410e-01
1.900000e+07	6.038760e-01	2.000000e+07	5.957890e-01	2.200000e+07	5.787500e-01
2.400000e+07	5.613880e-01	2.600000e+07	5.443210e-01	2.800000e+07	5.279040e-01
3.000000e+07	5.122500e-01	3.500000e+07	4.764060e-01	4.000000e+07	4.449440e-01
4.500000e+07	4.173750e-01	5.000000e+07	3.932090e-01	5.500000e+07	3.719910e-01
6.000000e+07	3.533180e-01	6.500000e+07	3.368370e-01	7.000000e+07	3.222490e-01
7.500000e+07	3.092950e-01	8.000000e+07	2.977570e-01	9.000000e+07	2.782100e-01
1.000000e+08	2.624190e-01	1.100000e+08	2.495110e-01	1.200000e+08	2.388350e-01
1.300000e+08	2.299010e-01	1.400000e+08	2.223360e-01	1.500000e+08	2.158540e-01
1.600000e+08	2.102330e-01	1.800000e+08	2.009250e-01	2.000000e+08	1.934300e-01

**Table A.1:** *An example of a CrossSections file.*

particle in electronvolt and the *cross section* for inelastic hadronic interaction in barn. After having read this file, the simulation knows total cross section as a function of incoming particle energy. Linear interpolation among closest points is done for energy values between two points. As this file was the original file in TENDL libraries, it is clear why cross section was zero below 1 MeV: no data were loaded below that energy, and therefore particle did not undergo inelastic hadronic interaction. This had already been noticed using the default Hadr03 example: for how big the detector was built, if energy was below 1 MeV no particles interacted at all, and therefore cross section could not be calculated.

## A.2. F files

The F files structure is a little bit more complicated. First, it is necessary to understand what those directories stand for and what can be found inside them. The structure has been inherited from the *ENDF-B-VII* libraries, and every directory contains data for different type of reactions. In particular, reaction type, directory name and MCNP numbering for that directory can be found in Table A.2.

This structure has been taken according to ParticleHP code itself, and MCNP numbering can be found in [59]. The case of neutronic inelastic data has been presented as it was the standard in the first ParticleHP, that was named NeutronHP at the time, but the same structure holds for protons and for the other particles as well. This means that in each directory there are files to read data about a given reaction channel: if the interested reaction for example is the (p,d), then a file inside directory F24 should be used.

Structure inside Fs directories is easy, as the user can just find a set of files named after isotopes, one for every nucleus that may undergo the corresponding reaction, similar to what happens in the `CrossSections` directory. Out of all these directories, one holds a different role from the others: that is

---

the F02. As other directories have exactly clear reaction channels, that directory is for the *anything* channel, and therefore may describe inclusive production of a specific particle. That directory is the one that has been modified to include alpha production from the proton on  $^{11}\text{B}$  reaction.

In the next section a brief explanation of how a single file works and what can be found inside will be given.

---

Reaction	Filename	MCNP numbering
(n,n')	F01	50-90,91,4
(n,anything)	F02	5
(n,2nd)	F03	11
(n,2n)	F04	16
(n,3n)	F05	17
(n,na)	F06	22
(n,n3a)	F07	23
(n,2na)	F08	24
(n,3na)	F09	25
(n,np)	F10	28
(n,n2a)	F11	29
(n,2n2a)	F12	30
(n,nd)	F13	32
(n,nt)	F14	33
(n,n3He)	F15	34
(n,nd2a)	F16	35
(n,nt2a)	F17	36
(n,4n)	F18	37
(n,2np)	F19	41
(n,3np)	F20	42
(n,n2p)	F21	44
(n,npa)	F22	45
(n,p)	F23	600-648,649,103
(n,d)	F24	650-698,699,104
(n,t)	F25	700-748,749,105
(n,3He)	F26	750-798,799,106
(n,a)	F27	800-848,849,107
(n,2a)	F28	108
(n,3a)	F29	109
(n,2p)	F30	111
(n,pa)	F31	112
(n,d2a)	F32	113
(n,t2a)	F33	114
(n,pd)	F34	115
(n,pt)	F35	116
(n,da)	F36	117

---

**Table A.2:** Structure of *F* files in ParticleHP.

---

## A.3. F files structure

The structure of F files has been understood looking inside Geant4 code, in particular in the class `G4ParticleHPInelasticBaseFS`. That class is the first class reading such files. Data are read in a cycle, and numbers follow the rules:

- the first item is a number, and is saved as *infotype*. It is just a check number and in common usage is not further used;
- the following two numbers are *dummy* points. They are just not saved. This happens only in the first dataset read in the file;
- the following number is a really important number saved as *dataType*. This number is used for the program to know what kind of data to expect;
- after the *dataType*, the stream of data is passed to another class reading data according to their type. After this different class finishes reading its data, the stream is returned to `G4ParticleHPInelasticBaseFS` and until the file is over reading is repeated starting from the beginning with the only exception that dummy numbers are not present anymore.

From this structure it is understandable how inside the same file more than one set of data can be read. The *dataType* possibilities are the following:

- 3: cross sections;
- 4: angular correlation;
- 5: energy distribution data;
- 6: energy and angular correlation data;
- 12: photon distribution filled with *mean* approach;
- 13: photon distribution filled with *partials* approach;
- 14: photon distribution filled with *angular* approach;
- 15: photon distribution filled with *energy* approach;

how data are read then depends on the type of data itself. As a complete description of ParticleHP is not the purpose of this work, here only two of these types will be discussed, in particular 3 and 6. These two are chosen as these two are the *dataType* in the file `F02/5_11_Boron`: the one modified to describe in a reliable way alpha production due to proton on boron reactions.

### A.3.1 dataType3: cross section

The first part of the `F02/5_11_Boron` file can be seen in Table A.3. This will be used for some clarity in explaining how this type of data are read from Geant4 simulations.

This file, just like the `CrossSections` one, begins with two words: one to recognize this is a NDL file and the following with the library version. After that, the *infotype* (1) is present, followed by the *dataType*, that is 3. After the *dataType* as this is the first dataset inside that file, two dummies are saved, in this case they are a pair of zeros. The following numbers are read by the class `G4ParticleHPVector`, responsible for reading *dataType* 3. The first number is the total number of data, here 45. Later in this file exactly 45 couples of numbers will be read: those are the data giving information about the cross section (in barns) for given energy (in electronvolt).

G4NDL  
TENDL-2014

	1				
	3				
	0	0	45		
1.000000e+06	3.487870e-01	2.000000e+06	3.588650e-01	3.000000e+06	3.830200e-01
4.000000e+06	4.514080e-01	5.000000e+06	4.903260e-01	6.000000e+06	5.358611e-01
7.000000e+06	5.586960e-01	8.000000e+06	5.707080e-01	9.000000e+06	5.823310e-01
1.000000e+07	5.865010e-01	1.100000e+07	5.983040e-01	1.200000e+07	6.287950e-01
1.300000e+07	6.302471e-01	1.400000e+07	6.296161e-01	1.500000e+07	6.261740e-01
1.600000e+07	6.246161e-01	1.700000e+07	6.184400e-01	1.800000e+07	6.114410e-01
1.900000e+07	6.038760e-01	2.000000e+07	5.957890e-01	2.200000e+07	5.787500e-01
2.400000e+07	5.613880e-01	2.600000e+07	5.443210e-01	2.800000e+07	5.279040e-01
3.000000e+07	5.122500e-01	3.500000e+07	4.764060e-01	4.000000e+07	4.449440e-01
4.500000e+07	4.173750e-01	5.000000e+07	3.932090e-01	5.500000e+07	3.719910e-01
6.000000e+07	3.533180e-01	6.500000e+07	3.368370e-01	7.000000e+07	3.222490e-01
7.500000e+07	3.092950e-01	8.000000e+07	2.977570e-01	9.000000e+07	2.782100e-01
1.000000e+08	2.624190e-01	1.100000e+08	2.495110e-01	1.200000e+08	2.388350e-01
1.300000e+08	2.299010e-01	1.400000e+08	2.223360e-01	1.500000e+08	2.158540e-01
1.600000e+08	2.102330e-01	1.800000e+08	2.009250e-01	2.000000e+08	1.934300e-01

**Table A.3:** First part of the 5\_11\_Boron file, with cross section data.

An issue may arise: these data are about cross sections, just like data previously described and showed in Table A.1. Then Geant4 has two different sets of data for the same goal. Through a *trial-and-error* approach it looks like Geant4 prefers to use data in the `crossSections` directory if available.

### A.3.2 data`Type`6: energy and angular correlation

Following Table A.3 data concerning energy and angular correlation can be seen. Part of that file has been reported in Table A.4.

Here only a small part of the file has been presented as reporting all the file would be needlessly too long. These data are read by the class `G4ParticleHPEnAngCorrelation`. First, we can see once again the *infotype* for the library (1) and the *dataType*, that is 6. After those numbers, the following are the mass of the target nucleus (here 10.911) in *uma*. This information would not be necessary because Geant4 already knows isotopes masses, but here it is reported once again. After the mass, the following number is called *frameFlag* (here 3). It is needed to understand the frame these data are taken in. Here 3 is an alias of 2 used especially for ParticleHP, and refers to the center of mass system. The following number, 23, is the number of products. This means that in this file, where the channels (p, anything) is presented, there are energy-angle correlation data for 23 different products. The next numbers *will be repeated 23 times*: these first lines are to introduce and set up overall parameters for these data, while next are referred to one of the products, and read by the class `G4ParticleHPProduct`.

Data continue with the code of the product, written as  $A \cdot 10^3 + Z$ . Here the code is `1.000000e+00`, corresponding to  $A = 1$  and  $Z = 0$ . This first set of data is about *neutrons* in the outgoing channel. After the code, the mass of the product is reported in *uma*, here the value is `1.000000e+00`. The following number (here a 0) is called *theIsomerFlag*, and so far Geant4 does not use this information.



5_11_Boron					
	1				
	6				
	10.9147	3	23		
1.000000e+00	1.000000e+00	0	1		
0.000000e+00	0.000000e+00				
	44				
	1				
	44	2			
1.000000e+06	0.000000e+00	3.000000e+06	0.000000e+00	4.000000e+06	1.572320e-01
5.000000e+06	1.937630e-01	6.000000e+06	2.284220e-01	7.000000e+06	2.314440e-01
8.000000e+06	2.580720e-01	9.000000e+06	2.741100e-01	1.000000e+07	2.748810e-01
1.100000e+07	2.847840e-01	1.200000e+07	2.690720e-01	1.300000e+07	2.646170e-01
1.400000e+07	2.529590e-01	1.500000e+07	2.534350e-01	1.600000e+07	2.282940e-01
1.700000e+07	2.367320e-01	1.800000e+07	2.479780e-01	1.900000e+07	2.644750e-01
2.000000e+07	2.831290e-01	2.200000e+07	3.288720e-01	2.400000e+07	3.760370e-01
2.600000e+07	4.227530e-01	2.800000e+07	4.650250e-01	3.000000e+07	5.099610e-01
3.500000e+07	6.075970e-01	4.000000e+07	6.980570e-01	4.500000e+07	7.608670e-01
5.000000e+07	8.235010e-01	5.500000e+07	8.671770e-01	6.000000e+07	8.986270e-01
6.500000e+07	9.338660e-01	7.000000e+07	9.628140e-01	7.500000e+07	9.846780e-01
8.000000e+07	1.009160e+00	9.000000e+07	1.055650e+00	1.000000e+08	1.105160e+00
1.100000e+08	1.143180e+00	1.200000e+08	1.186730e+00	1.300000e+08	1.220630e+00
1.400000e+08	1.256870e+00	1.500000e+08	1.283720e+00	1.600000e+08	1.316460e+00
1.800000e+08	1.375250e+00	2.000000e+08	1.429810e+00		
5011	2	1	32		
	1				
	32	2			
1e+06	2	0	2		
0.000000e+00	1.455492e-06	0.000000e+00	6.870528e+05	0.000000e+00	0.000000e+00
3e+06	2	0	2		
0.000000e+00	1.455492e-06	0.000000e+00	6.870528e+05	0.000000e+00	0.000000e+00

**Table A.4:** Part of the second part of the 5\_11\_Boron with energy-angular correlations.

The following number (here a 1) is saved as *theDistLaw*. This number is needed for the program to understand what distribution the following data are going to have. The possible values are:

- 0: unknown, at first assumed isotropic;
- 1: continuum energy-angular distribution;
- 2: discrete 2-body scattering;
- 3: isotropic emission;
- 4: Discrete 2-body recoil modification (not implemented yet);
- 5: not implemented yet;
- 6: N-Body phase space
- 7: Laboratory angular energy parametrisation

Depending on which value is present, a different class will contain data, and therefore there will be a different way to read data. Here, as the value is 1, the class `G4ParticleHPContEnergyAngular` will read data, but this operation will be achieved later.

---

Before that, there are two numbers refer to  $Q$ -values: the first is the *ground state  $Q$ -value* and the following is the *actual state  $Q$  value*, both expressed in electronvolt. So far only the former is used in simulations. The following numbers are used to compute the *yield* of the particle produced. This means that on average every reaction will produce a number of particles equal to the yield. Reading of the yield is made using the class `G4ParticleHPVector`. The first number (here 44) is the number of data couples that will be given (data couples are energy in electronvolt and adimensional yield), then the following numbers refer to the interpolation of data, granted by the class `G4InterpolationManager`. The 1 refer to the number of schemes that will be used, and it is followed by a set of couples that give first the range of the scheme (here 44) and then the type of the scheme (here 2). The number of couples must be equal to the number of schemes to use. The scheme 2 correspond to the `LINLIN` scheme: the simulation will do a linear interpolation both in the x axis and in the y axis when using yield data.

After the setup of the interpolation tool the yields can be read from the `G4ParticleHPVector` class, that reads the couples of numbers where the first is in electronvolt while the second is adimensional. In Table A.4 the last of these couples is  $(2.000000e+08, 1.429810e+00)$ .

When the yield has been saved, the class `G4ParticleHPContEnergyAngular` can finally begin reading the energy-angular correlation. The first thing is the target code (here 5011) written as  $Z \cdot 10^3 + A$ , then the following number is a code saved as *angularRep* (here 2). This is used to sample from the distribution, and different values correspond to different way to sample. The following number is used to set the interpolation scheme, just like before, and 1 is for the *histogram* scheme. The following number refer to the number of energies that will be presented in the file, here the value 32 is shown, therefore 32 different energies will be given. Then the others three number refer to interpolation, just like before, and have the same exact meaning.

After that, a set of energies is shown, each read by the class `G4ParticleHPContAngularPar`: first the energy in electronvolt, then the number of entries, the number of discrete entries and the number of angular parameters. Then, for every entry, three numbers are needed: the first is the energy (of the outgoing particle), and then a set of numbers equal to the one given before describe the angle.

## A.4. Modification to the ParticleHP

As said, two files were modified to well simulate the Reaction 1.2: the `CrossSections/5_11_Boron` and `F02/5_11_Boron`. The goal was to have a reliable alpha yield when studying the reaction of protons on  $^{11}\text{B}$ . The modifications touched two parts of the libraries:

- total reaction cross section;
- alpha production yield;

and the goal was to change *only alpha production yield*, while keeping the production of other nuclei and particles unchanged.

If the cross section was zero (i.e. below the threshold of 1 MeV), the modifications were a little bit easier to make. The yield has been set in fact to *one* both for alpha particles and  $^8\text{Be}$ , while the cross section has been set equal to the proton boron fusion reaction in the goal cross section. This way the simulation production cross section will be right.

---

When there was already a default cross section loaded (i.e. between 1 and 3.85 MeV) the cross section could not be changed as this would also change other particles production cross section. Then the routine followed by Geant4 itself has been followed: it was discussed how interpolation inside Geant4 is done linearly considering only the closest points. Then, the yield has been set equal to the ratio between the goal cross section and the linearly interpolated cross section for that energy. This routine has been repeated both for alpha particles and for  $^8\text{Be}$ . This way the production cross section agrees with the goal cross section, as confirmed from Figure 5.13.



# Bibliography

- [1] G. A. P. Cirrone, L. Manti, D. Margarone, G. Petringa, L. Giuffrida, A. Minopoli, A. Picciotto, G. Russo, P. Cammarata, F. and Pisciotta, et al. First experimental proof of proton boron capture therapy (pbct) to enhance protontherapy effectiveness. *Scientific Reports*, 8(1):1141, 2018.
- [2] M.Á. Nunes. *Protontherapy Versus Carbon Ion Therapy: Advantages, Disadvantages and Similarities*. Biological and Medical Physics, Biomedical Engineering. Springer International Publishing, 2015.
- [3] G. Delaney, S. Jacob, C. Featherstone, and M. Barton. The role of radiotherapy in cancer treatment: estimating optimal utilization from a review of evidence-based clinical guidelines. *Cancer*, 104(6):1129–1137, 2005.
- [4] World Health Organization. What is ionizing radiation? [https://www.who.int/ionizing\\_radiation/about/what\\_is\\_ir/en/](https://www.who.int/ionizing_radiation/about/what_is_ir/en/), 2009. [Online; accessed 1-March-2019].
- [5] G. Delaney, S. Jacob, C. Featherstone, and M. Barton. The role of radiotherapy in cancer treatment: estimating optimal utilization from a review of evidence-based clinical guidelines. *Cancer*, 104(6):1129–1137, 2005.
- [6] M. Höckel and P. Vaupel. Tumor Hypoxia: Definitions and Current Clinical, Biologic, and Molecular Aspects. *JNCI: Journal of the National Cancer Institute*, 93(4):266–276, 2001.
- [7] J. Foo and F. Michor. Evolution of acquired resistance to anti-cancer therapy. *J. Theor. Biol.*, 355:10–20, 2014.
- [8] J. Yang, J. B. Yue, J. Liu, and J. M. Yu. Repopulation of tumor cells during fractionated radiotherapy and detection methods (Review). *Oncol Lett*, 7(6):1755–1760, 2014.
- [9] O. Desouky and G. Zhou. Biophysical and radiobiological aspects of heavy charged particles. *Journal of Taibah University for Science*, 10(2):187–194, 2016.
- [10] A. Berman, S. St. James, and R. Rengan. Proton beam therapy for non-small cell lung cancer: Current clinical evidence and future directions. *Cancers*, 7:1178–1190, 2015.
- [11] T. Wenzl and J. J Wilkens. Modelling of the oxygen enhancement ratio for ion beam radiation therapy. *Physics in Medicine and Biology*, 56(11):3251–3268, 2011.
- [12] A. Peeters, J. P.C. Grutters, M. Pijls-Johannesma, S. Reimoser, D. De Ruyscher, J. L. Severens, M. A. Joore, and P. Lambin. How costly is particle therapy? cost analysis of external beam radiotherapy with carbon-ions, protons and photons. *Radiotherapy and Oncology*, 95(1):45 – 53, 2010.
- [13] J. Choi and J. O. Kang. Basics of particle therapy II: relative biological effectiveness. *Radiat Oncol J*, 30(1):1–13, 2012.
- [14] M. Dosanjh, U. Amaldi, R. Mayer, and R. Poetter. Enlight: European network for light ion hadron therapy. *Radiotherapy and Oncology*, 128(1):76 – 82, 2018.
- [15] P. Wardman. Chemical radiosensitizers for use in radiotherapy. *Clinical Oncology*, 19(6):397 – 417, 2007. Importance of Radiobiology to Cancer Therapy: Current Practice and Future Perspectives.

- 
- [16] G.E. Adams. Chemical radiosensitization of hypoxic cells. *Brit. Med. Bull.* 29: No. 1, 48-53(Jan 1973)., 1973.
- [17] Jack F. Fowler, Gerald E. Adams, and Juliana Denekamp. Radiosensitizers of hypoxic cells in solid tumours. *Cancer Treatment Reviews*, 3(4):227 – 256, 1976.
- [18] I. Martinez-Rovira and Y. Prezado. Evaluation of the local dose enhancement in the combination of proton therapy and nanoparticles. *Med Phys*, 42(11):6703–6710, 2015.
- [19] K. Haume, S. Rosa, S. Grellet, M. A. Smialek, K. T. Butterworth, A. V. Solov'yov, K. M. Prise, J. Golding, and N. J. Mason. Gold nanoparticles for cancer radiotherapy: a review. *Cancer Nanotechnol*, 7(1):8, 2016.
- [20] A. V. Verkhovtsev, A. V. Korol, and A. V. Solov'yov. Electron production by sensitizing gold nanoparticles irradiated by fast ions. *The Journal of Physical Chemistry C*, 119(20):11000–11013, 2015.
- [21] L. Stefancikova, E. Porcel, P. Eustache, S. Li, D. Salado, S. Marco, J. L. Guerquin-Kern, M. Refregiers, O. Tillement, F. Lux, and S. Lacombe. Cell localisation of gadolinium-based nanoparticles and related radiosensitising efficacy in glioblastoma cells. *Cancer Nanotechnol*, 5(1):6, 2014.
- [22] Geant4 collaboration. Overview | geant4.web.cern.ch. <http://geant4.web.cern.ch/>, 2017. [Online; accessed 1-March-2019].
- [23] K. Nedunchezian, N. Aswath, M. Thiruppathy, and S. Thirugnanamurthy. Boron Neutron Capture Therapy - A Literature Review. *J Clin Diagn Res*, 10(12):ZE01–ZE04, 2016.
- [24] R. F. Barth, M. G. Vicente, O. K. Harling, W. S. Kiger, K. J. Riley, P. J. Binns, F. M. Wagner, M. Suzuki, T. Aihara, I. Kato, and S. Kawabata. Current status of boron neutron capture therapy of high grade gliomas and recurrent head and neck cancer. *Radiat Oncol*, 7:146, 2012.
- [25] D. Yoon, J. Jung, and T. Suh. Application of proton boron fusion reaction to radiation therapy: A monte carlo simulation study. *Applied Physics Letters*, 105(22):223507, 2014.
- [26] A.J. Koning and D. Rochman. Modern nuclear data evaluation with the talys code system. *Nuclear Data Sheets*, 113(12):2841 – 2934, 2012. Special Issue on Nuclear Reaction Data.
- [27] H. W. Becker, C. Rolfs, and H. P. Trautvetter. Low-energy cross sections for  $^{11}\text{B}(p, 3\alpha)$ . *Zeitschrift für Physik A Atomic Nuclei*, 327(3):341–355, 1987.
- [28] N. Otuka et al. Towards a More Complete and Accurate Experimental Nuclear Reaction Data Library (EXFOR): International Collaboration Between Nuclear Reaction Data Centres (NRDC). *Nucl. Data Sheets*, 120:272–276, 2014.
- [29] INFN Laboratori Nazionali del Sud. Catana - infn - laboratori nazionali del sud. <https://www.lns.infn.it/en/application/catana.html>, 2017. [Online; accessed 1-March-2019].
- [30] CNAO fundation. Centro nazionale di adroterapia oncologica - home. <https://fondazionecnao.it/en/>, 2017. [Online; accessed 1-March-2019].
- [31] INFN Laboratori Nazionali del Sud. Introduction - infn - laboratori nazionali del sud. <https://www.lns.infn.it/en/about-us/introduction.html>, 2017. [Online; accessed 1-March-2019].
- [32] INFN Laboratori Nazionali del Sud. Superconducting cyclotron - infn - laboratori nazionali del sud. <https://www.lns.infn.it/en/accelerators/superconducting-cyclotron.html>, 2017. [Online; accessed 1-March-2019].
- [33] D. Battaglia, L. Calabbretta, L. Celona, P. Cirrone, G. Cuttone, F. Rosa, P. Lojacono, S. Nigro, M. Maggiore, V. Mongelli, et al. The infn experience in the hadron therapy field. 2019.

- 
- [34] INFN Laboratori Nazionali del Sud. Irradiation rooms - infn - laboratori nazionali del sud. <https://www.lns.infn.it/en/equipment/irradiation-rooms.html>, 2017. [Online; accessed 1-March-2019].
- [35] G. A. P. Cirrone, G. Cuttone, L. Raffaele, V. Salamone, T. Avitabile, G. Privitera, C. Spatola, D. Margarone, V. Patti, G. Petringa, et al. Clinical and Research Activities at the CATANA Facility of INFN-LNS: From the Conventional Hadrontherapy to the Laser-Driven Approach. *Front Oncol*, 7:223, 2017.
- [36] F. Bourhaleb, R. Cirio, G. A. P. Cirrone, G. Cuttone, M. Donetti, M. A. Garella, S. Giordanengo, N. Givechi, A. La Rosa, A. Luparia, et al. 121 on-line monitoring of the catana protontherapy beam with the strip ionization chamber mopi. *Radiotherapy and Oncology*, 76:S63–S64, 2005.
- [37] J. Pearce, R. Thomas, and A. Dusautoy. The characterization of the Advanced Markus ionization chamber for use in reference electron dosimetry in the UK. *Phys Med Biol*, 51(3):473–483, 2006.
- [38] N. A. Franken, H. M. Rodermond, J. Stap, J. Haveman, and C. van Bree. Clonogenic assay of cells in vitro. *Nat Protoc*, 1(5):2315–2319, 2006.
- [39] E. J Hall and (author.) Giaccia, A. J. *Radiobiology for the radiologist*. Philadelphia, PA : Wolters Kluwer Health/Lippincott Williams & Wilkins, seventh edition edition, 2012. Includes bibliographical references and index.
- [40] G. Obe, P. Pfeiffer, J. R. Savage, C. Johannes, W. Goedecke, P. Jeppesen, A. T. Natarajan, W. Martinez-Lopez, G. A. Folle, and M. E. Drets. Chromosomal aberrations: formation, identification and distribution. *Mutat. Res.*, 504(1-2):17–36, 2002.
- [41] R.M. Cassou and E.V. Benton. Properties and applications of cr-39 polymeric nuclear track detector. *Nuclear Track Detection*, 2(3):173 – 179, 1978.
- [42] S. Agostinelli, J. Allison, K. Amako, J. Apostolakis, H. Araujo, P. Arce, M. Asai, D. Axen, S. Banerjee, G. Barrand, et al. Geant4—a simulation toolkit. *Nuclear Instruments and Methods in Physics Research Section A: Accelerators, Spectrometers, Detectors and Associated Equipment*, 506(3):250 – 303, 2003.
- [43] R. Brun and F. Rademakers. Root — an object oriented data analysis framework. *Nuclear Instruments and Methods in Physics Research Section A: Accelerators, Spectrometers, Detectors and Associated Equipment*, 389(1):81 – 86, 1997. New Computing Techniques in Physics Research V.
- [44] N. Metropolis and S. Ulam. The monte carlo method. *Journal of the American Statistical Association*, 44(247):335–341, 1949.
- [45] Roger Eckhardt. Stan ulam, john von neumann, and the monte carlo method. *Los Alamos Science*, 15:131–136, 1987.
- [46] Geant4 collaboration. *Geant4 - Book for application developers*.
- [47] A. Kramida, Yu. Ralchenko, J. Reader, and and NIST ASD Team. NIST Atomic Spectra Database (ver. 5.6.1), [Online]. Available: <https://physics.nist.gov/asd> [2015, April 16]. National Institute of Standards and Technology, Gaithersburg, MD., 2018.
- [48] G. Petringa. Physics in geant4 - part 2. XIV Seminar on Software for Nuclear, Subnuclear and Applied Physics, 2017.
- [49] M. Tanabashi, K. Hagiwara, K. Hikasa, K. Nakamura, Y. Sumino, F. Takahashi, J. Tanaka, K. Agashe, G. Aielli, C. Amsler, et al. Review of particle physics. *Phys. Rev. D*, 98:030001, 2018.
- [50] Geant4 collaboration. *Geant4 - Physics Reference Manual*.
- [51] CERN. Root a data analysis framework. <https://root.cern.ch/>, 2018. [Online; accessed 1-March-2019].

- 
- [52] René B. *ROOT User's Guide*. CERN.
- [53] Nuclear Research and Consultancy Group (NRG). Talys: Home. <http://www.talys.eu/home/>, 2018. [Online; accessed 1-March-2019].
- [54] R. Capote, M. Herman, P. Obložinský, P.G. Young, S. Goriely, T. Belgya, A.V. Ignatyuk, A.J. Koning, S. Hilaire, V.A. Plujko, M. Avrigeanu, O. Bersillon, M.B. Chadwick, T. Fukahori, Zhigang Ge, Yinlu Han, S. Kailas, J. Kopecky, V.M. Maslov, G. Reffo, M. Sin, E.Sh. Soukhovitskii, and P. Talou. Ripl – reference input parameter library for calculation of nuclear reactions and nuclear data evaluations. *Nuclear Data Sheets*, 110(12):3107 – 3214, 2009. Special Issue on Nuclear Reaction Data.
- [55] Stephane Goriely Arjan Koning, Stephane Hilaire. *TALYS1.4 - User Manual*.
- [56] G. A. P. Cirrone, G. Cuttone, and S. E. Mazzaglia. Hadrontherapy a geant4-based tool for proton/ion-therapy studies. page 1630, Japan, 2010.
- [57] J. Benn, E.B. Dally, H.H. Müller, R.E. Pixley, H.H. Staub, and H. Winkler. Lifetime and energy of the ground state of  $8\text{be}$ . *Nuclear Physics A*, 106(2):296 – 312, 1967.
- [58] D. Mancusi, A. Boudard, J. Cugnon, J. David, P. Kaitaniemi, and S. Leray. Extension of the liège intranuclear-cascade model to reactions induced by light nuclei. *Phys. Rev. C*, 90:054602, 2014.
- [59] edited by M. Herman Members of the Cross Sections Evaluation Working Group and A. Trkov. *ENDF-6 Formats Manual: Data Formats and Procedures for the Evaluated Nuclear Data Files ENDF/B-VI and ENDF/B-VII*.
- [60] G.A.P. Cirrone, G. Petringa, A. Attili, D. Chiappara, L. Manti, V. Bravatà, D. Margarone, M. Mazzocco, and G. Cuttone. Study of the discrepancy between analytical calculations and the observed biological effectiveness in Proton Boron Capture Therapy (PBCT). *RAD journal*, 3(3):147–151, 2019.
- [61] D. Sanchez-Parcerisa, M. A. Cortés-Giraldo, D. Dolney, M. Kondrla, M. Fager, and A. Carabe. Analytical calculation of proton linear energy transfer in voxelized geometries including secondary protons. *Physics in Medicine and Biology*, 61(4):1705–1721, 2016.
- [62] Martin J. Berger, J S. Coursey, M A. Zucker. Estar, pstar, and astar: Computer programs for calculating stopping-power and range tables for electrons, protons, and helium ions (version 1.21). <http://physics.nist.gov/Star>, 1999.
- [63] Y. Kase, T. Kanai, N. Matsufuji, Y. Furusawa, T. Elsässer, and M. Scholz. Biophysical calculation of cell survival probabilities using amorphous track structure models for heavy-ion irradiation. *Physics in Medicine and Biology*, 53(1):37–59, 2007.



---

# Ringraziamenti

Ci sarebbero molte persone da ringraziare in conclusione a questo lavoro, quindi già mi scuso se sto dimenticando qualcuno.

Per iniziare, un grazie sentito ai miei relatori e correlatori: senza i consigli di Marco spesso non ce l'avrei fatta, ed é principalmente grazie a Giada e Pablo e alla loro disponibilità, pazienza e fiducia se sono riuscito a scrivere questa tesi. Inoltre un grazie va alle persone che mi hanno aiutato in questo lavoro, tra i quali Dr. Arce, Dr. Cammarata, Dr. Catalano, Prof. Manti e molti altri.

É anche doveroso ringraziare tutte le istituzioni che mi hanno aiutato in questi mesi di lavoro: l'Università di Padova che mi ha preparato e permesso di fare una tesi in trasferta, la Sezione di Padova dell'INFN che mi ha accolto e aiutato, i Laboratori Nazionali del Sud che mi hanno ospitato e permesso di prendere parte a numerosi esperimenti, il gruppo di organizzazione delle scuole di Geant4 che mi ha dato possibilità che mai avrei immaginato poco tempo fa, e il personale del Laboratorio di Biofisica delle radiazioni del dipartimento di fisica dell'Università di Napoli, che mi ha permesso di prendere parte a esperimenti e ha condiviso con me i risultati.

Ultime ma non ultime, tutte le persone che in questi anni di studio mi hanno supportato e sopportato: dalla mia famiglia che mi ha sempre spronato e aiutato da tutti i punti di vista, a Lisa che ha sempre creduto in me e c'è sempre stata, nonostante i momenti no, al gruppo di Padova che mi ha sempre aiutato senza pensarci due volte e ha reso l'università il periodo piú bello della mia vita: Francesco, Ivan, Marco, Gabriele, Giulio e in particolare il dottor Enrico, senza il quale a quest'ora starei ancora litigando con Linux e  $\text{\LaTeX}$ . Un ringraziamento va anche alla squadra *Crossfit 30037*, senza la quale avrei dato di matto tempo fa.